PUBLICATIONS OF THE ASTRONOMICAL SOCIETY OF THE PACIFIC, **120**:38–88, 2008 January

Taking the Measure of the Universe: Precision Astrometry with *SIM PlanetQuest*

STEPHEN C. UNWIN,[1] MICHAEL SHAO,[2] ANGELLE M. TANNER,[2] RONALD J. ALLEN,[3] CHARLES A. BEICHMAN,[4] DAVID BOBOLTZ,[5] JOSEPH H. CATANZARITE,[2] BRIAN C. CHABOYER,[6] DAVID R. CIARDI,[4] STEPHEN J. EDBERG,[2] ALAN L. FEY,[5] DEBRA A. FISCHER,[7] CHRISTOPHER R. GELINO,[8] ANDREW P. GOULD,[9] CARL GRILLMAIR,[8] TODD J. HENRY,[10] KATHRYN V. JOHNSTON,[11,12] KENNETH J. JOHNSTON,[5] DAYTON L. JONES,[2] SHRINIVAS R. KULKARNI,[4] NICHOLAS M. LAW,[4] STEVEN R. MAJEWSKI,[13] VALERI V. MAKAROV,[2] GEOFFREY W. MARCY,[14] DAVID L. MEIER,[2] ROB P. OLLING,[15] XIAOPEI PAN,[2] RICHARD J. PATTERSON,[13] JO ELIZA PITESKY,[2] ANDREAS QUIRRENBACH,[16] STUART B. SHAKLAN,[2] EDWARD J. SHAYA,[15] LOUIS E. STRIGARI,[17] JOHN A. TOMSICK,[18,19], ANN E. WEHRLE,[20] AND GUY WORTHEY[21]

Received 2007 August 19; accepted 2007 November 01; published 2008 January 22

ABSTRACT. Precision astrometry at microarcsecond accuracy has applications for a wide range of astrophysical problems. This paper is a study of the science questions that can be addressed using an instrument with flexible scheduling that delivers parallaxes at about 4 μas on targets as faint as $V = 20$, and differential accuracy of 0.6 μas on bright targets. The science topics are drawn primarily from the team key projects, selected in 2000, for the *Space Interferometry Mission PlanetQuest* (*SIM PlanetQuest*). We use the capabilities of this mission to illustrate the importance of the next level of astrometric precision in modern astrophysics. *SIM PlanetQuest* is currently in the detailed design phase, having completed in 2005 all of the enabling technologies needed for the flight instrument. It will be the first space-based long-baseline Michelson interferometer designed for precision astrometry. *SIM PlanetQuest* will contribute strongly to many astronomical fields, including stellar and galactic astrophysics, planetary systems around nearby stars, and the study of quasar and AGN nuclei. Using differential astrometry *SIM PlanetQuest* will search for planets with masses as small as Earth orbiting in the "habitable zone" around the nearest stars, and could discover many dozen if Earth-like planets are common. It will characterize the multiple-planet systems that are now known to exist, and it will be able to search for terrestrial planets around all of the candidate target stars in the *Terrestrial Planet Finder* and *Darwin* mission lists. It will be capable of detecting planets around young stars, thereby providing insights into how planetary systems are born and how they evolve with time. Precision astrometry allows the measurement of accurate dynamical masses for stars in binary systems. *SIM PlanetQuest* will observe significant numbers of very high- and low-mass stars, providing stellar masses to 1%, the accuracy needed to challenge physical models. Using precision proper-motion measurements, *SIM PlanetQuest* will probe the Galactic mass distribution, and, through studies of tidal tails, the formation and evolution of the Galactic halo. *SIM PlanetQuest* will contribute to cosmology through improved accuracy of the Hubble constant. With repeated astrometric measurements of the nuclei of active galaxies, *SIM PlanetQuest* will probe the dynamics of accretion disks around supermassive black holes, and the relativistic jets that emerge from them.

Online material: color figures

[1] Jet Propulsion Laboratory, California Institute of Technology, Pasadena, CA; stephen.unwin@jpl.nasa.gov.
[2] Jet Propulsion Laboratory, California Institute of Technology, Pasadena, CA.
[3] Space Telescope Science Institute, Baltimore, MD.
[4] Michelson Science Center, California Institute of Technology, Pasadena, CA.
[5] United States Naval Observatory, Washington, DC.
[6] Department of Physics and Astronomy, Dartmouth College, Hanover, NH.
[7] Department of Physics and Astronomy, San Francisco State University, San Francisco, CA.
[8] Spitzer Science Center, Pasadena, CA.
[9] Department of Astronomy, The Ohio State University, Columbus, OH.
[10] Department of Physics and Astronomy, Georgia State University, Atlanta, GA.
[11] Van Vleck Observatory, Wesleyan University, Middletown, CT.
[12] Pupin Physics Laboratories, Columbia University, New York, NY.
[13] Department of Astronomy, University of Virginia, Charlottesville, VA.
[14] University of California, Berkeley, CA.
[15] Astronomy Department, University of Maryland, College Park, MD.
[16] Landessternwarte Koenigstuhl 12, University of Heidelberg, 69117 Heidelberg, Germany.
[17] Department of Physics and Astronomy, University of California, Irvine, CA.
[18] Center for Astrophysics and Space Sciences, University of California at San Diego, La Jolla, CA.
[19] Space Sciences Laboratory, University of California, Berkeley, CA .
[20] Space Science Institute, Boulder, CO.
[21] Department of Physics and Astronomy, Washington State University, Pullman, WA.

1. INTRODUCTION

Astrometry is perhaps the most fundamental and oldest of all areas in astronomy, and it remains a cornerstone of the field for the 21st century. Accurate distances to astronomical objects are essential for deriving fundamental quantities like mass and luminosity. Photographic astrometry in the 19th and 20th centuries laid the foundation for our understanding of local stellar populations by identifying the inhabitants of the solar neighborhood (Gliese 1969; Luyten 1979). The Second US Naval Observatory CCD Astrograph Catalog (UCAC2) is a CCD-based survey covering most of the sky, with accuracies of 15–70 mas, depending on brightness (Zacharias et al. 2004), and utilizing the *Hipparcos* and Tycho-2 reference frame. Recent CCD-based astrometry over narrow fields has achieved an accuracy of <1 mas in a single measurement (Pravdo et al. 2005). On still smaller scales, Lane & Muterspaugh (2004) have demonstrated $\simeq 16$ μas measurements between the components of a 0.25″ binary, using the Palomar Testbed Interferometer at 2 μm. CCD parallaxes now achieve typical errors of 0.5 mas (Harris et al. 2005). Wide-angle astrometry using ground-based optical and near-IR interferometers now reaches 20 mas (Hummel et al. 1994). In the radio range, very long-baseline interferometry (VLBI) astrometry of quasars has allowed the creation of a quasi-inertial reference frame, the ICRF (International Celestial Reference Frame; Ma et al. 1998) with wide-angle accuracy of 0.25 mas.

Space-based astrometry has brought about a renaissance in the field. The ESA *Hipparcos* mission, which operated from 1989 to 1993, yielded an astrometric catalog of 118,000 stars down to 12.5 mag, with positional accuracy of 1 mas for stars brighter than $V = 11$. The European Space Agency (ESA) is now developing the *Gaia* mission as a next-generation astrometric survey mission (Perryman et al. 2001; Perryman 2002), and it is expected to develop a catalog of $\sim 10^9$ stars, with accuracy $\simeq$20–25 μas for stars brighter than $V = 15$.

In this paper, we present an overview of the impact of precision astrometry in many fields of astrophysics. We use NASA's *Space Interferometry Mission PlanetQuest* mission, hereafter *SIM*, as a specific example of a space-based facility instrument for astrometry. This mission has been under active development since 1996, based on concept studies made several years earlier (Shao 1993). A major objective of this paper is to show how microarcsecond-level astrometry is a powerful tool for 21st century astronomy. There are observing opportunities for new experiments with *SIM*, and this paper is intended as a resource for astronomers using precision astrometry in their research. Although presented in the context of the specific capabilities inherent to the *SIM* design, the topics represent very clearly the impact across many areas of astronomy in which precision astrometry plays a fundamental role. Most of the science investigations described here are drawn from the key projects of the *SIM* Science Team, which was selected via a NASA Announcement of Opportunity in 2000 (Unwin 2005 and references therein). The *SIM* Science Team members are coauthors on this paper.

Recommended by the 1990 NRC Decadal Survey (Bahcall 1991), *SIM* entered its formulation phase (Phase A) in 1997 October and was approved to enter Phase B in 2003 August. *SIM* was again endorsed by the 2000 NRC Decadal Survey (McKee & Taylor 2001) wherein it was assumed that *SIM* would be completed, making it unnecessary to rank it against new mission recommendations in that report. Technology development was completed in 2005 July and formally signed off by NASA Headquarters in 2006 March after extensive external independent review. Having completed nearly all of the formulation phase (Phase A/B), *SIM* is ready to enter the Implementation Phase, with mature designs, well-understood schedule and cost, and low technical and cost risk. Unfortunately, there is no official launch date, since budget pressures on NASA's Science Mission Directorate have resulted in NASA's delaying the implementation phase.

This paper covers the expected science contributions of *SIM* but does not describe any of the technical details of the instrument or mission. Brief descriptions of the instrument itself and the supporting technologies may be found in several technical papers (Laskin 2006; Marr 2006; Shao 2006). A companion paper (M. Shao & B. Nemati 2008, in preparation) explains the *SIM* instrument design, operation, performance, and calibration in more detail. The astrometric performance of *SIM* is based on an hierarchical error budget with more than 1000 terms, and with key sets of parameters verified in a series of testbeds developed during the formulation phase. Quoted performance numbers are current best estimates from the error budget and detailed instrument design.

As noted above, *SIM* stands for *Space Interferometry Mission*. *SIM* will be the first space-based Michelson interferometer for astrometry. The instrument will operate in the optical waveband using a 9 m baseline between the apertures. With a global astrometry accuracy of 3 μas for stars brighter than $V = 20$, it will measure parallaxes and proper motions of stars throughout the Galaxy with unprecedented accuracy. Operating in a narrow-angle mode, it will achieve a positional accuracy of 0.6 μas for a single measurement, equivalent to a differential positional accuracy at the end of the nominal 5 yr mission of ≤ 0.1 μas. This performance is about 1000 times better than existing capabilities on the ground or in space, and about 100 times better than the upcoming *Gaia* mission, for differential measurements. Such high accuracy will allow *SIM* to detect and measure unambiguous masses of terrestrial planets around stars in our Galactic neighborhood.

SIM is a targeted mission that measures the astrometric positions of stars, referencing the measurements to a grid of 1302 stars covering the entire sky. Its scheduling is highly flexible in the order of observations, their cadence, and the accuracy of each individual measurement. This contrasts with the *Hipparcos* and *Gaia* missions, which scan the entire sky according to a

predetermined scanning pattern. Many astrometry experiments can make effective use of, or in some cases require, this pointing capability—for instance, searches for terrestrial planets (especially in multiple-planet systems), stellar microlensing events, orbits of eccentric binary systems, and variable targets such as X-ray binaries and active galactic nuclei. Currently, the ICRF, defined by the locations of 212 extragalactic radio sources (Johnston et al. 1995; Ma et al. 1998) with most having errors less than 1 mas, is the standard frame for astrometry. *SIM* is expected to yield an optical reference frame at a level of about 3 μas; it will be "tied" to the ICRF by observing a number of radio-loud quasars in common.

This paper is divided into a number of sections, each covering a major area of *SIM* astrophysics. In § 2 we show how *SIM* can be used to search a large sample of nearby solar-type stars for Earth-like planets orbiting in the "habitable zone," and to take a planetary census of an even larger population of stars with a variety of spectral types, ages, and multiplicities. Section 3 describes a search for planetary systems around young stars with ages of 1–100 Myr, which will provide knowledge of the evolutionary history of planetary systems. In § 4 we explore how combining *SIM* with existing data sets extends our sensitivity to long-period planets and allows a very complete picture of planetary systems to be made. Section 5 shows how microarcsecond astrometry allows us to make fundamental advances in understanding the stellar mass-luminosity relation. In § 6 we show that *SIM* contributes to a range of problems dealing with the physics of "exotic" stellar objects such as neutron stars and black holes, and stars with circumstellar maser emission.

Sections 7, 8, and 9 cover stellar evolution, Cepheids, and the luminosity-age relation in globular clusters and constraints on the ages of clusters and the Galaxy. Section 10 explores the dynamics and evolution of our Galaxy using tidal streams, and § 11 explains how astrometric microlensing provides insight into the mass spectrum of dark bodies in the Galaxy. Sections 12 and 13 cover astrometric studies of the dynamical properties of our Galaxy, galaxies out to 5 Mpc, and the structure and properties of active galactic nuclei. In § 14 we present an application of *SIM* astrometry to cosmology. Section 15 describes how *SIM* will be able to make high dynamic range and high angular resolution images using the technique of aperture synthesis. In addition to its scientific significance, such data represent a demonstration of the future of high-resolution optical/IR imaging in space, similar to the way that the NRAO VLA[22] revolutionized ground-based radio imaging in the late 1970s. In § 16 we discuss a fundamental physics experiment with *SIM*.

Astrometric measurement techniques that support the science objectives are covered in the appendices. Appendix A discusses *SIM*'s "narrow-angle" precision astrometry mode, which is used for discovering planets around other stars and measuring their masses, as well as other science. In Appendix B we show how *SIM* measurements of "grid stars" are used to construct an astrometric reference frame for wide-angle astrometry, and how these measurements are tied to an inertial reference frame defined by ICRF quasars (Appendix C). Defining a nonrotating frame to high precision is essential for some of the science described in this paper. Appendix D explains the astrophysical criteria used to select suitable stars to serve as reference objects.

We conclude the paper (§ 17) with a recap of the major science areas, and an indication of new areas where the implications of microarcsecond-accuracy astrometry have yet to be explored in detail. This paper may serve as a guide to those interested in using precision astrometry to help further their research interests. *SIM* is a facility instrument, and opportunities will exist for the science community to propose new experiments. About half of the total observing time is assigned to the Science Team, but the remaining time is open and is not yet allocated. To assist researchers, § 17 includes a table showing the overall assignment of mission time, including open time for new programs.

2. THE SEARCH FOR POTENTIALLY HABITABLE PLANETS

Greek philosophers Epicurus, Metrodorus of Chios, and Lucretius pondered the possibility that many worlds like Earth existed. Aristotle and Plato argued that our world was unique. We are now in a position to resolve this 2400 year debate with NASA space missions such as *Kepler*, *SIM*, and the *Terrestrial Planet Finder* (*TPF*). *SIM* measures three key characteristics of a planet (1) its mass, (2) the size and shape of its orbit (semimajor axis and eccentricity), and (3) the inclination of its orbit—if there are multiple planets, this will tell if their orbits are coplanar. The planet's mass and orbit determine whether it can retain an atmosphere, develop a molten core and protective dynamo-generated magnetic field, and harbor oceans of liquid water. Such planet characteristics are believed to play vital roles in the formation and evolution of organic life.

Since 1995, over 200 exoplanets have been discovered, most by using the Doppler technique to monitor the gravitationally induced radial-velocity (RV) "wobble" induced by a planet (Marcy et al. 2005). Precise knowledge of the orbits and minimum planet masses are given in the *Catalog of Nearby Exoplanets* (Butler et al. 2006), which provides the physical and observational properties of known exoplanets orbiting within 3 AU. Twenty multiplanet systems have been discovered, spawning theoretical studies of the interactions between planets, their nascent protoplanetary disks, and other planets (Ford 2005; Ida & Lin 2005; Kley et al. 2005; Alibert et al. 2005; Chiang & Murray 2002; Tanaka & Ward 2004).

[22]The VLA is operated by the National Radio Astronomy Observatory, which is a facility of the National Science Foundation, operated under cooperative agreement by Associated Universities, Inc.

Most exoplanets found so far are gas giants or ice giants, with minimum masses greater than $M_{\rm Nep}$ and Jupiter-like radii gleaned from transit observations. The planet with lowest minimum mass found thus far by the Doppler technique has $M \sin i = 5.9\ M_\oplus$ and a period $P = 1.94$ d orbiting the star GJ 876 (Rivera et al. 2005). This discovery demonstrated that planet formation yields masses below $10\ M_\oplus$ and motivated questions regarding the occurrence and properties of rocky planets. Indeed, the distribution of masses of the well-characterized exoplanets around nearby stars (within 200 pc) rises steeply toward lower masses, at least as fast as $dN/dM \propto M^{-1.07}$. While planet detectability in current RV surveys becomes poor for masses below the mass of Saturn, the rise toward lower masses and the correlation of exoplanets with metal abundance suggest that planets grow from rocky or icy embryos toward larger masses. Such growth suggests that rocky planets should be at least as common as the giant planets, forming from the leftover planetesimals in a protoplanetary disk (Goldreich et al. 2004; Kenyon & Bromley 2006). The observed semimajor axes span a range of 0.02–6.0 AU with a rise observed in $dN/d\log a$. This suggests that planets of terrestrial masses may also be found at a wide range of orbital distances.

Recent simulations of the giant planet-formation process (Benz et al. 2006) produce large populations of low-mass planets whose growth was halted before they could become giant planets. These planets orbit beyond 1 AU of the parent star. Their results indicate that for every currently known exoplanet there should be many "failed" giant planet cores with masses smaller than $5\ M_\oplus$. Every solar-type star may have one or two low-mass planets.

Extrapolation of the RV-discovered distribution to 10 AU and integration over the entire range of semimajor axes indicates that at least 10% of all nearby FGK stars harbor gas giants in the inner few AU. Given the wide range of masses and orbital sizes of known planets, we expect that many rocky planets will orbit between 0.1 and 2 AU, having masses above $1\ M_\oplus$, just the domain in which *SIM* is uniquely sensitive. Note that the RV technique, with a precision of $1\ {\rm m\,s^{-1}}$, cannot detect planets of $1\ M_\oplus$ orbiting near 1 AU, as the RV semiamplitude will be $\sim 0.1\ {\rm m\,s^{-1}}$. Moreover, stellar surface jitter of $1\ {\rm m\,s^{-1}}$ makes improvement in the Doppler technique unlikely. Thus *SIM* offers a unique opportunity to detect Earth analogs, planets of $1\ M_\oplus$ in the habitable zones of nearby Solar-type stars.

Gaia is expected to detect many exoplanets, but for individual observations its astrometric precision will be many times lower than that of *SIM*, so its main discovery space is that of gas-giant planets (see Fig. 1). Searching the new domain of terrestrial planets will require the precision and flexibility offered by *SIM*, which can select the number and timing of observations, along with the number of reference stars, allowing a tailored study of each target.

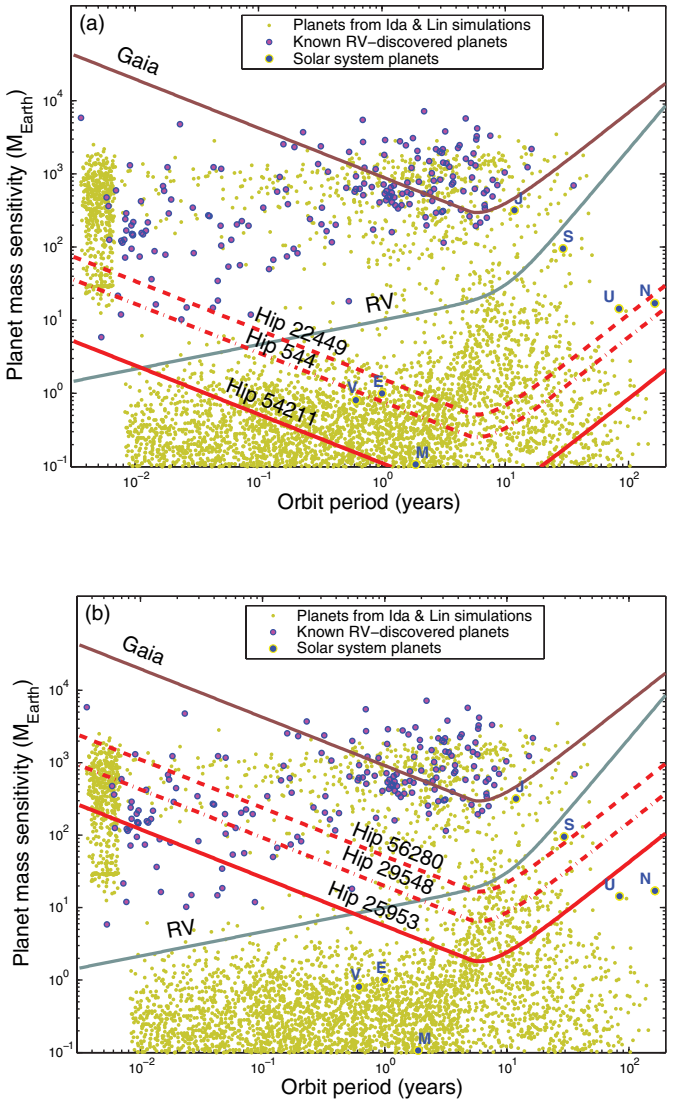

FIG. 1.—(*a*) Detailed view of the discovery space for rocky Earth-like (~1–10 $M_\oplus$) planets in the habitable zone (~0.7–1.5 AU for a G star), for the Earth analog survey of 129 stars described in § 2. The small dots represent a theoretical planet distribution (Ida & Lin 2005) for planets of 0.1–3000 $M_\oplus$. In this distribution gas giants have an envelope mass at least 10 times the mass of the central core; terrestrial planets initially formed within the ice line (2.7 AU for a solar luminosity star); icy planets formed outside the ice line; and hot Jupiters have periods ≤ 0.1 AU. Exoplanets discovered as of early 2007 and with semimajor axes > 0.03 AU are shown as filled circles. Planets in our solar system are labeled with single letters. Labeled curves represent the estimated sensitivity limits of indirect detection methods: for radial-velocity method (RV at $1\ {\rm m\,s^{-1}}$), and astrometry with *SIM* and *Gaia*. The *SIM* sensitivity in this space is a broad band, defined by the three lowest curves (labeled with specific *Hipparcos* star numbers). The lowest curve shows the "best" star (as computed from star mass and distance); the middle curve represents the median star; and the upper curve shows the least favorable star in the sample. Also shown is the effective sensitivity of *Gaia* for stars at 50 pc, a typical distance for *Gaia* targets. (*b*) Detailed view of the discovery space for the *SIM* 'Broad Survey' of 2100 stars, in which a much larger sample of stars is surveyed with less sensitivity than in the Earth analog survey. Symbols and curves have the same meaning as in (*a*).

2.1. Astrometric Detection of Terrestrial Planets

The angular wobble induced in a star by an orbiting planet is given by

$$\alpha = 3.00 \frac{M_\odot}{M_*} \frac{M_\mathrm{p}}{M_\oplus} \frac{a}{1\ \mathrm{AU}} \frac{1\ \mathrm{pc}}{D}\ \mu\mathrm{as}, \tag{1}$$

where α is the angular semiamplitude of the wobble in μas, M_p is the mass of the planet, M_* is the mass of the star, a is the orbital semimajor axis, and D is the distance to the system.

SIM's narrow-angle observing mode will allow for a single astrometric measurement precision of 0.6 μas for stars brighter than $V = 7$. Narrow-angle astrometry of each target star will be made relative to at least three reference stars selected to evenly surround the target star within 1.5°. The reference stars are K giants brighter than $V = 10$, within roughly 600 pc, so that the astrometric "noise" due to orbiting planets is minimized. RV observations prior to launch will detect brown-dwarf and stellar companions of the reference stars (Frink et al. 2001). A ten-chop sequence between a target and a reference star, with 30 sec integrations per chop, will achieve 0.85 μas differential measurement precision for $V = 7$ stars, including instrumental and photon-limited errors; this is more conservative than a scenario individually optimized for each target, which delivers 0.6 μas.

It is important to clearly define what constitutes astrometric detection of a planet. In this paper, for a star of a given mass and at a given distance we define the effective mass sensitivity as the mass of a planet that *SIM* can detect with false-alarm probability (FAP) of 1%, and a detection probability of 50%. Effective mass sensitivities can be determined for lists of actual planet-search target stars using Monte Carlo simulations of detection of stellar reflex motion due to Keplerian planet orbits. Effective mass sensitivity provides a good metric of *SIM*'s planet-finding capability for a given target star, because it depends only on assumptions about the *SIM* instrument and the known characteristics of target stars, without assumptions about the poorly known properties of the planets under study, e.g., their mass distribution, semimajor-axis distribution, and frequency of occurrence.

SIM's capability of detecting planets orbiting in the habitable zones of nearby stars for several hypothetical planet surveys has been investigated in detail by Catanzarite et al. (2006). In their simulations, each target was allocated the same amount of observing time. In this section we present a different approach, in which each target star is searched to a specific mass sensitivity. Thus the simulated observing program computes observing time based on the mass and distance of each star individually. This takes advantage of recent Microarcsecond Metrology (MAM) testbed results at JPL, indicating that *SIM*'s systematic noise floor is below 0.1 μas after many repeated measurements, opening up the possibility of detecting sub–Earth-mass planets around the closest stars. The current best estimate of *SIM*'s single-measurement accuracy is 0.6 μas. Both the number of "visits" during the 5 yr mission (nominally ~100 1D measurements in each of two orthogonal baseline orientations) and the spacing of those visits, are flexibly scheduled, allowing follow-up of the most interesting targets during the mission. Approximately 40% of *SIM*'s 5 yr mission time is available for planet searching in narrow-angle mode.

2.2. The Lowest-Mass Planets Detectable by *SIM*

The threshold planet mass detectable by *SIM*, for a given orbital radius around a star of given mass and distance, can be estimated in several ways. Sozzetti et al. (2002) used a χ^2-based test of the null hypothesis for detection. They derived a detection threshold of $S = 2.2$, where S is the "scaled signal," the ratio of the angular radius of the astrometric wobble and the astrometric measurement accuracy. This criterion has been widely quoted in the planet-search community. It is, however, overly simplistic to deem a planet detectable only if the amplitude of the angular wobble is greater than the astrometric measurement accuracy. Such an estimate fails to account for both the advantage of large numbers of observations, N_obs, and for the temporal coherence of the orbital position.

In our own Monte Carlo study (Catanzarite et al. 2006), planet detection is accomplished by using a *joint periodogram*, the sum of the periodogram power in the astrometric measurements along two orthogonal baseline directions, after fitting out a model of position offset, proper motion, and parallax. From the simulations we derive and validate a more appropriate planet detectability criterion.

We define SNR as the ratio of the angular wobble to the standard error of the observation:

$$\mathrm{SNR} = \frac{\alpha}{\sqrt{2}\sigma/\sqrt{N_\mathrm{2D}}} \tag{2}$$

where N_2D is the number of two-dimensional measurements, σ is the single-measurement accuracy, and the factor of $\sqrt{2}$ is inserted because the measurement is differential. *SIM* measurements are one-dimensional; each target is measured and then reobserved within a day or so with a baseline orientation that is quasi-orthogonal to that of the first measurement. So the number of two-dimensional measurements is half the number N of 1D measurements. Replacing N_2D with $N/2$, we have

$$\mathrm{SNR} = \frac{\alpha\sqrt{N}}{2\sigma} \quad \text{or} \quad \mathrm{SNR} = 0.5S\sqrt{N}, \tag{3}$$

in terms of the scaled signal S. It is the SNR rather than "scaled signal S" which properly determines detectability; we find that a planet with a SNR of 5.4 is detectable half the time at the 99% confidence level. With 200 observations, our detectability criterion is equivalent to $S = 0.76$, a factor of 3 below that quoted in Sozzetti et al. (2002). With 200 observations at 0.85 μas differential accuracy, *SIM* achieves mass sensitivities of $\approx 0.2\ M_\oplus$ at the midhabitable zones of the nearest few targets.

To illustrate the detection process we show in Figure 2 how the joint periodogram, by simultaneously using data from the two orthogonal baseline directions, is able to reliably detect a planet in the low signal-to-noise regime where a simple χ^2 test would reject it.

2.3. *SIM* Planet Surveys

Discovery and characterization of many Earth-like planets is one of *SIM*'s most important scientific objectives. Up to half of the *SIM* observing time will be devoted to three planet surveys, each with distinct science objectives:

1. A "deep survey" of up to several hundred stars located within 30 pc, for the lowest-mass planets detectable by *SIM*. The Deep Survey is expected to yield a significant number of Earth-like planets.

2. A "broad survey" of ~2100 stars over a variety of spectral types, ages, and multiplicities, for planets with masses of a few $M_\oplus$ and greater. It will explore the diversity of planetary systems, providing a more complete picture of planetary systems than is possible with, say, RV or direct imaging surveys alone.

3. A "young planet survey" of ~200 stars with ages in the range 1–100 Myr. This survey, when combined with the results of planetary searches of mature stars, will allow us to test theories of planetary formation and early solar-system evolution.

In this section we discuss the objectives of the deep durvey and broad survey. See § 3 for details of the young planet survey.

The most effective observing strategy for detecting low-mass planets will depend on the fraction of stars expected to have terrestrial planets ($\eta_\oplus$). We expect results from the *Kepler* mission (planet detection via transits) to inform that strategy. The basic argument is simple: if Earths are rare, then *SIM* should concentrate on a larger sample of hundreds of stars to get as much information on as many systems as possible. If, on the other hand, terrestrial planets are common, we would like to probe as many systems as possible for potentially habitable planets. With this goal in mind, it makes sense to search each target to the same mass sensitivity, instead of measuring each target to the same accuracy, as was adopted in our previous work (Catanzarite et al. 2006).

To emphasize this "mass-limited" approach to the search, we term this survey the "Earth analog survey". We allocate to each target enough integration time to allow a planet of 1 $M_\oplus$ to be detected at the radius of its midhabitable zone (as determined from its spectral type). We find that with an assignment of 40% of a 5 yr mission, and a single-measurement accuracy of 0.6 μas, *SIM* can probe the midhabitable zone of 129 stars for 1.0 $M_\oplus$ planets (Table 1). Essentially, one can regard this as the survey yield for the idealized case of δ-function distributions for planet mass and planet orbit radius (1 $M_\oplus$ at 1 AU for a G2V star). Although unrealistic, this measure of performance avoids having to make assumptions about the distributions. (In § 2.4 below, we show a second simulation of the planet yield, this time basing it on distributions from A. Cumming G. W. Marcy & R. P. Butler (2008, in preparation).

The discovery space (planet mass vs. orbit radius) for the Earth analog survey is shown in Figure 1*a*, with the 129 stars filling a band in the lower portion of the plot. Distributing the observing time over a larger target list allows one to detect more terrestrial planets, albeit at higher masses. Table 1 shows the expected *SIM* yield for three different values of the search depth. A survey to a sensitivity of 3 $M_\oplus$ would encompass more nearby stars than would likely be observed by the *TPF* mission. In each survey, the mass sensitivity improves with orbit radius, out as far as orbits with periods $\lesssim$5 yr (see Fig. 1*a*). Note that these surveys are intended to be illustrative; at the time of *SIM* launch, the best available data from all sources will be used to design a survey which might represent a combination of the approaches in Table 1.

In the broad survey, *SIM* will probe 2100 stars for planets. As its name implies, this planetary census includes stars of all spectral types (including O, B, A, and early F, which are not accessible to RV measurements), binary stars, stars with a broad range of age and metallicity, stars with dust disks, evolved stars, white dwarfs, and stars with planets discovered with RV surveys. Each class addresses specific features of the planet-formation process: *Are metals necessary for giant planet formation? Does the number of planets decline slowly with time due to dynamical evolution? What is the relation between dust disks and planets?*

Using about 4% of a 5 yr mission, each star will be measured 100 times at 4 μas per measurement. Figure 1*b* shows the discovery space for the broad survey, which is expected to yield a large sample of hot, cold, rocky, ice-giant and gas-giant planets, as well as multiple-planet systems for tests of planet-formation theories. Orbit solutions will determine masses and inclinations, and elucidate planetary system architecture for multiple-planet systems.

SIM's discoveries will complement future exoplanet missions. *SIM* will complete the planetary system architecture for stars with planets identified by *Kepler* and *COROT*. Where *Kepler* and *COROT* find the rocky planets *SIM* will find the gas-giant planets. Furthermore, it will provide high quality parallaxes (and thus accurate angular diameters) of stars around which planets have been detected by transits. *SIM* resolves the uncertainty in determining planetary orbit radii from transits. *SIM* determines the orbit, so that it can provide the time-dependent location of the planet in the sky, which is critical for any follow-up program, such as *TPF*.

2.4. Expected Planet Yields for *SIM* Surveys

We estimate the likely yield of planets from *SIM* observations under plausible assumptions regarding their frequency of occurrence and distributions as a function of mass and orbit radius. Tentative target lists have been selected for the survey of nearby main-sequence stars (Marcy et al. 2005; Shao 2006). Our

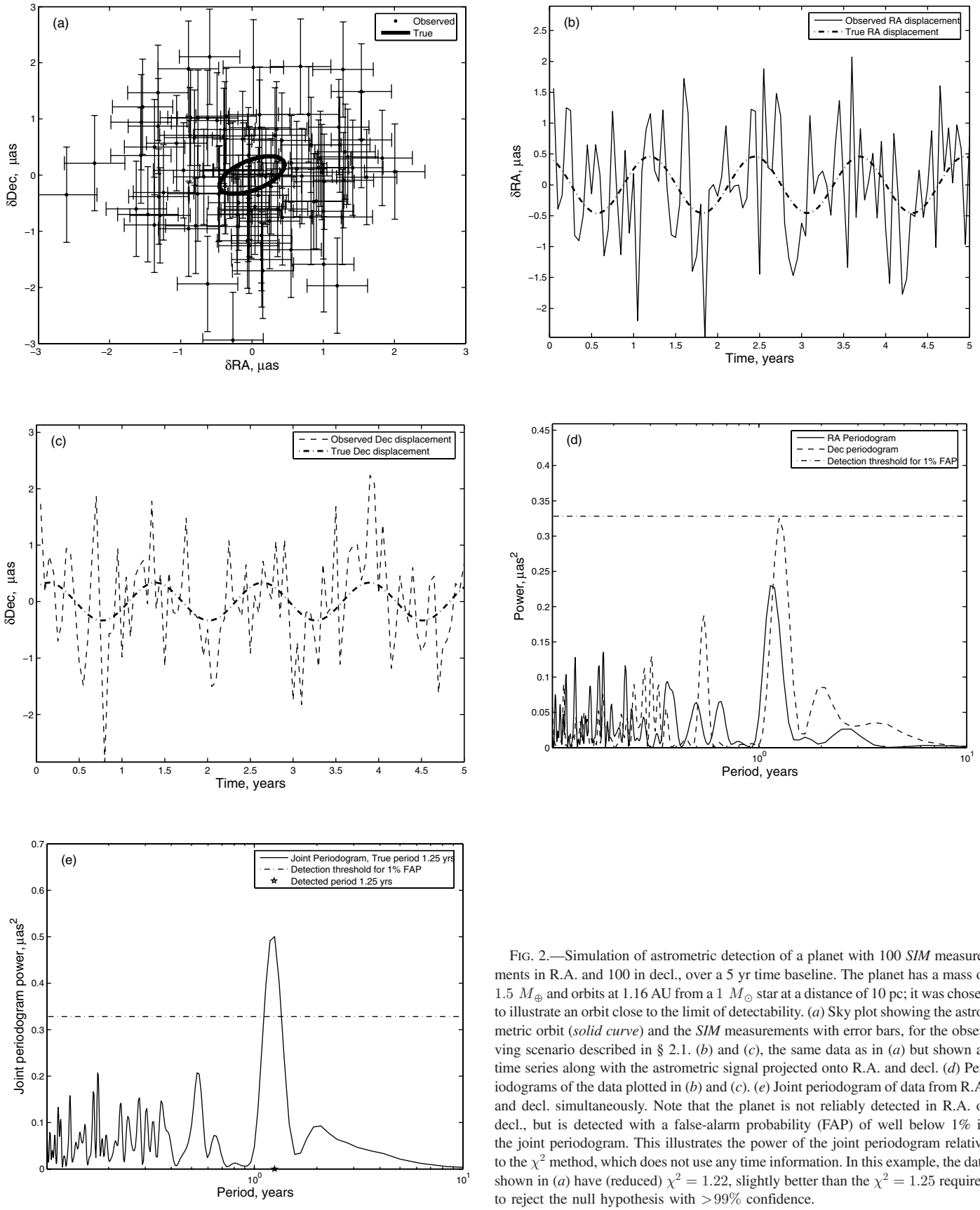

FIG. 2.—Simulation of astrometric detection of a planet with 100 *SIM* measurements in R.A. and 100 in decl., over a 5 yr time baseline. The planet has a mass of $1.5\ M_{\oplus}$ and orbits at 1.16 AU from a $1\ M_{\odot}$ star at a distance of 10 pc; it was chosen to illustrate an orbit close to the limit of detectability. (*a*) Sky plot showing the astrometric orbit (*solid curve*) and the *SIM* measurements with error bars, for the observing scenario described in § 2.1. (*b*) and (*c*), the same data as in (*a*) but shown as time series along with the astrometric signal projected onto R.A. and decl. (*d*) Periodograms of the data plotted in (*b*) and (*c*). (*e*) Joint periodogram of data from R.A. and decl. simultaneously. Note that the planet is not reliably detected in R.A. or decl., but is detected with a false-alarm probability (FAP) of well below 1% in the joint periodogram. This illustrates the power of the joint periodogram relative to the χ^2 method, which does not use any time information. In this example, the data shown in (*a*) have (reduced) $\chi^2 = 1.22$, slightly better than the $\chi^2 = 1.25$ required to reject the null hypothesis with $>99\%$ confidence.

TABLE 1
PLANET MASS-LIMITED SURVEYS WITH *SIM*

	Mass sensitivity	Number of stars surveyed
Survey 1	1.0 $M_\oplus$	129
Survey 2	2.0 $M_\oplus$	297
Survey 3	3.0 $M_\oplus$	465

NOTES.—In a mass-limited survey, observing time on each star is calculated to yield the given mass sensitivity for a planet at the center of the habitable zone, computed from the star's distance, estimated mass, and spectral type (see § 2.3). Stars are rank-ordered in observing time, and the resulting number of stars that can be surveyed to a given mass sensitivity is shown as a function of planet mass, for three different sensitivity levels.

simulations use actual star lists, since catalogs of nearby stars are almost complete, except for late-type stars (Duquennoy & Mayor 1991). Target lists for the simulations are derived from an initial list of 2350 stars taken from the *Hipparcos* catalog, with distances of less than 30 pc (Turnbull & Tarter 2003). We excluded stars with luminosity greater than 25 $L_\odot$, thereby eliminating giants from our sample. To eliminate the possibility of fringe contamination from a binary companion, we applied the following selection rules: stars with a companion closer than 0.4″ were excluded; for stars with a companion that was separated by 0.4″ to 1.5″, both were included as target-star candidates if the magnitude difference was >1; otherwise, both companions were excluded. If the target-star candidate had a wide binary companion that was separated by more than 1.5″, the companion was added to the list of target-star candidates. Surviving candidates were rank-ordered by effective mass sensitivity.

Although the sensitivity for planet detection at each target is of primary significance in assessing the capability of any proposed planet survey, it is also important to understand the yield: how many planets we do we expect to find and what is their expected mass distribution? As discussed in § 2.3, planet detection sensitivity may be derived from knowledge of instrument performance, the target list, the observing scenario, and the available observation time for each star. To predict the expected survey yield requires knowledge (or plausible assumptions) of mass and orbit distributions of planets and their occurrence frequency, for solar-type stars.

Discoveries from the golden age of RV surveys (Butler et al. 2006) have given us robust knowledge of planetary statistics for orbits out to 3 AU and masses down to a few Saturns. But the surveys are incomplete for planets on more distant orbits; and though a handful of planets with masses in the terrestrial range have been discovered, these are in very close-in orbits. Though RV is advancing toward detection of Earth-mass planets orbiting M stars, terrestrial planets in the habitable zones of solar-type stars will remain beyond its capability, except possibly for a handful of nearby stars with extremely low variability such as α Cen B. On the other hand, information on orbital and mass distributions and occurrence frequency of terrestrial planets around Sun-like stars will be forthcoming from the *Kepler* mission in a few years; and *COROT* will very soon yield statistics of Neptune-class planets.

At this time we can only estimate planetary statistics in the terrestrial-mass regime by extrapolation from observational results and the expectations of planet-formation theorists. To this end we created a simple hybrid model based on the power-law mass and period distributions derived from the RV observational data, obtained from surveys of solar-type stars (A. Cumming, G. W. Marcy & R. P. Butler 2008, in preparation). For simplicity, in our model we assume that each star has a maximum of one planet. We extrapolated these power laws to orbits out to 10 AU, and to masses down to the terrestrial-mass regime. To account for the prevalence of "failed cores" expected by many theorists (e.g., Ida & Lin 2005), we increased the occurrence frequency of terrestrial planets by a factor of 5. The model distributions are depicted graphically in Figure 1. Some recent studies suggest that the planet occurrence rate is lower in low-mass stars (Butler et al. 2004, 2006; Endl et al. 2006; Johnson et al. 2007), and Gould et al. (2006) deduce that about a third of low-mass stars may have cold Neptunes, whereas extrapolation from A. Cumming, G. W. Marcy & R. P. Butler (2008, in preparation) indicates that only 5% of solar-type stars have Neptunes at all separations.

Our hybrid power-law model has the following properties for solar-type stars: 73% of stars have terrestrial-mass planets (0.3–10 $M_\oplus$); $\simeq$10% of stars have terrestrial-mass planets in the habitable zone (0.7–1.5 AU); 5% of stars have Neptune-class planets (10 $M_\oplus$ to 0.1 $M_{\rm Jup}$); and 16% of stars have Jupiter-class planets (0.1–10 $M_{\rm Jup}$). According to this model, the overall occurrence frequency of planets is 95%. Our predictions of Neptunes and Jupiters are probably close to reality, since they involve little extrapolation from observational data, but the terrestrial-mass planet prediction is sensitive to our extrapolation.

Using this hybrid power-law model, we estimate planet yields for the Earth analog and broad surveys via Monte Carlo simulation. For each survey target star we generate 1000 planets, with masses and periods drawn randomly from the model described above. For each planet we generate a circular orbit, with parameters other than mass and period randomized. We calculate the reflex motion trajectory of each target star due to its planet, and sample it 100 times uniformly over a time baseline of 5 yr. This results in a time series of 100 pairs of simulated right ascension and declination true star positions. This database of planets and orbits is then stored away. Next we create 1000 "sky realizations"; each realization results from assigning to 95% of the target stars a planet randomly drawn from the database; according to the statistics of our model, 5% of the targets have no planet. Finally, we generate a simulated survey for each sky realization by perturbing each stellar reflex motion trajectory with parallax, and single-measurement error of 0.6 μas. We

preprocess the simulated observational data by fitting out a model of position, parallax, and proper motion, running the fit residuals through the joint periodogram (see § 2.2) with the detection threshold set to allow only a 1% chance of false detections. Each simulated survey therefore has a set of "input" planets, and for each a subset of those are detected with *SIM*. The most useful representation of the results are histograms of the ensemble averages of input and detected masses for the simulated surveys and planets.

Figure 3*a* shows the expected histogram for input versus detected terrestrial planet masses in the Earth analog survey. The histogram shows fractional counts because it is a mean over 1000 simulated surveys. Results for the complete range of planet masses are shown in Table 2. In the habitable zone, *SIM* would detect 61% of all the terrestrial planets, including almost half of all planets with masses in the range 1–1.5 $M_{\oplus}$, and nearly every planet of higher mass.

We repeated the methodology described above, with the same hybrid power-law distributions for the input planets, on the *SIM* broad survey of 2100 stars. In Figure 3*b* we show the mean of the mass histograms (logarithmic mass bins extending over entire mass range) for 1000 simulated surveys. Table 3 shows that we expect *SIM* to find 7% of the terrestrial planets, 2% of all terrestrial planets in the habitable zone, 47% of the Neptune-class planets, and 87% of the Jupiter-class planets.

It is important to realize that the planet yields predicted by these simulations depend on many parameters, e.g., the *SIM* single-measurement accuracy, the observing scenario and time devoted to each target, the mass and orbit radius distributions of the planets, and, of course, the frequency of occurrence of those planets. In particular, we note that the fractions of habitable-zone terrestrial planets that are input to the simulations are different in Tables 2 and 3, due to different characteristics of the survey stars. The broad survey target list includes a larger number of low-mass stars; about half have masses $< 0.5\ M_{\odot}$. Though our hybrid power-law model is derived from observations of solar-type stars, we have assumed that it also applies to low-mass stars. One feature of the model is that there is a decrease in the number of planets per dex as the orbit radius becomes smaller than about 0.7 AU. Since the habitable zones of low-mass stars are entirely within 0.7 AU, these stars will accordingly have fewer habitable-zone planets than solar-type stars, and this is reflected in the tables.

To summarize, *SIM* will be capable of detecting a significant fraction of the expected population of planets for a large sample of stars within 30 pc. As the first planned instrument capable of detecting terrestrial planets around nearby stars, *SIM*'s planet yield will in fact test the degree to which the above model assumptions are valid. *SIM*'s scientific discoveries will likely reveal the erstwhile hidden regime of rocky planets, and make possible the first thorough checks of the predictions of current theories of planet formation.

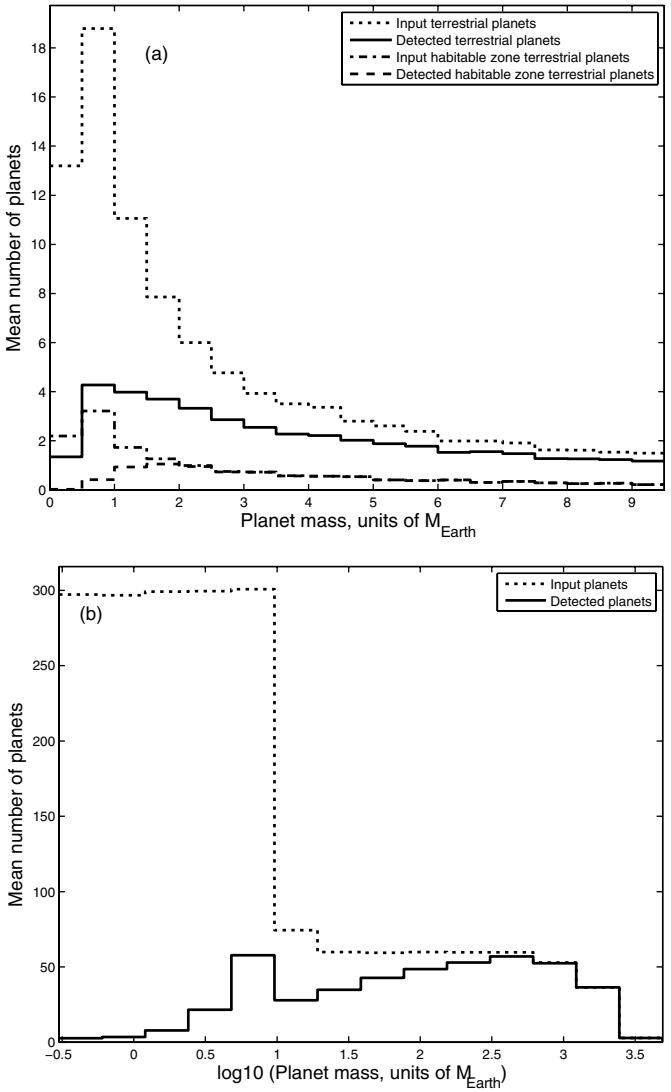

FIG. 3.—(*a*) Histogram of the expected yield of terrestrial planets for the *SIM* Earth analog survey observing program and assumed planetary orbit and mass distributions, and a normalized planet occurrence rate, described in § 2.4. This histogram is a mean of 1000 simulated surveys in which geometric parameters of the model orbits were randomized. The mean input distribution of terrestrial ($M < 10\ M_{\oplus}$) planets is shown as the dotted curve, and the mean number of terrestrial planets detected in the survey by *SIM* as the solid curve. For terrestrial planets in the habitable zone only, the corresponding curves are shown as dash-dotted and dashed lines, respectively. The integral planet counts are summarized in Table 2. Note that the yield of planets, especially at the low-mass end, depends sensitively on both the assumed planetary model parameters and the observing strategy. (*b*) The same as in (*a*) but for the 2100 star broad surve', which includes stars spanning the entire main sequence. This survey would discover planets over a wide range of masses and orbit radii that are largely unexplored by other detection methods. The integral planet counts are summarized in Table 3.

2.5. Physical Parameters of Habitable Planets

SIM will provide a wealth of planetary astrophysics, including the masses, orbital radii, and orbital eccentricities of rocky

TABLE 2
EXPECTED YIELD OF *SIM* EARTH ANALOG SURVEY OF 129 STARS

Planet type	Number detected	Total number in sample	Fraction detected
Terrestrial, 0.3 to 10 $M_\oplus$	43.0 ± 5.0	94.0 ± 5.1	0.46
Terrestrial (habitable zone)	9.6 ± 2.9	15.7 ± 3.7	0.61
Ice giant, 10 $M_\oplus$ to 0.1 $M_{\rm Jup}$	5.3 ± 2.2	6.1 ± 2.4	0.87
Gas giant, 0.1 to 10 $M_{\rm Jup}$	21.1 ± 4.2	21.3 ± 4.3	0.99

NOTE.—Based on 1000 Monte Carlo survey realizations, assuming the distribution of planets from the hybrid model discussed in § 2.4.

planets around the nearest stars. It will also find correlations between rocky planets and stellar properties such as metallicity and rotation.

SIM and *TPF*/*Darwin* together, along with *Kepler*, provide a valuable combination of information about rocky planets. Each mission brings results that illuminate a different portion of the multidimensional space that represents the field of exoplanet research. *Kepler* offers the occurrence rate of small planets. *SIM* provides the masses and orbits of planets around nearby stars, identifying the candidate Earths. *TPF*/*Darwin* measures radii, chemical composition, and atmospheres. In some cases, images from *TPF*/*Darwin* may provide feedback which allows reanalysis of old *SIM* data, helping orbit determination, especially for multiple-planet systems.

Imaging surveys (such as *TPF* and *Darwin*) require lists of target stars for observation, ideally those for which rocky planets have been detected. Assuming that the fraction of stars with Earths in the habitable zone, $\eta_\oplus$, is 0.1, *SIM* will produce a list of target stars for *TPF* enriched by a factor of at least 2 in rocky planets between 0.5 and 2.0 AU relative to a *TPF*-only sample. For many of these stars, *SIM*'s orbital solution will be precise enough to predict the best timing for a direct observation. This information is crucial for direct imaging, since a planet in the habitable zone can spend much of its time hidden in the glare of the parent star. Indeed, habitable rocky planets detected by *SIM* will likely reside at angular separations of at least 100 mas from the host star. Such tantalizing rocky planets will become high priority targets for those instruments, both on the ground and in space, that can perform high-contrast imaging. With sufficiently long integration times and on-band, off-band filters, early imaging of Earth-like planets around the very nearest stars may be achieved in advance of *TPF* and *Darwin*. *SIM* will also identify those stars that *TPF* and *Darwin* should avoid, notably those with large planets near the habitable zone that render any Earths dynamically unstable. Of course, *SIM* also detects those Saturn- or Neptune-mass planets located at 2 AU, valuable in themselves for planetary astrophysics.

As a benchmark, one may assume that at least 10% of stars have a rocky planet between 0.5 and 2.0 AU. If so, *Kepler* will find them in its transit survey of stars 400–1000 pc away; and *SIM* is likely to find the first rocky planets orbiting in the habitable zones of Sun-like stars closer than 30 pc. Although no rocky planets will be detected in common between the two missions, *SIM* could detect gas giants orbiting *Kepler* target stars for which rocky planets have been detected via transits. (Multiple-planet detections by *Kepler* will likely be rare due to the very stringent coplanarity requirement.)

Detections of rocky planets will spawn theoretical work about geophysically plausible interior structures for such planets. *SIM* measures planet masses, which is *the* basic physical parameter for any planet. Imaging of Earth-mass planets around all stars within 30 pc remains beyond current technical ground-based capabilities as such planets are 10^{10} times fainter than the host star and will be 28th magnitude, comparable to the background patchwork of high-redshift galaxies. Adding to the challenge, planets in somewhat edge-on orbital planes will spend a significant fraction of the time located within the diffraction-limited angle of the host star. The next generation of space-based telescopes, represented by *TPF* and *Darwin*, will have a rich discovery space to explore. *SIM* will pave the way by conducting an inventory of rocky planets around nearby stars.

TABLE 3
EXPECTED YIELD OF *SIM* BROAD SURVEY OF 2100 STARS

Planet type	Number detected	Total number in sample	Fraction detected
Terrestrial, 0.3 to 10 $M_\oplus$	98.3 ± 9.5	1511.6 ± 20.4	0.07
Terrestrial (habitable zone)	2.4 ± 1.6	154.2 ± 12.0	0.02
Ice giant, 10 $M_\oplus$ to 0.1 $M_{\rm Jup}$	47.1 ± 6.6	99.8 ± 9.6	0.47
Gas giant, 0.1 to 10 $M_{\rm Jup}$	303.5 ± 16.6	347.4 ± 17.4	0.87

NOTE.—Based on 1000 Monte Carlo survey realizations, assuming the distribution of planets from the hybrid model discussed in § 2.4.

2.6. The Impact of Starspots on Astrometric Planet Detection

Stellar variability manifests itself in different ways in photometric, astrometric, and RV data. In this subsection we estimate the expected astrometric centroid jitter due to variability of the planet-search target stars, and assess the impact on astrometric planet detection.

The 30 yr record of satellite observations of the Sun's photometric variability shows an rms of 0.042% (Fröhlich 2006). Variations on timescales of days to decades can be attributed to the evolution and rotational modulation of magnetic surface phenomena, e.g., sunspots and faculae (Wenzler et al. 2005). In general, photometric variability in a star due to starspots introduces noise in measurements of both its photocenter and radial velocity. This noise, in turn, imposes limits on the mass of a planet detectable by these types of measurements.

To investigate the size of the effect, we developed a simple dynamic sunspot model that accurately captures the known behavior of the Sun's photometric variations in both time and frequency domains (J. H. Catanzarite, M. Shao & N. M. Law 2008, in preparation). Starspot noise has a "red" power spectral density (PSD), showing strong variation with frequency, and our model takes account of this. The important frequencies are those associated with the duration of a measurement (about an hour), the length of an observing campaign (up to a few years), and the orbital period of the planet one is trying to detect.

We used our dynamic sunspot model to characterize the jitter in the radial velocity and in the astrometric centroid. For the Sun, we find typical rms jitter of 7×10^{-7} AU in the astrometric centroid, and $0.3\ \mathrm{m\,s^{-1}}$ in the radial velocity. Because of the shape of the PSD, a simple rms does not adequately represent the noise contribution to planet detection. To gauge the impact on planet detection, we sampled the centroid and the RV signal from our sunspot model once every 11 days (100 epochs) over three years. From the PSD of the resulting time series, we found that the noise level in the centroid due to starspots is 4×10^{-7} AU for orbit periods longer than 0.6 yr, equivalent to the astrometric signal (at 10 pc) of a $0.1\ M_{\oplus}$ planet in a 1 AU orbit, and well below the sensitivity of *SIM* at this distance.

This level of centroid jitter translates (at 10 pc) to an astrometric noise of 0.04 μas, substantially below *SIM*'s noise floor of 0.085 μas achieved with 100 observations with a differential accuracy of 0.85 μas (see § 2.1). We therefore conclude that if the Sun were at 10 pc, starspot noise would not impact the astrometric detection of terrestrial planets with orbit periods longer than 0.6 yr.

RV measurements of solar-type stars are subject to variability due to starspots. The PSD in radial velocity is flat in the same region of frequencies, with a noise level of $0.2\ \mathrm{m\,s^{-1}}$, comparable to the signal of a $1\ M_{\oplus}$ planet in a 1 AU orbit. In addition, RV measurements may also be subject to astrophysical noise from other processes involving velocity field fluctuations, such as p-modes. For this reason, the estimated RV jitter due to starspots is only a lower bound to the noise in RV measurements. Astrometry is not affected by these other processes, so our dynamic starspot model is a good representation of the dominant astrophysical noise source for astrometric planet detection. A detailed discussion of our starspot simulations is forthcoming (J. H. Catanzarite, M. Shao & N. M. Law 2008, in preparation).

2.7. Detecting Multiple Planets

Of the planet-bearing stars identified by the RV technique, 20 are revealed to have multiple-planet systems, comprising 13% of the sample. Sozzetti et al. (2003) and Ford (2006) have investigated astrometric orbit fitting for multiple-planet systems. Our own simulations show that with 200 observations, *SIM* can detect and characterize systems with two or three short-period planets as long as their periods are well separated, which should be the case if they are in dynamically stable orbits. Gas-giant companions with periods longer than the mission length are hard to detect, because *SIM* would detect an acceleration but not obtain data for a closed orbit (Gould 2001). However, *SIM* can generate valuable statistical data on long-period planets, even if the periods are very uncertain, because these planets are undetectable with RV measurements and too faint for direct imaging. In intermediate cases, combined RV and astrometric data should constrain the orbits and make orbit solutions tractable (Eisner & Kulkarni 2002).

2.8. Early-Mission Detection of Planets

Precision astrometry requires knowledge of the *SIM* baseline length and orientation. A set of baseline vectors for each tile is derived as part of the astrometric grid solution. Early in the mission, the grid accuracy, and the reconstruction of baseline vectors, is relatively poor, but it improves rapidly after about 9 months of data have been taken. An observing and analysis technique termed grid-based differential astrometry (GBDA) has been developed to make effective use of early observations of planet-search targets. Details of the method are given in Appendix A. To demonstrate the GBDA approach, we modeled the detection of the planet orbiting Tau Boo, previously detected by the RV method (Butler et al. 1997). It has a Jupiter-like planet in a 3-day orbit, and an expected astrometric signature of 9.0 μas. The model shows that this planet would be readily detected, even with limited baseline knowledge from the grid. Thus *SIM* will be able to make useful detections of planetary systems very early in the mission.

3. JUPITER-MASS PLANETS AROUND YOUNG STARS

A *SIM* young planets survey, targeted toward 150–200 stars with ages from 1 to 100 Myr, will help us understand the formation and dynamical evolution of gas-giant planets. The host stars of the majority of the more than 200 exoplanets found to

date are mature main-sequence stars that were chosen based on their having quiescent photospheres for the successful measurement of small Doppler velocities (< 10 m s^{-1}). Similarly, stellar photospheres must be quiescent at the millimagnitude level for transit detections because a Jupiter-mass planet transiting a solar-type star reduces the photometric signal by about 1.4%. Since young stars have RV fluctuations or rotationally broadened line widths of *at least* 500 m s^{-1} and brightness fluctuations of many percent, optical RV measurements accurate to < 100 m s^{-1} or transit observations cannot be used to detect planets around young stars. The near-IR is more promising, and a number of groups are attempting RV observations to improve on these limits and find a few "hot Jupiters" within 0.1 AU.

A few potentially planetary mass objects have been detected at 20–100 AU from young (<10 Myr) host stars by direct, coronagraphic imaging, e.g., 2MASSW J1207334−393254 (Chauvin et al. 2005) and GQ Lup (Neuhauser et al. 2005). However, these companions are only inferred to be of planetary mass by comparison to uncertain evolutionary models that predict the brightness of young Jupiters as a function of mass and age (Wuchterl & Tscharnuter 2003; Baraffe et al. 2002; Burrows et al. 1997). Since dynamical determinations of mass are impossible for objects on such distant orbits, it is difficult to be sure that these are planets and not brown dwarfs. Nor is it even clear that the origin of these distant young Jupiters is due to the same formation processes as planets found closer. Multiple fragmentation events (Boss 2001), rather than core accretion in a dense disk (Ida & Lin 2005), may be responsible for the formation of these objects orbiting so far from their star.

As a result of the selection biases of the radial velocity, transit, and direct imaging techniques, we know little about the incidence of planets around young stars in orbits close to their stars, leaving us with many questions about the formation and evolution of gas-giant planets.

Using equation (1), a Jupiter orbiting 5.2 AU away from a 0.8 $M_\odot$ star at the distance of the youngest stellar associations (1–10 Myr) such as Taurus (140 pc) and Chamaeleon would produce an astrometric amplitude of 44 μas. At the 25–50 pc distance of the nearest young stars (10–50 Myr), such as members of the β Pic and TW Hya groups, the same system would have an astrometric amplitude in excess of 100 μas. Moving a Jupiter into a 1 AU orbit would reduce the signal by a factor of 5.2, or 50 μas for a star at 25 pc and 8 μas for one in Taurus. In its narrow-angle mode, *SIM* will have a single-measurement accuracy (SMA) of 0.6 μas (1σ); observations made during wide-angle observations (Appendix B) will have SMA $\simeq 4$ μas. Thus a search for gas giants falls well within *SIM*'s capabilities and forms the core of the *SIM*-YSO program. Figure 4 shows *SIM*'s expected astrometric accuracy for the *SIM*-YSO survey as a function of planet mass and semimajor axis. Also plotted is the expected RV accuracy achievable with present day infrared echelle spectrometers. Unlike RV surveys, *SIM* will be able to detect Jupiter-mass planets at radii out to several AU around young stars.

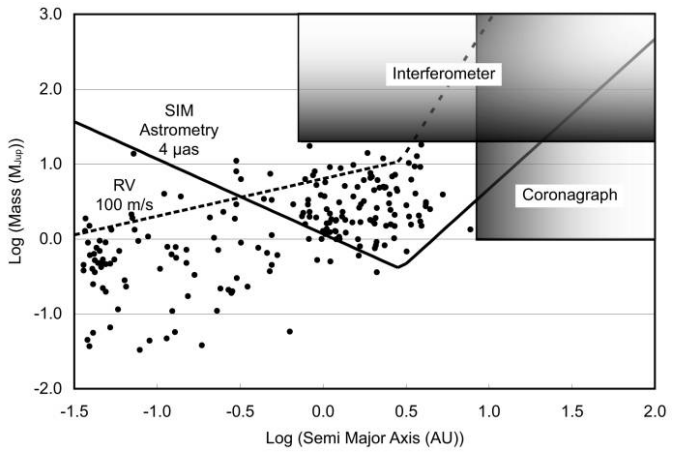

FIG. 4.—Planet mass detection sensitivity for the *SIM*-YSO survey (*solid curve*) in M_J versus orbital semimajor axis. Estimated capabilities for a large ground-based coronagraph (taken to be a diameter $d = 30$ m telescope at $\lambda = 1.6$ μm operating an angular distance of $4\lambda/d$) and a near-IR interferometer (85 m baseline at $\lambda = 1.6$ μm and an intermediate stellar distance of 50 pc) are shown as shaded boxes. Also plotted are the properties of the known RV detected planets (*dots*). RV accuracy for YSOs (*dashed curve*) is limited to about 100 m s^{-1} (§ 3). Except for RV, the sensitivity limits assume a distance of 140 pc.

3.1. Science Goals

In a *SIM* survey of 200 young stars, we expect to find anywhere from 10–20 (assuming that only the presently known fraction of stars, 5%–10%, have planets) to 200 (all young stars have planets) planetary systems. We have set our sensitivity threshold to ensure the detection of Jupiter-mass planets in the critical orbital range of 1 to 5 AU. These observations, when combined with the results of planetary searches of mature stars, will allow us to test theories of planetary formation and early solar-system evolution. By searching for planets around pre–main-sequence stars carefully selected to span an age range from 1 to 100 Myr, we will learn at what epoch and with what frequency giant planets are found at the water-ice "snowline" where they are expected to form (Pollack et al. 1996). This will provide insight into the physical mechanisms by which planets form and migrate from their place of birth, and about their survival rate.

With these *SIM* observations in hand, we will have data, for the first time, on a series of important questions: What processes affect the formation and dynamical evolution of planets? When and where do planets form? What is the initial mass distribution of planetary systems around young stars? How might planets be destroyed? What is the origin of the eccentricity of planetary orbits? What is the origin of the apparent dearth of companion objects between planets and brown dwarfs seen in mature stars? How might the formation and migration of gas-giant planets affect the formation of terrestrial planets?

Our observational strategy is a compromise between the desire to extend the planetary mass function as low as possible and the essential need to build up sufficient statistics on planetary occurrence. About half of the sample will be used to address the "where" and "when" of planet formation. We will study classical T Tauri stars (cTTs), which have massive accretion disks, as well as post-accretion, weak-lined T Tauri stars (wTTs). Preliminary studies suggest the sample will consist of ~30% cTTs and ~70% wTTs, driven in part by the difficulty of making accurate astrometric measurements toward objects with strong variability or prominent disks. The second half of the sample will be drawn from the closest young clusters with ages starting around 5 Myr, to the 10 Myr thought to mark the end of prominent disks, and ending around the 100 Myr age at which theory suggests that the properties of young planetary systems should become indistinguishable from those of mature stars. The properties of the planetary systems found around stars in these later age bins will be used to address the effects of dynamical evolution and planet destruction (Lin et al. 2000). Since we will also measure accurate parallaxes, we will have good luminosities for the host stars, and will use these to help estimate ages.

3.2. Astrophysical Noise

The photospheric activity that affects radial velocity and transit measurements affects astrometric measurements, but, as we will now show, at a level consistent with the secure detection of gas-giant planets. From measurements of photometric variability (Bouvier & Bertout 1989; Bouvier et al. 1995) plus Doppler imaging (Strassmeier & Rice 1998), T Tauri stars are known to have active photospheres with large starspots covering significant portions of their surfaces (Schussler et al. 1996) as well as hot spots due to infalling accreting material (Mekkaden 1998). These effects can produce large photometric variations which can significantly shift the photocenter of a star. Using a simple model for the effect of starspots on the stellar photocenter (Tanner et al. 2007), for a typical T Tauri star radius of $3R_{\odot}$ we see that the astrometric jitter is less than 3 μas for R-band variability less than 0.05 mag. Thus, the search for Jovian planets is plausible for young stars less variable than ~0.05 mag in the visible even without a correction for jitter that may be possible using astrometric information at multiple wavelengths. Note that since both the astrometric signal and the astrometric jitter scale inversely with distance, there is no advantage (from the jitter standpoint) to examining nearby stars even despite their larger absolute astrometric signal. Other astrophysical noise sources, such as offsets induced by the presence of nebulosity and stellar motions due to nonaxisymmetric forces arising in the disk itself, are negligible for appropriately selected stars. Finally, it is worth noting that searching for terrestrial planets will be difficult until stars reach an age such that their photometric variability falls below 0.001 mag and the corresponding astrometric jitter below 0.5 μas.

3.3. The Sample

The youngest stars in the sample will be located in well-known star-forming regions such as Taurus, the Pleiades, Scorpius-Centaurus and TW Hydra (Tanner et al. 2007) and will be observed in narrow-angle mode, which is capable of achieving a single-measurement accuracy of 0.6 μas. Somewhat older stars, such as those in the β Pictoris and TW Hydrae Associations, are only 25–50 pc away and can be observed with less mission time in wide-angle mode, capable of 4 μas single-measurement accuracy. We have adopted the following criteria in developing our initial list of candidates: (a) stellar mass between 0.2 and 2.0 $M_{\odot}$, (b) $R < 12$ mag for reasonable integration times, (c) distance less than 140 pc to maximize the astrometric signal to be greater than 6 μas, (d) no companions within 2″ or 100 AU for instrumental and scientific considerations, respectively, (e) no nebulosity to confuse the astrometric measurements, (f) variability $\Delta R < 0.1$ mag, and (g) a spread of ages between 1 and 100 Myr to encompass the expected time period of planet-disk and early planet-planet interactions.

A literature search and precursor observing program (described in Tanner et al. 2007) was carried out to identify and validate stars according to these criteria. The observing program included adaptive optics imaging with the Palomar 5 m, VLT 8 m, and Keck 10 m telescopes to look for M star or brown-dwarf companions, RV measurements with the McDonald 2.7 m and HET telescopes, as well as the Magellan telescope to look for M star or brown-dwarf companions, and photometric observations with smaller telescopes to look for variability. The variability program proved to be the most stringent filter with roughly 50% of the sample showing photometric dispersion in excess of 0.1 mag. We now have a validated list of 75 stars meeting all of the above criteria. More stars will be added to the precursor program to bring the total up to the desired number of 150–200 stars. With the available observing time allocated to this program (1600 h), we will be able to make 75–100 visits to each star (up to 50 2D visits), which, spread over 5 years, will be enough to identify and characterize up to 3 planets per star having periods ranging from less than a year up to 2.5 years. For narrow-angle targets we will take advantage of the natural clustering of young stars to share requisite observations of ~5 reference stars, typically $R = 10$–12 mag K giants, with multiple (2–8) science stars within a 1° radius. With additional observations during a 10 year extended mission, it will possible to find planets out to 5 AU.

A secondary goal of the program is to put our knowledge of stellar evolution on a firmer footing by measuring the distances and orbital properties of ~100 stars precisely enough to determine the masses of single and binary stars to an accuracy of 1%. This information is required to calibrate the pre–main-sequence tracks (e.g., Baraffe et al. 2002) that serve as a chronometer ordering the events that occur during the evolution of young stars and planetary systems. To accomplish the goals of this program, we will observe a few dozen binary T Tauri stars as well

as stars with gas disks observed (in millimeter lines of CO) to exhibit Keplerian rotation. With accurate orbits and distances for these systems, it will be possible to determine accurate stellar properties for comparison with stellar evolution models.

4. HOW UNIQUE IS THE SOLAR SYSTEM?

SIM is most sensitive to orbits with periods in the range of ~1–5 yr (Fig. 1), with the most sensitivity to periods close to the mission length. *SIM* is well-suited to detect Earth-like planets in the habitable zone around nearby stars (see § 2 and Catanzarite et al. 2006). For periods up to ~10 yr, estimates of orbital parameters, including period, can be made, but as the period lengthens, the uncertainties grow quickly. In the limiting case, *SIM* can only make a detection of the acceleration due to a companion (Gould 2001). Even though the parameters of any one such target may not be well-determined, important statistical conclusions can be drawn from an ensemble of long-period systems. Independent data, especially over a long-time baseline, can greatly improve our knowledge of long-period companions. For many targets, there will be a 10–15 yr baseline of RV measurements to draw on.

Combining astrometry from a "*SIM* quick look" (SQL) survey with data from the *Hipparcos* astrometric mission (ESA 1997) would constrain orbits of 100 yr or more, and this could be done for several thousand *Hipparcos* stars. Below, we show results from a simulation of the extraction of planets from the combined dataset. Orbits of a $1\ M_{\rm Jup}$ planet can be reliably characterized up to periods of about 10 yr, $10\ M_{\rm Jup}$ planets up to 80 yr, and stellar companions up to 320 yr.

4.1. Masses and Periods of Long-Period Planets

Long-period extrasolar giant planets appear to be rare: only 25 have periods above 5 yr and just one has a period slightly longer than that of Jupiter. Taking the selection effects into account, Tabachnik & Tremaine (2002) estimate that 3% of Sun-like stars should have a planet with a period between 2 days and 10 yr and a mass of 1–10 $M_{\rm Jup}$. For our simulation, we adopt the normalization of Sozzetti (2005), which is 1.62 times that computed by Tabachnik & Tremaine (2002).

We define a solar system giant analog (SSGA) as a planet (or planets) whose mass and period fall within the range of the giants of our solar system (i.e., with a period between 12 and 165 yr and mass of 0.05–$1\ M_{\rm Jup}$). Such systems may or may not contain lower-mass planets, in closer orbits, but the astrometric signatures of SSGAs would normally dominate, and would remain detectable in distant systems for which terrestrial planets are below the detection limit. Because the extrasolar giant planet period distribution function increases with period, systems dominated by giant planets should be rather common, and we estimate that 12.6% of Sun-like stars could harbor SSGAs.

We also define a more massive version of the solar system giant analog, with mass between 1 and $13\ M_{\rm Jup}$, as a massive solar system giant analog or MSSGA. These are predicted to be quite abundant, and of course are easier to detect: 20% of the total number of planetary systems with periods up to 165 years and occurring around 7.9% of single stars.

4.2. A Survey for Solar-System Analogs

To identify likely long-period planetary systems we combine data from an SQL survey with *Hipparcos* data (ESA 1997). This method uses the astrometric parameters as determined from a fit to the *SIM* data to predict the position at the *Hipparcos* epoch. Differences between the observed and predicted positions indicate the presence of a companion (Olling 2007b); *SIM* data allow for the determination of the seven astrometric parameters of an "acceleration" solution (in addition to the two positions, two proper motions, and parallax). Additional *SIM* observations would help with reliable extraction of accelerations. In any case, the aim of the survey would primarily be to reject the main-sequence (MS) binaries that have huge signals. Either way, a *SIM* survey would produce a sample rich in planetary and/or brown-dwarf (BD) companions.

For truly single stars, the *SIM* data will be an excellent predictor of positions recorded in the twentieth century. However, if the star has a companion, the short-term proper motion determined from a SQL survey can be very different from the center-of-mass motion. For a face-on, circular system, the semimajor axis of the orbit, orbital speed, acceleration, and the derivative of the acceleration are all substantial for nearby MSSGA systems. For a $1\ M_{\odot}$ star at a distance of 20 pc, and a $1\ M_{\rm Jup}$ planet, we can show that MSSGAs with periods in the range of 5 to 160 yr are readily detectable. This issue has been well-studied, in the context of FK5 and *Hipparcos* astrometry, by Wielen et al. (2001 and references therein).

Due to the short observing span with respect to the orbital period, SQL data effectively determine the instantaneous proper motion and acceleration due to orbital motion. The long-time baseline τ between the SQL and *Hipparcos* epochs allows us to compute a metric, $\Delta_{xy}(\tau) \equiv [\Delta_x^2(\tau) + \Delta_y^2(\tau)]^{1/2}$, which is independent of phase for circular, face-on orbits (Olling 2007b). The $\Delta_{xy}(\tau)$ diagnostic is useful when it exceeds the astrometric error.

The χ^2_ν figure of merit is useful in revealing MSSGA, BD, and MS companions. For orbital periods between 5 and 320 yr, the (reduced) χ^2_ν values uncover 11%, 39%, and 73% of the companions in the MSSGA, BD, and MS mass range, respectively, if we use only the *SIM* data to compute χ^2_ν. Here we ignore the effects of inclination and eccentricity, which complicate the characterization of the companion, although they will not lower the χ^2_ν and Δ_{xy} values very much (Makarov & Kaplan 2005; Olling 2007b). Including the available non-*SIM* astrometry significantly increases the yield to 46%, 90%, and 99.8% for the three mass ranges respectively. These results indicate that

low-mass companions can be efficiently detected by combining SQL and *Hipparcos* data. We find that the orbits of a 1 or 10 $M_{\rm Jup}$ MSSGA can be characterized up to periods of 10 or 80 yr, respectively, and for stellar companions up to 320 yr (Olling 2007b). The $\Delta_{xy,\mu}$ values are significant up to 1200 or 5000 years for companions with mass 0.08 or 1.0 $M_{\odot}$, respectively.

4.3. Very Long-Period Companions

There is strong evidence that the intrinsic multiplicity rate due to either stars or planets is close to 100% among *Hipparcos* MS stars (Olling 2005). The lack of cataloged companions is most likely due to selection effects. Thus, those systems without signs of binarity in a SQL + Hipparcos survey are likely to have either substellar companions with an unknown period, or very long-period stellar companions. An extended *SIM* survey would further explore these poorly characterized systems.

An extended *SIM* astrometric survey would be significantly more sensitive than the initial quick look survey. Applying the Δ_{xy} analysis presented above to the extended *SIM* survey indicates that the MSSGAs can be detected with masses as low as 0.1 $M_{\rm Jup}$ in 10 yr orbits. The maximum period for which a 1 $M_{\rm Jup}$ planet can be reliably detected is extended by a factor of 4 (to 40 yr) and for 10 $M_{\rm Jup}$ by a factor of 2 (to 160 yr). Thus SQL + Hipparcos plus an extended *SIM* survey can uncover a very significant part of the MSSGA parameter space.

Given the importance of accurate pre-*SIM* astrometry, we note that large-scale ground-based photometric surveys such as Pan-STARRs will also provide astrometry at the required (sub-mas) level (Chambers 2005). Also, data from the *Gaia* mission (Perryman 2002) will help explore and characterize SSGAs more fully.

5. PRECISION *M-L* RELATION FOR EXTREME STELLAR TYPES

Mass is the most fundamental characteristic of a star. It governs a star's entire evolution—determining which fuels it will burn, what color it will be, and how long it will live. It is crucial to our understanding of stellar astrophysics that we determine stellar masses to high accuracy. Knowing the masses of main-sequence stars answers basic stellar astrophysics questions such as: What is the mass-luminosity relation for the highest mass and also the lowest-mass stars? What is the initial mass function? What is the mass content of the Galaxy and how does it evolve? In fact, the dependence of luminosity upon mass—the mass-luminosity relation (MLR)—is one of the few stellar relations sufficiently fundamental to be applicable to many areas of astronomy. With the exception of the H-R diagram, it is the single most important "map" of stellar astronomy. To answer truly fundamental astrophysical questions about stars, the ultimate goal is to determine masses to 1% accuracy, which will allow us to challenge stellar models more severely than ever before. Because of *SIM*'s exquisitely accurate astrometric capabilities, coupled with its faint magnitude limit, we can develop a well-stocked "toolbox" of MLRs that can become the standards against which all stars are measured.

Here, we consider the extreme ends of the main sequence, where *SIM* will be crucial in making real progress in defining the MLR. In the case of the most massive stars, *SIM*'s extreme accuracy will allow us to reach further across the Galaxy to pick up the rare O- and B-type binaries needed for mass determinations. For their much less massive cousins, the red M dwarfs, *SIM*'s faint limit provides the ability to measure the orbital motions of objects all the way to the end of the stellar main sequence, and into the regime of the substellar brown dwarfs.

There are two tactics that can be used to pin down the most massive and least massive stars—measurements of individual systems in the field and the calibration of the so-called third and fourth parameters, metallicity and age, by targeting stars in clusters for which those quantities are known.

5.1. Massive O and B Stars

Massive stars are key contributors to the energy budget and chemical enrichment of the Galaxy, but little is presently known about their masses (see Fig. 5). There are only five known eclipsing binaries among the O stars that have reasonably well-established masses (Harries et al. 1998), and this lack of data has seriously hindered our understanding of the evolution of massive stars. One unknown, for example, is the maximum mass possible for a star. Interior models for massive stars predict that stable stars can exist with initial masses of 120 $M_{\odot}$, but the most massive object among the five eclipsing binaries is only 33 $M_{\odot}$. Furthermore, indirect methods of estimating mass by comparison with model evolutionary tracks and through spectroscopic diagnostics lead to discrepancies as large as a factor of 2 (Herrero et al. 2000). *SIM* will record the photocentric and/or absolute orbits of many binaries, and by combining this information with spectroscopic data it will be possible to determine accurate distances, inclinations, and masses. An excellent example is the massive binary HD 93205, which consists of an O3V + O8V pair in a 6.08 day orbit. *SIM* observations will show a 45 μas photocentric variation that will yield the first accurate mass for a star at the top of the main sequence (only known to be in the range of 32–154 $M_{\odot}$; Antokhina et al. 2000).

SIM will also provide the first accurate masses of the evolutionary descendants of massive stars. The most massive stars develop strong outflows later in life and appear as Wolf-Rayet (WR) stars. *SIM* measurements of the WR binary WR 22 (WN7 + O9III; Schweickhardt et al. 1999) will show a 250 μas astrometric variation through the 80.3 day orbit. These measurements will provide the mass of this extraordinary object, currently estimated to be 55 ± 7 $M_{\odot}$, the most massive star known. Intermediate-mass B stars in close binaries are believed to suffer extensive mass transfer and mass loss during the

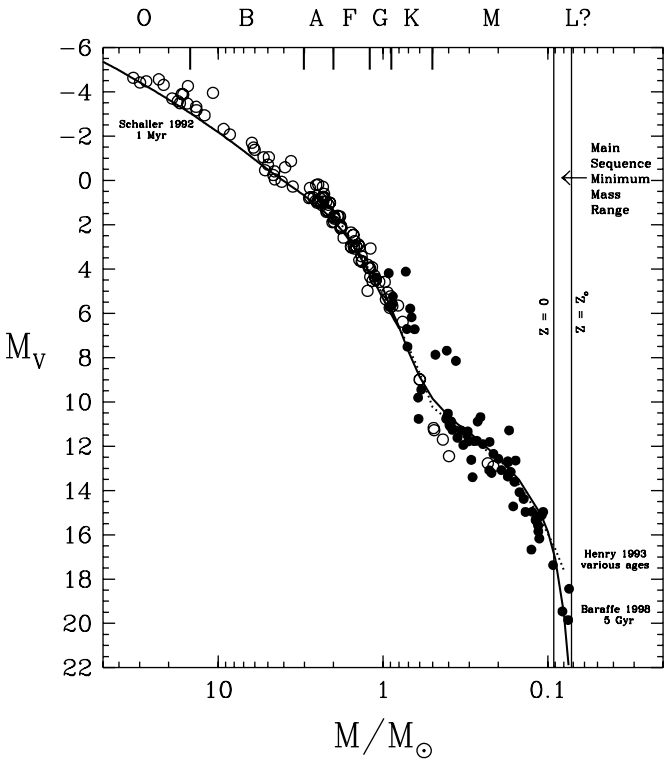

FIG. 5.—Mass-luminosity relation in 2007, using eclipsing binary data (*open circles*) from Andersen (1991) and others, supplemented with visual, speckle, and interferometric binary data (*filled circles*). Model curves for the mass-luminosity relation at the indicated ages and solar metallicity are shown, from Schaller et al. (1992) at the higher masses and Baraffe et al. (1998) at the lower masses. The empirical fit of Henry & McCarthy (1993) for stars with masses 0.08 to 2.0 $M_\odot$ is indicated with a dotted line.

Roche lobe overflow phase. The best example of this evolutionary stage is the enigmatic binary, η Lyr (Bisikalo et al. 2000), which consists of a bright, 3 $M_\odot$ star losing mass to a 13 $M_\odot$ star hidden in an extensive accretion disk. The astrometric orbital motion of the bright component will amount to 820 μas, and *SIM* will provide accurate mass estimates at this key evolutionary stage. Finally, two other examples of massive stars with longer periods include HD 15558 (O5e) and HD 193793 (WR), with periods of 1.2 and 7.9 yr, respectively. At distances of 1.3 and 2.6 kpc, each system has a semimajor axis of 5–10 mas, easily within reach of *SIM*.

5.2. Low-Mass M Stars and Brown Dwarfs

Red dwarfs dominate the solar neighborhood, accounting for at least 70% of all stars, and represent nearly half of the Galaxy's total stellar mass (Henry et al. 1999; Fig. 6). These stars have spectral type M, $V = 9$–20, and masses 0.08–0.50 $M_\odot$ (Henry & McCarthy 1993; Henry et al. 1994). The MLR remains ill-defined for M dwarfs, so their contribution to the mass of the Galaxy is a guess at best, and the conversion of a luminosity function to a mass function is problematic. At masses less than ~0.20 $M_\odot$ an accurate MLR can provide a strict test of stellar evolutionary models that suggest the luminosity of such a low-mass star is highly dependent upon age and metallicity. Finally, the MLR below 0.10 $M_\odot$ is critical for brown-dwarf studies because accurately known masses can convincingly turn a candidate brown dwarf into a bona fide brown dwarf.

In recent decades, the masses of red dwarfs have been determined using a combination of infrared speckle interferometry and HST-FGS, and occasionally via RV efforts. The number of red dwarfs with accurate mass measurements less than 0.20 $M_\odot$ has increased from four in 1980 (Popper 1980) to 22 (Henry et al. 1999). The sample of more massive red dwarfs in the range $0.50\ M_\odot > M > 0.20\ M_\odot$ has also increased, with particular improvement in the quality of the available masses.

SIM is critical for M dwarf systems because they are typically faint and do not allow high-precision RV measurements due to their slow orbital motion and poorly separated spectral lines. In addition to accurate orbital monitoring, *SIM* will provide two crucial pieces of information required to reduce mass errors to the 1% level, where they become astrophysically interesting: parallaxes and mass fractions. As an example, we examine the nearby binary Gl 748, which represents the current state-of-the art accuracies for red dwarf masses (2.4%). *SIM* can improve the mass by reducing the error in the semimajor axis of the absolute orbit (147.0 ± 0.7 mas) by a factor of 18 (to 0.04 mas, or 10 times the nominal astrometric accuracy of *SIM* for Global Astrometry) and the error in the parallax (98.06 ± 0.39 mas) by a factor of 10. The result would be mass errors of only 0.1%.

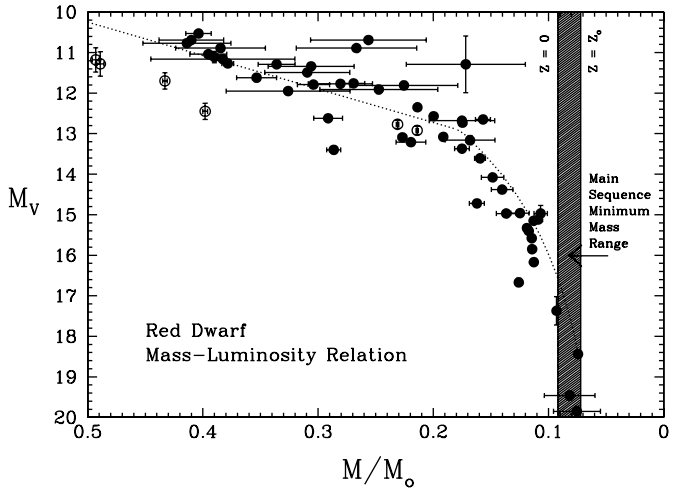

FIG. 6.—Zoom in of the mass-luminosity relation in 2007, focusing on red dwarfs. Eclipsing binary data are represented by open circles, and other binaries (visual, speckle, and interferometric) by filled circles. The empirical fit of Henry et al. (1999) is indicated with a dotted line, as well as the range of minimum masses for main-sequence stars, depending on metallicities. Note the disconnect between some of the eclipsing and visual binary points, as well as the need for a revision to the fit (toward lower masses) for the lowest-mass stars.

Mass is the best discriminator between stars and brown dwarfs. An object's mass determines whether or not temperatures in the object's core are sufficiently high to sustain hydrogen fusion—the defining attribute of a star. L dwarfs are objects with smaller masses and cooler temperatures (~1500–2000 K) than those of M dwarfs, but no accurate masses of L dwarfs have yet been measured, so the models of L dwarfs are completely untested by data. Several hundred L dwarfs have been discovered to date, and appropriate systems observable at *SIM*'s faint limit are being found. One example is GJ 1001 BC at a distance of 13 pc. With an orbital period of ~4 yr, this system is ideally suited to the nominal *SIM* mission lifetime.

6. THE LATE STAGES OF STELLAR EVOLUTION

The first discovery of an X-ray binary occurred over four decades ago when Scorpius X-1 was detected during a New Mexico rocket flight (Giacconi et al. 1962). Although the nature of Sco X-1 was not immediately clear, it was not long before Shklovskii (1967) suggested the correct explanation that Sco X-1 is a neutron star accreting from a stellar companion. Over the years, in excess of 25 X-ray satellites have found hundreds of X-ray binaries with neutron star or black hole accretors exhibiting a rich variety of physical phenomena. Studies of these systems allow us to probe the most extreme physical conditions in the universe, including magnetic fields at the surfaces of neutron stars that can be in excess of 10^{12} Gauss (Coburn et al. 2002), densities in neutron star cores that may be as much as an order of magnitude above nuclear densities (Lattimer & Prakash 2004), and gravitational fields near black holes and neutron stars that can provide tests of strong gravity (Psaltis 2004).

Studies of accreting stellar mass black holes also improve our understanding of active Galactic nuclei (AGN) and quasars. X-ray binaries with relativistic jets are often called microquasars (Mirabel et al. 1992) because of the similarities between these systems and quasars. However, detailed comparisons between the two populations are hampered by uncertain distances to the microquasars, making parameters like total luminosity and jet velocity uncertain.

While much has been learned about the physics of X-ray binaries, it is evident that more precise measurements of physical properties are required to make further progress in testing theory. Some of the properties that are the least accessible using current instrumentation, such as the source distance (d), proper motion, and binary inclination (i), will be readily measured using *SIM*. Here, we discuss some of the issues related to the physics of X-ray binaries that *SIM* will help address.

For these sources as well as for other radio-emitting stars, it will be possible to combine *SIM*'s observations with very long baseline interferometry (VLBI) observations to place the radio components within an absolute reference frame that is accurate to 3 μas.

6.1. Masses of Neutron Stars

Neutron stars (NSs) provide a unique opportunity to understand what happens to matter as densities are increased beyond the density of nuclei. Thus, measuring the NS equation of state (EOS) has important implications for nuclear physics, particle physics, and astrophysics, and measuring NS masses, radii, or both provide constraints on the EOS. The NSs for which accurate mass measurements have been made lie very close to the canonical value of $1.4\ M_\odot$ (Thorsett & Chakrabarty 1999), and EOSs with normal matter (neutrons and protons) as well as exotic matter (e.g., hyperons, kaon condensates, and quark matter) can reproduce this mass for a large range of radii (Lattimer & Prakash 2004). However, more recently, there are indications that some systems may harbor higher mass, 1.8–2.5 $M_\odot$, NSs (Barziv et al. 2001; Clark et al. 2002; Nice et al. 2005) and confirming these high NS masses by reducing the uncertainties would lead immediately to ruling out a large fraction of the proposed EOSs.

SIM will be capable of making precise orbital measurements for a large number of high-mass X-ray binary (HMXB) systems. These systems typically have O- or B-type companions with ~25 HMXBs being brighter than $V \sim 15$. They also have orbital periods ($P_{\rm orb}$) of days to a couple of years, and their wide orbits give large astrometric signatures. Taking estimates of HMXB parameters ($P_{\rm orb}$, d, and the component masses) from Liu, van Paradijs & van den Heuvel (2000) as well as more recent literature, we find that 21 likely NS HMXBs have orbital signatures (the semimajor axis of the optical companion's orbit) of $a_{\rm sig} \geq 5$ μas and eight HMXBs have $a_{\rm sig} \geq 40$ μas. Detailed simulations that account for the optical source brightnesses (Tomsicket al.2005) show that *SIM* is expected to be capable of detecting orbital motion for 16 NS HMXBs (see Fig. 7).

The most interesting among these 16 systems are those for which the projected size of the NS's orbit ($a_{\rm x} \sin i$) has already been measured (Bildsten et al. 1997). The five sources for which this is the case are Vela X-1, X Per, 3A 0535+262, GX 301–2, and PSR B1259–63. *SIM* measurements, along with $a_{\rm x} \sin i$, will immediately yield a NS mass measurement. Perhaps Vela X-1 is the most tantalizing, as it is suspected of having an overmassive NS. The current NS mass measurement for Vela X-1 is $M_{\rm x} = 1.86 \pm 0.16\ M_\odot$ (1 σ errors) (Barziv et al. 2001). In 40 hr of narrow-angle *SIM* observations of Vela X-1, it will be possible to measure $M_{\rm x}$ to 3.9% (Tomsick et al. 2005). This is a major improvement over the current mass measurement and will be sufficient to determine if Vela X-1 harbors an overmassive NS. As our estimate of the astrometric signature for Vela X-1 is 9.5 μas, the microarcsecond measurement accuracy provided by *SIM* is critical.

6.2. Masses of Stellar Black Holes

Black holes (BHs) are among the most fascinating celestial objects. Stellar BHs in our galaxy accreting from a normal star

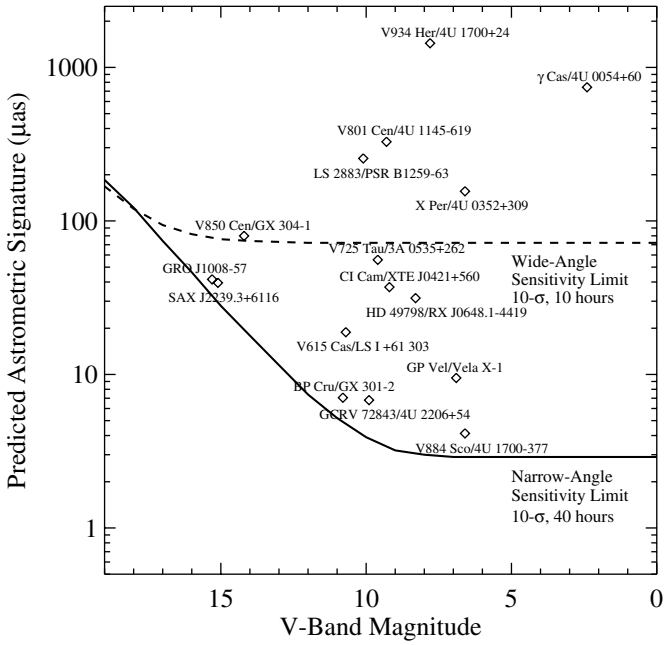

FIG. 7.—Expected astrometric signature from orbital motion vs. V-band magnitude for the 16 neutron star and neutron star candidate high-mass X-ray binaries that we expect to have large enough signatures to be detected by *SIM*. The solid line shows the 10 σ narrow-angle *SIM* sensitivity limit found from simulations (Tomsick et al. 2005) where 40 hour-long observations are made, and we have a priori knowledge of the binary orbital period. The dashed line shows the 10 σ wide-angle *SIM* sensitivity limit for 20 half-hour-long observations.

facilitate investigation of disk accretion and relativistic jets. The mass is a fundamental property of a stellar BH and has critical implications for the evolution of BH binaries. Although BHs and NSs are often difficult to distinguish, it is believed that a compact object that is more than 3 $M_\odot$ is probably a BH while objects less than 3 $M_\odot$ could be either a BH or a NS. Present measured masses of 20 confirmed BHs have possible masses ranging from 3 to 18 $M_\odot$ (Remillard & McClintock 2006). The masses of stellar BHs have large uncertainties due to the unknown orbital inclination, parallax, and other systematic errors.

As an example, our understanding of the nature of the galactic BH Cyg X-1 could change substantially depending on its true distance and the companion's mass. The mass of the BH in Cyg X-1 is estimated as 10 $M_\odot$ (Herrero et al. 1995). However, the companion star of Cyg X-1 might be undermassive for its early spectral type. Additionally, there is a huge range of distance estimates for the system: *Hipparcos* measurements place it at 1724 ± 1000 pc, VLBI estimates 1400 ± 900 pc, and spectral analysis places it at 2000 2500 pc. If the lower companion mass and nearest distance are adopted, the mass of Cyg X-1 could be as low as 3 $M_\odot$. *SIM* can refine the mass measurements for X-ray binaries that are thought to harbor BHs. Currently, the main uncertainty in the component masses arises from uncertainty in the binary inclination and distance to the system, quantities that will be measured accurately by *SIM*. For the case of Cyg X-1, the ~20 $M_\odot$ supergiant companion has an orbital astrometric signature of 27 μas at a distance of 2.5 kpc or 34 μas at 2.0 kpc. Thus, the orbit of Cyg X-1 can be easily resolved by *SIM*, allowing the binary inclination to be determined accurately and the semimajor axis to be determined to better than 2% (Pan & Shaklan 2005). *SIM*'s measurements, combined with X-ray spectroscopic and photometric observations and VLBI observations, will give us a complete physical picture of stellar BHs for the first time.

SS 433 is an HMXB and microquasar with unique relativistic baryonic jets that precess with a 162 day period (Margon 1984). Although there is evidence to support the presence of a BH in the system (Hillwig et al. 2004), the nature of the compact object is still debated. Due to the uncertainty in the compact object's mass, the orbital astrometric signature is also uncertain, but could easily be 10–30 μas. Because the object is bright ($V = 14$), *SIM* narrow-angle measurements are feasible, and a detection of its orbital motion would allow for a definitive answer regarding the nature of the compact object.

6.3. Formation and Evolution of Black Holes and Neutron Stars

The evolutionary endpoints of massive stars result in compact objects, such as white dwarfs, NSs, or BHs. It is of great importance to investigate their birth place, asymmetric birth kicks, and the path of formation and evolution of these compact objects. In theory, a BH can be formed in two different ways: a supernova (SN) explosion or the collapse of a massive star without an energetic explosion. These formation mechanisms can be distinguished by unique information contained in the kinematic history. If a galactic BH or a NS is formed in a supernova event, very often a supernova remnant is nearby. It is crucial to use three-dimensional space velocity measurements to determine the object's runaway kinematics and the galactocentric orbits (see Mirabel & Rodrigues 2003 and references therein). Unfortunately, the current measurement precision of transverse velocities is limited. The image superposition technique with *HST* has a precision of $\approx$1 mas for proper motions and an error of 16% for velocities (Mirabel et al. 1992). *SIM* can provide at least 2 orders of magnitude improvement for kick velocity measurements, and can identify associations between a compact object and supernova remnant for many X-ray binaries.

For the scenario where a BH is formed without a supernova event, the most important issues include determination of its birth place, measurements of its galactocentric orbit, and a thorough investigation of its space environment (Pan & Shaklan 2005). So far, only Cyg X-1 provides observational evidence of this outcome, because it appears to have proper motion in common with the association OB-3 and there is no nearby supernova remnant. For this type of BH formation, key parameters, such as inclination, kick velocity, distance, and masses,

are either indirectly known or lack sufficient precision from current observations.

6.4. LMXB Distances and Constraints on Physical Parameters

As most X-ray binaries are too far away for parallax measurements, distance measurements for these systems are, for the most part, highly uncertain. It is not unusual for an X-ray binary's only distance estimate to be based on a companion's spectral type and a system brightness, and these estimates can be uncertain by a factor of 2 or more. This leads to uncertainty about many basic system parameters such as luminosities, mass accretion rates, radii of NSs (Rutledge et al. 2002), sizes of accretion disks, and jet velocities (Fender 2006).

SIM will be able to measure the distances of low-mass X-ray binaries (LMXBs), and we have used Liu et al. (2001), as well as more recent literature, to compile a list of LMXBs. As LMXBs tend to be optically faint, the main selection criterion is V-band magnitude. Although the optical brightness can be strongly variable for transients, these systems spend most of their time in quiescent (i.e., low flux) states. There are 27 LMXBs with $V < 20$ for which *SIM* parallax measurements will be feasible. For the brightest few sources ($V = 12$–13), it will be possible to measure distances to accuracies as high as 2% using 1 hr of *SIM* time. While more time will be required for the fainter sources, accurate distance measurements will still be feasible. For the 19 sources on our list with $V > 17$, we typically expect to obtain distance measurements to 5% accuracy using, on average, 5 hr of *SIM* time per source. Thus, these systems make excellent use of *SIM*'s ability to observe fainter targets.

The LMXBs on our target list include microquasars such as V4641 Sgr and GRO J1655–40 for which accurate distance measurements will provide a test of whether their jet velocities actually exceed $0.9c$. Observations of Cen X-4 will allow improved constraints on NS radius measurements, and we will be able to determine if the brightest persistent NS systems (such as Sco X-1 and Cyg X-2) and the brightest X-ray bursters (such as 4U 1636–536) reach the Eddington limit.

6.5. Active Stars and Micro-Quasars

There are various types of stars that produce continuum emission at radio wavelengths, including RS CVn binaries, eclipsing Algol-type binaries, X-ray binaries, novae, pre–main-sequence stars, and microquasars. Two areas in which a *SIM* astrometric mission would have a significant impact in the study of radio stars are (1) establishing a link between the ICRF and the optical reference frame and (2) the location of the radio emission and the mechanism by which it is generated.

Traditionally, links between the radio and optical frames have been determined through observations of radio stars. At optical wavelengths, the *Hipparcos* Catalog currently serves as the primary realization of the celestial reference system. The link between the *Hipparcos* Catalog and the ICRF was accomplished through a variety of ground- and space-based efforts (Kovalevsky et al. 1997; Lestrade et al. 1999). The standard error of the alignment was estimated to be 0.6 mas at epoch 1991.25, with an estimated error in the system rotation of 0.25 mas yr^{-1} per axis (Kovalevsky et al. 1997). For future astrometric missions such as *SIM*, the link between the ICRF and the optical frame will be established through direct observations of the quasars. However, observations of a number of radio stars should provide a useful check on this important frame tie.

In a series of radio observations made with connected element interferometers (Johnston et al. 2003; Boboltz et al. 2003, 2007; Fey et al. 2004), positions and proper motions of $\sim$50 radio stars were determined in the ICRF. One goal of this program was to investigate the current accuracy of the ICRF-*Hipparcos* frame tie. Most recently, Boboltz et al. (2007) compared radio star positions and proper motions with the *Hipparcos* Catalog data, and obtained results consistent with a nonrotating *Hipparcos* frame with respect to the ICRF. These studies demonstrate the methods by which the optical and radio frames can be linked on levels of a few milliarcseconds using radio stars. Such a connection between a future *SIM* optical frame and the ICRF will require much more accurate VLBI observations in the radio, and will take into account phenomena related to the orbits of the close binary companions.

In addition to establishing a link between frames, observations of active radio stars performed with ground-based VLBI and *SIM* will greatly enhance our understanding of these objects. Many of the stars emitting in the radio are close RS CVn and Algol-type binaries with separations < 20 mas and orbital periods < 20 days. *SIM* will provide unprecedented insight into the process of radio emission and mass transfer for such stars. For example, the prototype radio star, Algol, is a triple system. From VLBI measurements, it was concluded that the two orbital planes of the close and far pairs are perpendicular to each other, rather than being coplanar (Pan et al. 1993). Research to determine the cause of such perpendicular orbits in stellar evolution theory is ongoing (Lestrade et al. 1993).

In both RS CVn and Algol-type binaries it is unclear where exactly the radio emission originates relative to the two stars in the system. Competing mechanisms for generating radio emission are reviewed in Ransom et al. (2002) and include phenomena such as gyrosynchrotron radiation from polar regions of the active K-giant star (Mutel et al. 1998), emission from coronal loops originating on the K giant (Franciosini et al. 1999), and emission from active regions near the surface of both stars with possible channeling of energetic electrons along interconnecting magnetic field lines (Ransom et al. 2002). An astrometric mission such as *SIM* should provide stellar positions on the 10 μas level, and the full three-dimensional orbits required to distinguish between the various emission mechanisms.

SIM will also have the flexibility to coordinate observations with ground-based instruments such as the VLBA to allow the location of the radio emission relative to the stars as a function of time, even for the shortest period (~1 day) binaries. In addition, studies of the dynamics of radio jets from microquasars will take advantage of *SIM*'s flexible "target of opportunity" scheduling. Most microquasars are X-ray transients, and when they undergo their month- to yearlong outbursts they become millions of times brighter in X-rays and thousands of times brighter in the optical, and they often produce observable radio jets. *SIM* observations of an outburst will provide the precise absolute location of the compact object and accretion disk, which is critical for interpretation of the locations and velocities of the jets.

A final issue regarding radio stars and microquasars is the establishment of the linear scale sizes of the systems through accurate parallax measurements. Existing parallax measurements are sometimes in conflict. For example, with *Hipparcos*, the distance to the microquasar LS I +61 303 was found to be 190 pc; however, VLBI observations place it at a distance of 1150 pc (Lestrade 2000). Through accurate parallax measurements, *SIM* will provide the linear scale sizes necessary to relate the radio emission to stellar positions and to constrain theoretical models of radio star and microquasar emission.

6.6. Late-type Stars with Maser Emission

The evolution of stars along the asymptotic giant branch (AGB), including Mira variables, semiregular variables, and supergiants, is accompanied by significant mass loss to the circumstellar envelope (CSE). The nature of this mass-loss process and the mechanism by which spherically symmetric AGB stars evolve to form axisymmetric planetary nebulae (PNe) is not well understood.

The circumstellar maser emission (OH, H_2O, and SiO) associated with many AGB stars provides a useful probe of the structure and kinematics of the nearby circumstellar environment. Figure 8 shows a schematic view of the inner CSE of a typical AGB star with masers. The various maser regions can be studied at radio wavelengths with VLBI, while the star itself, the molecular atmosphere, and the circumstellar dust can be studied using long-baseline interferometry in the optical and infrared.

While ground-based techniques provide a powerful tool to study AGB stars, there are still unanswered questions for which *SIM* could provide crucial information. For example: (1) What is the underlying cause of the transition of symmetrical AGB stars to asymmetrical PNe (e.g., unseen binary companions, nonradial pulsations)? (2) What are the positions of AGB stars relative to the circumstellar masers within the CSE? (3) What is the linear scale size of the CSE?

A review of the current research regarding PNe shaping is presented in Balick & Frank (2002). Theoretical models involve interacting stellar winds, magnetic field shaping, astrophysical jets, and unseen companions. Observational radio-IR-optical interferometric studies probe the inner regions of the progenitor AGB stars and provide evidence for asymmetry (Monnier et al. 2004; Boboltz & Diamond 2005), significant magnetic fields (Vlemmings et al. 2006), and highly collimated astrophysical jets (Imai et al. 2002; Boboltz & Marvel 2005). Whatever the mechanism for shaping PNe from AGB stars, it must be operating at the innermost scales of the CSE. This is just the regime that *SIM* will be able to probe.

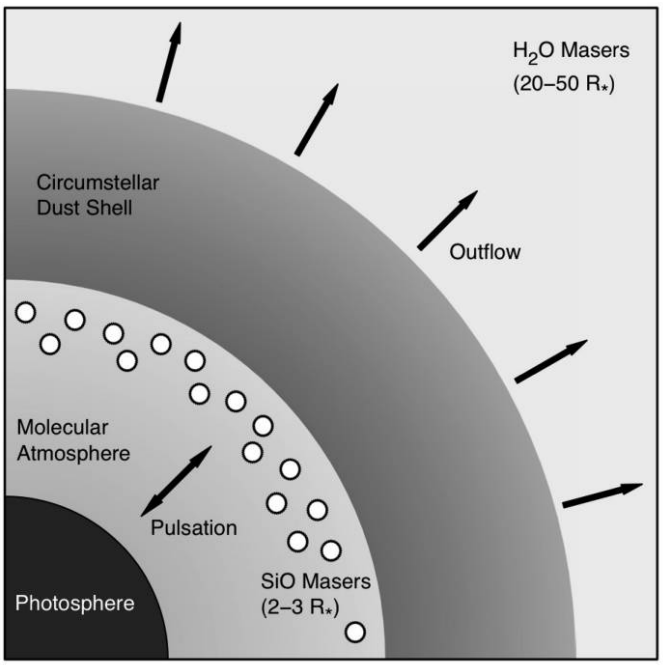

FIG. 8.—Schematic view of the radial structure of the envelope of a typical AGB star with circumstellar maser emission. Interferometry in the optical, near-infrared, and mid-infrared can be used to study the photosphere, the molecular atmosphere and the circumstellar dust. VLBI at radio wavelengths can be used to study the circumstellar SiO and H_2O masers.

Figure 9 illustrates the problem of referencing optical-IR interferometry to radio interferometry results. Shown are the results of a joint Very Large Telescope interferometer (VLTI) and very long baseline array (VLBA) study of the Mira variable S Ori (Wittkowski et al. 2007). The stellar diameter, represented by the dark circle in the center, was measured with the VLTI while the circumstellar SiO masers were imaged concurrently with the VLBA. The referencing of the star to the masers is purely conjectural, however, with additional astrometric information from *SIM*, this assumption would become unnecessary.

A similar astrometric problem is demonstrated by recent H_2O maser observations of disks toward silicate carbon stars. In the case of the star V778 Cyg, Szczerba et al. (2006) were able to use Tycho astrometric data to associate the H_2O masers with an unseen companion orbiting the carbon-rich AGB star. A si-

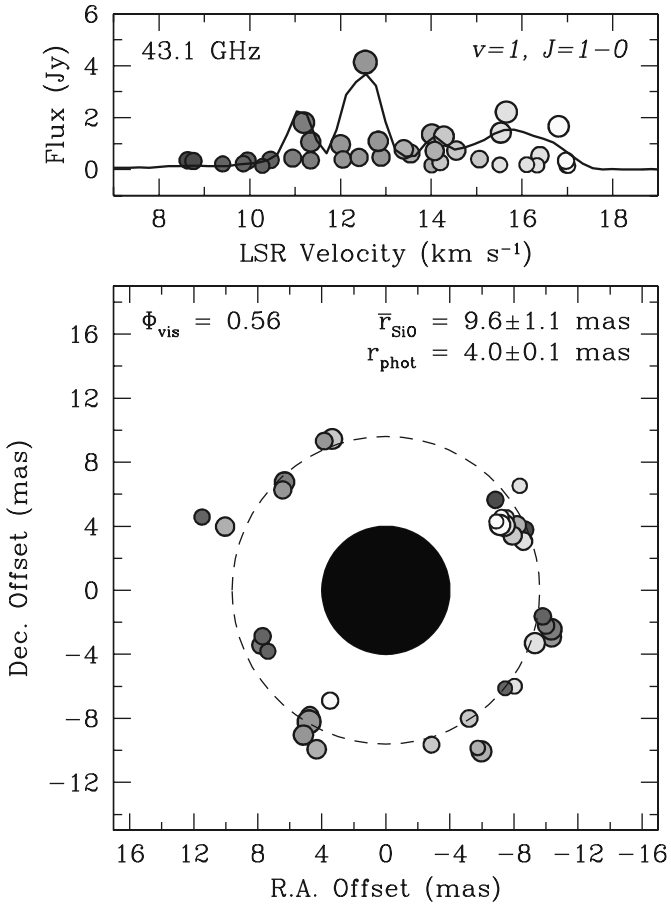

FIG. 9.—The $v = 1$, $J = 1$–0 SiO maser emission toward the Mira variable S Ori at a stellar phase $\Phi_{\rm vis} = 0.56$, as measured by the VLBA. The top panel shows the spectrum formed by plotting maser intensity versus velocity. The bottom panel plots the spatial and velocity distribution of the masers with point shading representing the corresponding velocity bin in the spectrum and point size proportional to the logarithm of the flux density. The dashed circle is based on the mean angular distance of the SiO masers from the center of the distribution. The dark circle in the center illustrates the angular size of the continuum photosphere as determined from VLTI measurements (Wittkowski et al. 2007).

milar disk has been observed for the carbon star EU And, also traced by H_2O masers; however, it is impossible to determine whether the disk is associated with the AGB star with the available astrometric data. With *SIM* astrometry, such a determination would be routine.

Finally, *SIM* will greatly improve the study of AGB stars by providing the precise parallax distances essential to establishing a linear scale size for the star and the various regions of the CSE. Knowledge of these scale lengths is important for theories relating to the chemistry of CSEs, the formation points of circumstellar masers and dust, and the strength of the stellar magnetic field. Furthermore, the linear velocity of circumstellar gas as traced by maser proper motions has yet to be accurately determined for many stars without precise distances.

7. STELLAR EVOLUTION, EXTRAGALACTIC DISTANCES, AND GALAXY FORMATION

The study of normal galaxy evolution will be greatly enhanced not only by *SIM* projects that target dynamics and dark matter, but also by those that target the distance scale. We show in this section that better distances translate to much more precise information on the chemical and age structure of the various stellar populations that make up the Galaxy and external galaxies. *SIM* can be used to obtain parallax distances to Galactic (disk; Population I) clusters. This will complement *SIM*'s Population II (halo and thick disk) distance-scale investigations described in § 9.

A critical step in studying ages and chemical compositions of stellar populations is to establish a collection of standard clusters, mostly Galactic clusters, for which distances, reddenings, abundances, and ages will be derived with unprecedented accuracy. *SIM* is critical to this task by providing accurate parallax distances. These standard clusters can then be used to tightly constrain theoretical isochrone sets more stringently than ever before. The isochrones, in turn, give ages for clusters and also for galaxies via integrated-light models, and precision studies of galaxy evolution are the ultimate aims enabled by this *SIM* study. Morphological look-back studies (e.g., GEMS; Rix et al. 2004) and spectroscopic surveys (e.g., COMBO-17; Wolf et al. 2004) dovetail nicely with stellar population studies that earlier predicted in a broad way what the direct observations are finding. That is, spiral galaxies look as if they have had quasi-continuous star formation for long epochs, as expected, but elliptical galaxies, while mostly dead today, have also had much more complex star formation histories than one would suppose, not too drastically different from spirals (Worthey 1998).

A plethora of questions regarding field versus cluster environment, chemical evolution, and morphological evolution remain, and are likely to remain for many years. Present age errors intrinsic to isochrone-based models are of the order of 30% (Charlot et al. 1996), but the clusters studied by *SIM* should allow for increased precision for better understanding of galaxy evolution at all redshifts. A reasonable goal in this regard is 5% age precision for favorable, well-observed extragalactic stellar populations from the next generation of large, ground-based spectroscopic telescopes.

But an absolute 5% age precision requires a much better grip on the systematics of stellar populations than presently exists. With precise distances from *SIM*, distance will no longer contribute significantly to the uncertainties, and instead other effects will dominate. For example, the uncertainty in heavy element abundance (Z) propagates approximately as $\delta \log \text{ age} = -3/2\delta \log Z$ (Worthey 1994) using stellar temperatures as age indicators, as one is forced to do for integrated-light applications. This implies that overall heavy element abundance uncertainty be less than 0.02 dex, a goal reached only rarely at present, but which should be very common in the near future. The detailed, element-by-element composition also matters.

Worthey (1998) estimates that abundance ratio effects need to be tracked and calibrated if they induce more than a 7 K shift in stellar temperature. Progress on such detailed effects is underway and should be available in a few years. Progress on bolometric corrections, absolute flux scale, and stellar color-$T_{\rm eff}$ relations can also be expected shortly. A standard cluster set provides tie-down points for stellar modelers, which relate intimately to the interpretation of high-redshift stellar population studies.

SIM will measure parallax distances to the Galactic clusters (supplemented by the globular cluster distances described in § 9). The luminosity of the main-sequence turnoff (MSTO) in the color-magnitude diagram is the best age indicator: the one with the smallest errors (Chaboyer 1995) and the one that ties most directly to the "fusion clock" of the hydrogen-burning star. Distance uncertainty is currently the dominant uncertainty, and that will be removed by *SIM* (to less than 1% for most individual Galactic clusters, and perhaps 1% for the Globular clusters in aggregate). After abundance effects, the remaining uncertainty is that of interstellar extinction, which may prove to be the dominant uncertainty in the end, although progress is being made in that area as well.

The target clusters were chosen to fulfill the following science goals. (1) We would like to see extragalactic stellar population age estimates with 5% absolute precision, at least for "red envelope" galaxies. This requires that isochrone sets be calibrated to the standard cluster set, and that the clusters themselves have well-determined ages (Table 4). (2) Of the many distance-scale issues that are benefitted by *SIM*, another important one is the surface-brightness fluctuation method (Tonry & Schneider 1988; Mei et al. 2005) that can be used to chart local galaxy flows and matter distributions. This method depends directly on the isochrone sets and is thus tied to the standard cluster set. (3) In our Galaxy, the standard clusters can be tied in to the photometry of the rest of the globular and open cluster system in order to investigate the chemical and dynamical history of the Galaxy. In external galaxies this is filtered through the isochrone sets. (4) The cluster ages themselves are important. (5) Finally, the clusters were chosen to be as massive as possible in order to attempt to populate the rarer, post-hydrogen-burning phases of evolution. These phases are the current frontier of stellar evolution, and the more constraints we can place, the better off we are.

TABLE 4

CLUSTERS SELECTED FOR POPULATION STUDIES

Cluster	Distance (kpc)	E (B-V)	[Fe/H]	Age (Gyr)
NGC 6528	9.1	0.6	−0.2	12
Palomar 6	7.3	1.5	~0.0	12
NGC 6440	8.4	1.1	−0.3	12
Collinder 261	2.2	0.27	−0.2	9
NGC 6791	4.2	0.1	0.4	8
Melotte 66	2.9	0.2	−0.4	7
NGC 6253	1.5	0.2	0.4	5
Messier 67	0.8	0.02	−0.1	4
NGC 2420	2.2	0.02	−0.4	4
Berkeley 18	5.8	0.46	0.0	4
NGC 6819	2.4	0.05	0.1	2
NGC 7789	1.9	0.22	−0.2	1.7
IC 4651	0.9	0.15	0.1	1.5
NGC 2243	4.5	0.05	−0.5	1.1
NGC 2477	1.2	0.3	0.0	1.0
NGC 6134	0.9	0.4	0.3	0.9
Messier 44	0.2	0.0	0.2	0.7
NGC 1817	2.0	0.33	−0.3	0.4
NGC 2324	3.8	0.11	−0.8	0.4
NGC 2099	1.4	0.3	0.1	0.4

NOTE.—This list is given in order of decreasing age. All parameters given are approximate.

The primary selection criterion is to cover as much age versus metallicity parameter space as the Galaxy allows. This makes "oddball" clusters with atypical abundances very important. For instance, young and metal-poor clusters are rare in the Galaxy, so NGC 2243 becomes a very important cluster. The globular clusters do not reach supersolar abundance, so the old, metal-rich cluster NGC 6791 becomes a valuable tie-point. The clusters to be observed with *SIM* cover about 1.5 dex in age, and are listed in Table 4.

8. CEPHEIDS IN THE MILKY WAY

SIM's contributions to Cepheid science are at least fourfold: (1) Approximate Cepheid distances are fairly easily estimated, so that once a variable star is identified as a Cepheid it will be useful for Galactic rotation-curve studies if a *SIM*-based parallax and proper motion are available. (2) An accurate distance calibration allows for an accurate determination of extinction and metallicity effects on the inferred absolute luminosity. (3) The physics of the pulsation mechanism (including the mysterious amplitude decline of Polaris) can be studied in great detail for those nearby Cepheids where the extinction is small and/or well measured (such as in clusters), and for Cepheids that are members of binary systems where accurate mass measurements can be made. (4) The changing color of the Cepheids during its pulsation phase ($\Delta(V-I) \sim 1.1\Delta V$; Olling (2007b), private communication) could help calibrate *SIM*'s color-dependent astrometric terms, while on average, ΔV increases with period: $\Delta V \sim \log P_{\rm days}$ (e.g., Bono et al. 2000).

The second and third points are essential for our understanding and usage of Cepheids as extra-galactic distance indicators. Currently, our lack of detailed understanding of the physics of the pulsation mechanism (i.e., the calibration of the period-luminosity-color relation) yields galaxy distances which carry systematic uncertainties of the order of $\pm 5\%$ (Pietrzyński et al. 2006; Macri et al. 2006). A better understanding of the physics would likely result in smaller systematic errors, and, hence, in an easier method for determining accurate distances to a large number of galaxies. For example, it has been claimed that

"bump Cepheids" can be used to determine distances below the 2% level. This method is based on a detailed analysis of the light-profile and nonlinear pulsation models (e.g., Keller & Wood 2006).

The Milky Way is the only galaxy for which we can perform detailed three-dimensional dynamical studies, because all six phase-space parameters can be determined for a number of tracers of the gravitational potential. Such studies are essential for the interpretation of velocity fields of external galaxies, especially those at high redshift, which are used to infer galaxy-formation scenarios. Young stars such as Cepheids (age ~ 50 Myr) are very sensitive to small- and large-scale perturbations of the potential (Mayor 1974), and are thus very useful to study the dynamical effects of, for example: (1) the bar, (2) spiral structure, (3) the Gould Belt, and (4) the warp. For such studies, the apparent magnitude is not important, just the distance and space velocity. Cepheids are useful for these kind of studies because they can be identified based on their periodic signal (Metzgeret al. 1998). A total of about 900 Galactic Cepheids are currently known (Welch 1998), while only the 200-odd nearest of these stars are typically used in studies of Galactic dynamics (Zhu 2000; Metzger et al. 1998; Feast & Whitelock 1997; Pont et al. 1997; Pontet al. 1994; Caldwell & Coulson 1987). The Cepheid sample provides a unique opportunity to perform very detailed studies of the dynamics of disk galaxies. Many of these Cepheids are too distant for *Gaia*, but are easy targets for *SIM*. Because the binarity rate among Cepheids is large ($\gtrsim 80\%$; Szabados 2003), it is crucial to monitor the Cepheids astrometrically throughout the *SIM* mission.

Cepheids in the Milky Way suffer a significant amount of extinction (A_V). For example, the nearest 180 stars in the sample of Pont and collaborators (Pont et al. 1994; Pont et al. 1997) have $A_V = 1.7 \pm 1$ mag, where the extinction correction is uncertain by about 0.1 mag. In general, it is hard to determine extinction better than to ± 0.05 mag for stars with Cepheid colors, even with the *Gaia* instrument suite (Jordi et al. 2006). Currently, the extinction is estimated from an intrinsic period-color relation (e.g., Laney & Stobie 1994; Caldwell & Coulson 1986) which is calibrated on Cepheids in open clusters. If more accurate methods become available to determine extinction, the Galactic relation between period, luminosity, color, metallicity, etc., would be very-well calibrated. Cross-validation of such a calibration would be available via the Cepheids in galaxies with rotational-parallax distances (see § 14.3): M 31 and M 33 (employing *SIM*) and the LMC (from *Gaia* data).

The "expanding photosphere" or "Baade-Wesselink" or "Barnes-Evans" or "infrared surface brightness" method has been used for many years to yield "geometric" distances for Cepheids. In this method, one can equate the integral of the changing radial velocity of the stellar envelope during the pulsation cycle to observed changes in radius. In principle, this method is very accurate because the radial velocities can be measured very accurately, while the radii of nearby Cepheids can be measured employing ground-based interferometry or via a surface-brightness color relation. However, this method also suffers from zero-point issues (Gieren et al. 2005) that may depend on, for example, metallicity, period, and pulsation mode. Thus, a large sample of Cepheids with a range of physical properties is required to establish this relation firmly. *SIM* could provide a much better calibration of this method than *Gaia* because *SIM* can reach the required distance accuracies at both faint and bright magnitudes.

A final, perhaps philosophical, point is that Cepheids are variable stars, and it is through this variation that we can learn much more about the internal structure and atmospheric physics than for normal stars. For example, the confirmation by helioseismology of the standard solar model firmly established neutrino oscillations, and hence proved that neutrinos are massive.

9. ACCURATE AGES AND DISTANCES FOR POPULATION II OBJECTS

The metal-poor stars in the halo of the Milky Way Galaxy were among the first objects formed in our Galaxy. These Population II stars are the oldest objects in the universe whose ages can be accurately determined. Age determinations for these stars allow us to set a firm lower limit to the age of the universe and to probe the early formation history of the Milky Way. The age of the universe determined from studies of Population II stars may be compared to the expansion age of the universe and used to constrain cosmological models. Globular clusters (GCs) provide the best opportunity to determine ages of Population II (hereafter Pop II) stars, as it is easy to identify the various evolutionary sequences in a GC color-magnitude diagram. The MSTO luminosity is the best stellar "clock" that can be used to determine the absolute ages of GCs (e.g. Demarque 1980; Rood 1990; VandenBerg 1990; Renzini 1991; Chaboyer et al. 1996).

The theoretical isochrones in Figure 10 demonstrate how age affects the color-magnitude diagram for a cluster of stars with uniform age and metallicity. It is immediately apparent that the MSTO and subgiant regions are most sensitive to age differences. The MSTO becomes redder and fainter as a cluster of stars gets older. Thus, in principle one could determine the age from the color of the turnoff, independent of distance.

The predicted colors of MSTO stars are subject to a great deal of uncertainty. To quantify this, we ran a Monte Carlo simulation to determine the uncertainty in the calculation of isochrones. First, distribution functions for the various input parameters used in a stellar evolution code (such as the opacities, nuclear reaction rates, treatment of convection, and oxygen abundance) are determined based on the known uncertainties in the determination of each of the various quantities. Isochrones are then calculated for a given set of input parameters that are drawn at random from the specified distribution function. This procedure was then repeated 1119 times in order to determine how the known uncertainties in the input parameters

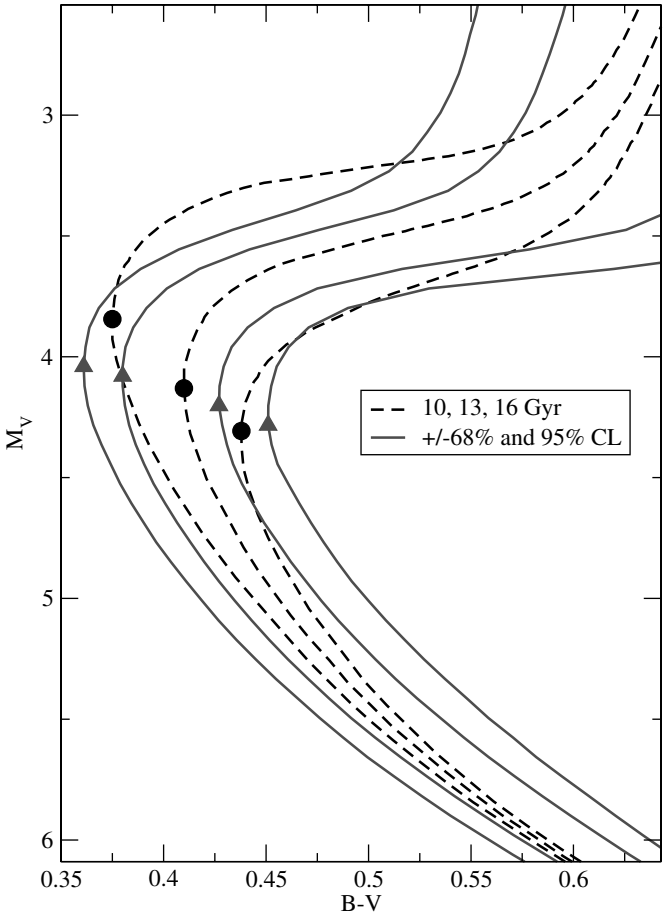

FIG. 10.—Theoretical isochrones with $[Fe/H] = -1.6$ calculated using the stellar evolution code described in Bjork & Chaboyer (2006), showing the change in the position of the MSTO (*solid circles*) when the age of the standard 13 Gyr isochrone is changed by ± 3 Gyr (*dashed curves*). The effects of changes in other parameters (e.g., nuclear reaction rates, opacities, treatment of convection, and oxygen abundance) were evaluated using the Monte Carlo simulation described in § 9, and are shown as the $\pm 68\%$ and $\pm 95\%$ confidence levels in a standard isochrone (*solid curves*), with corresponding MSTO (*triangles*). See the electronic edition of the PASP for a color version of this figure.

required for stellar evolution calculations affect the theoretical isochrones. The results may be represented as confidence contours in the color-magnitude diagram. Full details are given in Bjork & Chaboyer (2006). Figure 10 illustrates the large uncertainty in the predicted colors of the MSTO for a given age and metallicity, by comparing the Monte Carlo isochrones to standard isochrones with different ages. The uncertainty in the theoretical calculation of the MSTO color leads to an error of approximately ± 2 Gyr ($1\ \sigma$). In contrast, theoretical uncertainty in the MSTO luminosity is considerably lower, of the order of ± 1 Gyr.

The largest uncertainty in the determination of globular cluster ages based upon the MSTO luminosity is the distance scale for Population II objects. A 1% error in the distance leads to a $\simeq 2\%$ error in the derived age (e.g., Chaboyer et al. 1996). *SIM* will be able to determine distances to globular clusters and other stars in the halo with unprecedented accuracy, thereby significantly reducing the uncertainty in the derived ages of metal-poor stars. Table 5 provides basic data on the 21 globular clusters that will be observed with *SIM*. These clusters were chosen based upon the following properties: (a) distance from the Sun, (b) metallicity, (c) reddening, and (d) whether the cluster is thought to belong to the Old Halo (OH), Young Halo (YH), or Thick Disk (TD) (column [3]). This grouping of globular clusters is based on their kinematics, metallicity, and horizontal branch morphology (Da Costa & Armandroff 1995).

For each globular cluster, we plan to observe approximately six red giant branch stars with an accuracy of 7 μas. We will average together the parallaxes of all the confirmed members to obtain a final parallax to the cluster with an accuracy of 4 μas, which supported by the expected accuracy of the *SIM* grid of about 3 μas. This will determine the distances to the individual globular clusters with an accuracy of 1% to 5% (column [7] in Table 5), which is a factor of 2 to 10 times better than currently achieved. The current uncertainties in the globular

TABLE 5
TARGET GLOBULAR CLUSTERS

NGC (1)	[Fe/H] (2)	Group (3)	Nrr (4)	E $(B-V)$ (5)	$D_\odot$ (kpc) (6)	σ_D (%) (7)	σ_{age} (%) (8)
6341	−2.29	OH	25	0.02	8.1	4	8
7099	−2.12	OH	10	0.03	7.9	4	8
4590	−2.06	YH	41	0.04	10.1	5	10
6397	−1.95	OH	…	0.18	2.2	1	5
6541	−1.83	OH	…	0.12	7.4	3	8
6809	−1.81	OH	10	0.07	5.3	2	6
5139	−1.62	OH	152	0.12	5.1	2	7
5272	−1.57	YH	260	0.01	10.0	5	10
6752	−1.55	OH	…	0.04	3.9	2	5
6205	−1.54	OH	3	0.02	7.0	3	7
6218	−1.48	OH	…	0.19	4.7	2	8
3201	−1.48	YH	85	0.21	5.1	2	8
5904	−1.29	OH	123	0.03	7.3	3	8
288	−1.24	OH	…	0.03	8.1	4	8
362	−1.16	YH	13	0.05	8.3	4	8
6723	−1.12	OH	29	0.05	8.6	4	9
6362	−1.06	OH	33	0.09	7.5	3	8
6652	−0.85	YH	…	0.09	9.4	4	10
104	−0.76	TD	1	0.05	4.3	2	5
6838	−0.73	TD	…	0.25	3.8	2	7
6352	−0.70	TD	…	0.21	5.6	3	9

NOTES.—Values taken from the Harris (1996) compilation, unless otherwise noted.

Explanations of individual columns: Group: OH = Old Halo, YH = Young Halo, D = Thick Disk (Da Costa & Armandroff 1995); Nrr—Number of RR Lyrae stars in the cluster (from compilation by B. W. Carney 2003, private communication); $D_\odot$—distance from the Sun; these values are uncertain by $\pm 10\%$; σ_π—percent uncertainty in the parallax, assuming 4.6 μas accuracy; σ_{age}—percent uncertainty in the age estimate including contributions due to uncertainties in the distance determination, reddening, photometric zero point, and metallicity determination.

cluster distance scale is dominated by systematic errors, while our distance scale will be dominated by random errors. This will allow us to average together the age of the most metal-poor globular clusters in our sample, thereby significantly reducing the uncertainty in the determination of the mean age of the oldest globular clusters.

In order to determine the expected accuracy in our absolute age estimate for the oldest, most metal-poor globular clusters, a Monte Carlo simulation was performed, similar to that outlined in Bjork & Chaboyer (2006). In this simulation, we varied all of the sources of error in our age determinations within their expected uncertainties, including the reddening determinations, photometric zero-points, parallax uncertainties, uncertainties in the exact composition of the stars (helium abundance, oxygen abundance and iron abundances), and uncertainties in the stellar models (including nuclear reaction rates, opacities, treatment of convection, model atmospheres, and diffusion). The distribution function for each of the individual input parameters was determined by a careful consideration of the expected uncertainties in the various quantities when *SIM* delivers its final parallaxes. The simulation showed that we will determine the absolute age of the oldest globular clusters to an accuracy of $\pm 3\%$, or ± 0.4 Gyr.

To study the relative age distribution of stars in the halo, *SIM* will observe 60 metal-poor turnoff or subgiant branch stars in the field. To illustrate the expected accuracy of our relative age determinations for the field halo stars and the globular clusters in our *SIM* program, we ran a Monte Carlo simulation, which allowed the true distance to the object to vary within its current estimated uncertainties, and which took into account the uncertainties in the *SIM* distance and reddening determinations and in the chemical composition of the stars. We find that the field stars will have a typical uncertainty of ± 0.6 Gyr, while the globular cluster ages will have an error of ± 0.9 Gyr (column [8] in Table 5). From these simulations we conclude that we will be able to detect age differences of the order of 1 Gyr between various stellar populations.

10. EXPLORING GALACTIC STELLAR POPULATIONS AND DARK MATTER ON GALACTIC SCALES

N-body simulations of the formation of structure in the universe in the presence of dark matter (and dark energy) show galaxies (and all large structures) building up hierarchically. The active merging history on all scales demonstrated by high-resolution, cold dark matter (CDM) numerical simulations has had remarkable success in matching the observed properties of the largest structures in the universe, like galaxy clusters, but are a challenge to reconcile with the observed properties of structures on galactic scales. The Milky Way and its satellite system is a particularly important laboratory for testing specific predictions of the CDM models, most especially because high accuracy astrometric observations enabled by *SIM* will allow definitive tests of dynamical effects specifically predicted by CDM.

SIM will make possible unprecedented opportunities to explore stellar dynamics with a precision that will allow critical measurements of gravitational potentials from Local Group size (see Section 11) to Milky Way, dwarf galaxy, and star cluster scales. We outline in more detail below several specific important *SIM* contributions that will bear directly on tests of dark matter (DM) and the evolution of galaxies like the Milky Way and its stellar populations.

10.1. Probing the Outer Halo with Tidal Tails

At large distances from the Galactic center (>30 kpc), the stellar distribution is far from homogeneous. Standard methods of estimating the depth of the Milky Way's gravitational potential using a tracer population whose orbits are assumed to be random and well-mixed would be systematically biased under these circumstances (e.g., Yencho et al. 2006). However, these inhomogeneities themselves are thought to have formed through the infalling and disruption of satellites, and therefore we actually have more information about the stars in these lumps than in a truly random sample. For example, we know that stars that are clearly part of a stream of debris were once all part of the same satellite. We can use this knowledge to map the mass distribution in the Galaxy. If we could measure the distances, angular positions, line-of-sight velocities and proper motions of debris stars, we could integrate their orbits backward in some assumed Galactic potential. Only in the correct potential will the path of the stream stars ever coincide in time, position, and velocity with that of the satellite (see Fig. 11).

SIM measurements combined with ground-based line-of-sight velocities should provide everything needed to undertake the experiment; however, obtaining precision trigonometric parallaxes of numerous distant debris stars would involve a significant investment of *SIM* observing time. On the other hand, distances could be estimated either by using accurate photometric parallaxes (calibrated with *SIM*) for red giant or horizontal branch stars or by exploiting our expectations for the orbital energy distribution in the debris. In the latter case, we know the mean offset of the leading and trailing debris from the satellite's own orbital energy (Johnston 1998) and hence can solve the energy equation for the distances to stars in each of these groups by assuming each has this mean energy (Johnston et al. 1999). This should be more accurate than using a photometric parallax, so long as the offset in orbital energy is less than $\delta d(d\Phi/dr)$, where δd is the uncertainty in distances and $d\Phi/dr$ is the gradient in the assumed Galactic potential.

If we find a coherent stream but not the associated satellite, the same techniques apply, but with the parent satellite's position and velocity as additional free parameters. The usefulness of Galactic tidal streams for probing the Milky Way potential has long been recognized, and the results of astrometric space missions to provide the last two dimensions of phase-space

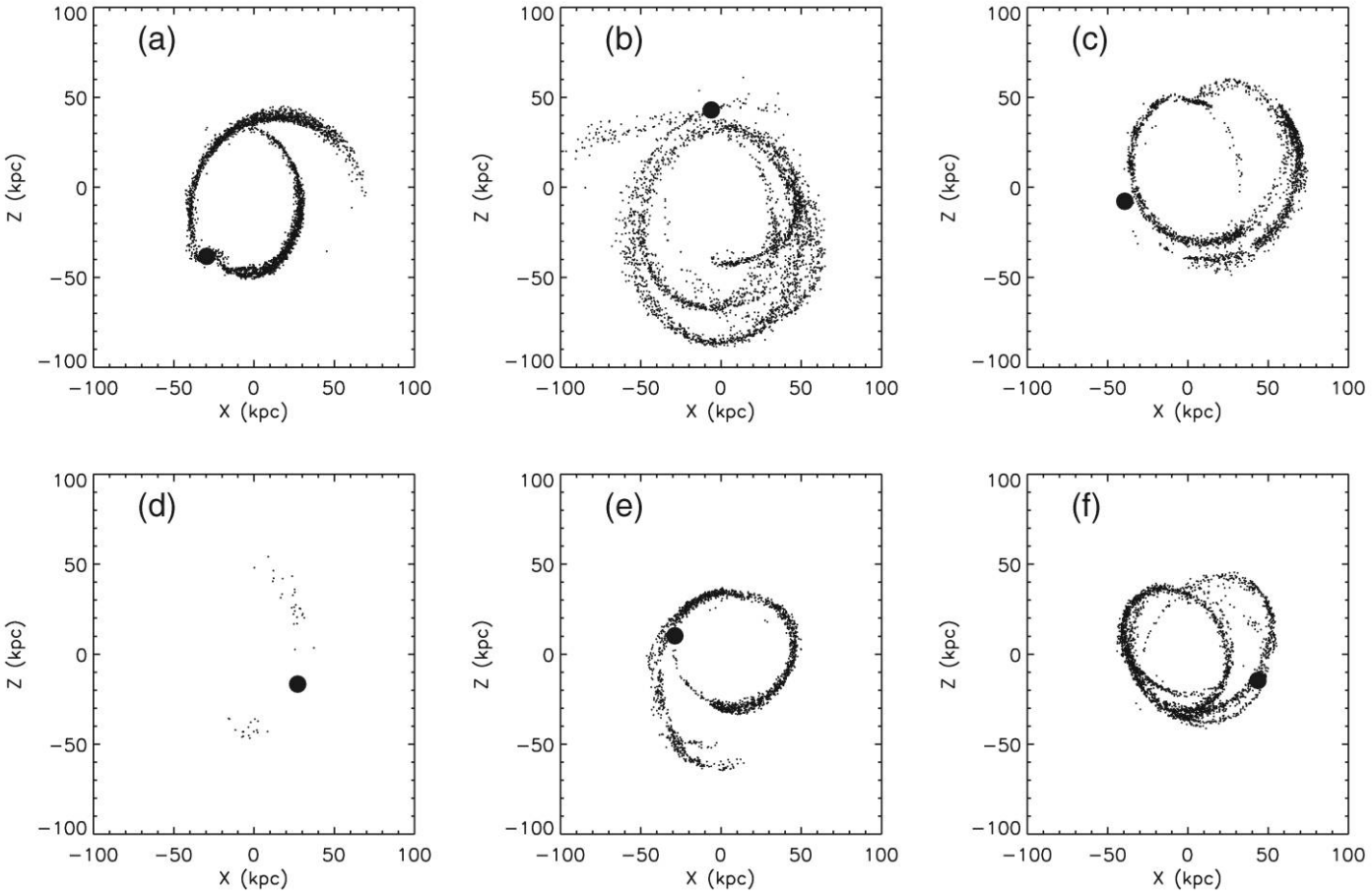

FIG. 11.—Demonstration of the sensitivity of *SIM* to the Galactic potential using stellar streams. A Sagittarius-like tidal stream was created by the disruption of a dwarf satellite in a time-independent Galactic potential through a semianalytical N-body simulation (Law et al. 2005). This resulted in the tidal stream demonstrated in panel (*a*). Complete 6D phase-space information on stars in the stream will be derived using the astrometric data from *SIM*. With such data in hand, guesses may be made on the strength and shape of the Galactic potential, and the orbits of the individual stars in the tidal streams run backward under these assumed potentials. Panels (*b*) and (*c*) demonstrate what happens when the strength of the Galactic potential is underestimated by varying degrees: When the orbits are run backward, the tidal stream stars orbit at too large a radius and do not converge to a common phase-space position. In panels (*e*) and (*f*) the strength of the Galactic potential has been overestimated, and when the clock is run backward the tidal stream stars assume orbits that are too small and once again do not converge on a common phase-space position. In panel (*d*) a Galactic potential of the correct strength was guessed, and when the stream star orbits are run backward, the tidal stream stars collect back into the core of the parent satellite.

information for stream stars has been eagerly anticipated (e.g., Johnston et al. 1999; Peñarrubia et al. 2006).

Applying this method to simulated data observed with the μas yr^{-1} precision proper motions possible with *SIM* and km s^{-1} radial velocities suggests that 1% accuracies on Galactic parameters (such as the flattening of the potential and circular speed at the solar circle) can be achieved with tidal tail samples as small as 100 stars (Johnston et al. 1999; Majewski et al. 2006). Dynamical friction is not an important additional consideration if the change in the energy of the satellite's orbit in $N_{\rm orb}$ orbits is less than the range in the energies of debris particles. For $N_{\rm orb} = 3$, this condition is met for all satellites except the LMC, SMC, and Sagittarius. Evolution of the Galactic potential does not affect the current positions of tidal debris, which respond adiabatically to changes in the potential and therefore yield direct information on the *present* Galactic mass distribution independent of how it grew (Peñarrubia et al. 2006).

Ideally, stars from several different tails at a variety of distances from the Galactic center and orientations with respect to the Galactic disk would be probed. It is also important to sample the tidal tails out to points where stars were torn from the satellite at least one radial orbit ago and hence have experienced the full range of Galactic potential along the orbit (Johnston 2001). Finally, the stars also need to have proper motions measured sufficiently accurately that the difference between their own and their parent satellite's orbits are detectable—this translates to requiring proper motions of the order of 100 μas yr^{-1} for Sgr but 10 μas yr^{-1} for satellites that are farther away.

The possible existence of a significant fraction of the halo in the form of dark satellites has been debated in recent years

(Moore et al. 1999; Klypin et al. 1999). These putative dark subhalos could scatter stars in tidal tails, possibly compromising their use as large-scale potential probes, but astrometric measurements of stars in these tails could, on the other hand, be used to assess the importance of substructure (Ibata et al. 2002; Johnston et al. 2002). Early tests of such scattering using only radial velocities of the Sgr stream suggest a Milky Way halo smoother than predicted (Majewski et al. 2004), but this represents debris from a satellite with an already sizable intrinsic velocity dispersion. Because scattering from subhalos should be most obvious on the narrowest, coldest tails (e.g., from globular clusters) these could be used to probe the DM substructures, whereas the stars in tails of satellite galaxies such as Sgr, with larger dispersions initially and so less obviously affected, can still be used as global probes of the Galactic potential.

In the last few years a number of well-defined Galactic tidal tails have been discovered at a wide range of radii and, with *SIM*, can be used to trace the Galactic mass distribution as far out as the virial radius with an unprecedented level of detail and accuracy. For example, M-giant stars associated with Sgr have now been traced entirely around the Galaxy (Majewski et al. 2003), the globular clusters Pal 5 and NGC 5466 both have tidal tails traced to over 20° from their centers (Grillmair & Johnson 2006; Belokurov et al. 2006a; Grillmair & Dionatos 2006a), two apparently cold streams over 60° long have been discovered in the Sloan Digital Sky Survey (Grillmair & Dionatos 2006b; Grillmair 2006a; Belokurov et al. 2006b), and the nearby "Anticenter," or "Monoceros" stream has been shown to be broken up into dynamically colder "tributaries" (Grillmair 2006b). In the outer Galaxy, there are suggestions of debris associated with the Ursa Minor, Carina, Sculptor, and Leo I dSphs (Palma et al. 2003; Majewski et al. 2005; Westfall et al. 2006; Muñoz et al. 2006b; Sohn et al. 2007), and evidence for outer halo debris from the Sgr dSph (Pakzad et al. 2004). With *SIM*, for the first time it will be possible to probe the full three-dimensional shape, density profile, and extent of (and substructure within) an individual DM halo.

10.2. Hypervelocity Stars

Hypervelocity stars (HVS) were postulated by Hills (1988), who showed that the disruption of a close binary star system deep in the potential well of a massive black hole could eject one member of the binary at speeds exceeding $1000\ \mathrm{km\,s^{-1}}$. HVSs can also be produced by the interaction of a single star with a binary black hole (Yu & Tremaine 2003). These remarkable objects have now been discovered: Brown et al. (2006) report on five stars with Galactocentric velocities between 550 and $720\ \mathrm{km\,s^{-1}}$ and argue persuasively that these are HVSs in the sense that they are "unbound stars with an extreme velocity that can be explained only by dynamical ejection associated with a massive black hole." It is likely that many more HVSs will be discovered in the next few years, both by ground-based surveys and by the *Gaia* mission.

The acid test of whether these remarkable objects are HVSs is whether their proper motions are consistent with trajectories that lead back to the Galactic center. The magnitudes of the known HVSs range from 16 to 20, so their proper motions should be measurable by *SIM* with an accuracy of a few $\mu\mathrm{as\,yr^{-1}}$. At the estimated distances of these stars (20 to 100 kpc) a velocity of $500\ \mathrm{km\,s^{-1}}$ corresponds to a proper motion of 1000 to $5000\ \mu\mathrm{as\,yr^{-1}}$, so *SIM* should be able to determine the orientation of their velocity vectors to better than 1%.

If these measurements confirm that the HVSs come from the Galactic center, then we can do more. For many stars, *SIM* will be able to measure all six phase-space coordinates, but for HVSs, the orbits are far more tightly constrained because we know the point of origin. Gnedin et al. (2005) have pointed out that the nonspherical shape of the Galactic potential—due in part to the flattened disk and in part to the triaxial dark halo—will induce nonradial velocities in the HVSs of 5–$10\ \mathrm{km\,s^{-1}}$, corresponding to 10–$100\ \mu\mathrm{as\,yr^{-1}}$. Each HVS thus provides an independent constraint on the potential, as well as on the solar circular speed and distance to the Galactic center.

10.3. Dark Matter within Dwarf Galaxies

Dwarf galaxies, and particularly dSph galaxies, are the most DM-dominated systems known to exist. Due to the small scale sizes (~1 kpc) and large total mass-to-light ratios (approaching $100\ M_\odot/L_\odot$), the dSphs provide the opportunity to study the structure of DM halos on the smallest scales. The internal structure of the dSphs, as well as their commonality within the Local Group, make possible a new approach to determining the physical nature of DM with *SIM*.

CDM particles have negligible velocity dispersion and very large central phase-space density, resulting in cuspy density profiles over observable scales (Navarro et al. 1997; Moore et al. 1998). Warm dark matter (WDM), in contrast, has smaller central phase-space density, so that density profiles saturate to form constant central cores. Due to the small scale sizes of dSphs, if a core is a result of DM physics then the cores occupy a large fraction of the virial radii, which makes the cores in dSphs more observationally accessible than those in any other galaxy type. Using dSph central velocity dispersions, earlier constraints on dSph cores have excluded extremely warm DM, such as standard massive neutrinos (Lin & Faber 1983; Gerhard & Spergel 1992). More recent studies of the Fornax dSph provide strong constraints on the properties of sterile neutrino DM (Goerdt et al. 2006; Strigari et al. 2006).

The past decade has seen substantial progress in measuring radial velocities for large numbers of stars in nearby dSph galaxies (Armandroff, Olszewski & Pryor 1995; Tolstoy et al. 2004; Wilkinson et al. 2004; Muñoz et al. 2005, 2006a; Walker et al. 2006). In all dSphs, the projected RV dispersion profiles are roughly flat as far out as they can be followed, with mean

values between 7 and 12 km s^{-1}. From these measurements, the DM density profiles are obtained by assuming dynamical equilibrium and solving the Jeans equation (Richstone & Tremaine 1986). In this analysis, the surface density of the stellar distribution is required, and in all dSphs these stellar distributions are well-fitted by King profiles, modulo slight variations. In the context of equilibrium models, the measured velocity profiles typically imply at least an order of magnitude more mass in DM than in stars, and imply mass-luminosity ratios that increase with radius—in some cases quite substantially (e.g., Kleyna et al. 2002)—though at large radii tidal effects may complicate this picture (Kuhn 1993; Kroupa 1997; Muñoz et al. 2005; Muñoz et al. 2006b; Sohn et al. 2007). Knowing whether mass follows light in dSphs or the luminous components lie within large extended halos is critical to establishing the regulatory mechanisms that inhibit the formation of galaxies in all subhalos (§ 10.1).

Unfortunately, for equilibrium models the solutions to the Jeans equation are degenerate in that the dark matter density profiles are equally well-fitted by both cores or cusps. In particular, there is a strong degeneracy between the inner slope of the DM density profile and the velocity anisotropy, β, of the stellar orbits; this leads to a strong dependency of the derived masses on β. Radial velocities alone cannot break this degeneracy (Fig. 12), even if the present samples of radial velocities are increased to several thousand stars (Strigari et al. 2007). The problem is further compounded if we add triaxiality, Galactic substructure, and dSph orbital shapes to the allowable range of parameters.

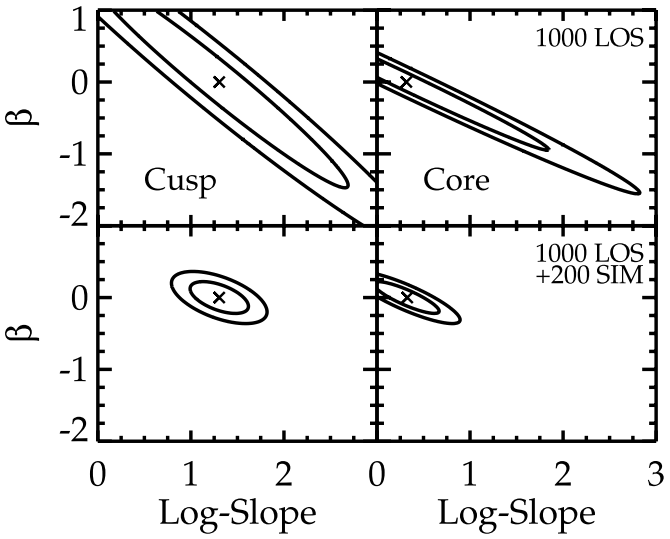

FIG. 12.—Demonstration of the ability to recover information on the nature of dark matter using observations of dSph stars, from analytical modeling by Strigari et al. (2007). Each panel shows the the 68% and 95% confidence regions for the errors in the measured dark halo density profile (log) slope (measured at twice the King core radius) and velocity anisotropy parameter β for a particular dSph; small crosses indicate the fiducial input model values. In the upper plots, derived from line-of-sight (RV) velocities for 1000 stars, the two parameters are highly degenerate, for both a cusp model (*left panel*), and core model (*right panel*). The addition of 200 proper motions from *SIM* providing 5 km s^{-1} precision transverse velocities (*lower panels*) dramatically reduces the uncertainty in both parameters.

The only way to break the mass-anisotropy degeneracy is to measure more phase-space coordinates per star. The Jeans equation written for the transverse velocity dispersion probes the anisotropy parameter differently than that for the radial-velocity dispersion. Thus, combining proper motions with the present samples of radial velocities will provide orthogonal constraints and has the prospect to break the anisotropy-inner slope degeneracy.

The most promising dSphs for this experiment will be the nearby (60–90 kpc away) systems Sculptor, Draco, Ursa Minor, Sextans, and Bootes, for which the upper giant branches require proper motions of stars with $V \simeq 19$. The latter four of these dSphs include the most DM-dominated systems known (Mateo 1998; Muñoz et al. 2006a), as well as a system with a more modest M/L (Sculptor). While Sagittarius is closer still, its strong interaction with the Galaxy and obvious tidal distortions indicate a system clearly not in dynamical equilibrium; thus it offers an interesting, possibly alternative case study for establishing the internal dynamical effects of tidal interaction. To sample the velocity dispersions properly will require proper motions of > 100 stars per galaxy with accuracies of 7 km s^{-1} or better (less than 15 μas yr^{-1}). Detailed analysis shows that with about 200 radial velocities and 200 transverse velocities of this precision, it will be possible to reduce the error on the log-slope of the dark matter density profile to about 0.1 (Strigari et al. 2007). This is an order of magnitude smaller than the errors attainable from a sample of 1000 radial velocities, and sensitive enough to rule out nearly all WDM models (see Fig. 12). Obtaining the required transverse velocities, while well beyond the capabilities of *Gaia*, is well matched to the projected performance of *SIM*.

10.4. Galactic Satellite Proper Motions

Knowing the bulk proper motions of the dSphs is key to modeling not only their structure and evolution, but whether they correspond to the predicted dark subhalos and how they relate to the two primary solutions to the missing satellites problem, i.e., the "very massive dwarf" versus the "very old dwarf" pictures (Mashchenko et al. 2006). The derived orbits of the dSphs can be compared directly to predictions for the orbits of infalling DM substructure (Ghigna et al. 1998; Benson 2005; Zentner et al. 2005). These orbits can also be used to test for the reality of the purported dynamical families (e.g., Lynden-Bell & Lynden-Bell 1995; Palma et al. 2002) hypothesized to be the product of the breakup of larger systems (Kunkel 1979; Lynden-Bell 1982), to determine the possible connection of their apparent alignment to local filaments (Libeskind et al. 2005),

and to verify whether distant systems like Leo I (e.g., Sohn et al. 2007) are bound to the Milky Way and can be used as test particles for measuring the mass profile of the Galaxy.

The proper motions of the more distant satellites of the Milky Way are expected to be on the order of hundreds of μas yr^{-1}, and to derive transverse velocities good to $\sim$10 km s^{-1} ($\sim$10%) requires a bulk proper-motion accuracy of $\sim$10 μas yr^{-1} for the most distant satellites (Leo I, Leo II, Canes Venatici), in which the brightest giant stars have $V \sim 19.5$. The constraints are slightly more relaxed for satellites at roughly 100 kpc distances, $\sim$20 μas yr^{-1} for systems with brightest stars at $V \sim 17.5$. Such measurements for individual stars are well within the capabilities of *SIM*, which could derive the desired bulk motions for Galactic satellites with only a handful of stars per system (suitably placed to account for rotation and other internal motions, § 10.3).

With much less per star precision, but many more stars, attempts to measure dSph galaxy proper motions from the ground with long time baselines (e.g., Scholz & Irwin 1994; Schweitzer et al. 1995; Schweitzer et al. 1997), with the *Hubble Space Telescope* and short time baselines (Piatek et al. 2002), and with combinations of both ground and *HST* data (Dinescu et al. 2004) still lead to bulk motions measurements with uncertainties of order the size of the motion of the dSph, and with significantly different results (e.g., two recent measures of the proper motion of the Fornax dSph differ at the 2 σ level (Dinescu et al. 2004 vs. Piatek et al. 2002). Even for the closer Magellanic Clouds, there still remain significant and disturbing variations in the derived proper motions (Jones et al. 1994; Kroupa et al. 1994; Kroupa & Bastian 1997; Anguita et al. 2000; Momany & Zaggia 2005; Kallivayalil et al. 2006; Pedreros et al. 2006). These inconsistencies not only reflect the difficulty of beating down random uncertainties with $\sqrt{N}$ statistics in systems with limited numbers of sufficiently bright stars—a problem that will be severe in the most recently discovered dSphs, where the populations of giant stars number at most in the tens (e.g., Willman et al. 2005b; Belokurov et al. 2006c; Zucker et al. 2006)—but also in dealing with numerous systematic problems, such as establishing absolute proper-motion zero points (see discussion in Majewski 1992; Dinescu et al. 2004). With its μas-level extragalactic astrometric reference tie-in, and intrinsic per-star proper-motion precision, *SIM* will make definitive measures of the proper motions of the Galactic satellites that will overcome the previous complications faced by satellite proper-motion studies.

The same stellar precisions conferred by *SIM* to the study of distant dwarf satellites and star clusters (§ 10.5) may also be applied to proper motions of individual distant field stars, whose full space motions can be derived and used as additional point mass probes of the Galactic potential, whether they are part of tidal streams or a well-mixed halo population.

10.5. Globular Cluster Proper Motions

Globular clusters, which have a spatial distribution that spans the dimensions of the Milky Way and which readily lend themselves to abundance and age assessments, have long served as a cornerstone stellar population for understanding galaxy evolution. Several distinct populations of globular clusters are known: a disk (Armandroff 1989) and/or bulge (Minniti 1996) population and at least two kinds of halo clusters (Zinn 1996). Since Searle & Zinn (1978), the notion that halo globular clusters were formed in separate environments—"protogalactic fragments"—later accreted by the Milky Way over an extended period of time has been a central thesis of Galactic structure studies. More recently, direct substantiation of the hypothesis for at least some clusters has come from the identification of clusters that are parts of the Sagittarius stream (Ibata et al. 1995; Dinescu et al. 2000; Majewski et al. 2004; Bellazzini et al. 2002, 2003) and the Monoceros structure (Crane et al. 2003; Frinchaboy et al. 2004; Bellazzini et al. 2004). These systems represent more obvious "dynamical families" associated with recent mergers having readily identifiable debris streams, but presumably such mergers were even more common in the early Galaxy. Ancient mergers may have tenuous stellar streams today, and their identification will require 6D phase-space information to locate objects of common energy and angular momentum. Tracing ancient mergers via their identified progeny will provide key insights into the evolution of substructure and star clusters in hierarchical cosmologies (Prieto & Gnedin 2006).

Of course, halo globular clusters will serve as valuable test particles for determining the halo potential, but these cluster data will also play an essential role in understanding clusters as stellar systems. The dynamical evolution of small stellar systems is largely determined by external influences such as disk and bulge shocks (e.g., Gnedin et al. 1999), so determining cluster orbits by measuring their proper motions will dramatically improve our understanding of their evolution and address the long-standing issue of whether the present population of these systems is the surviving remnant of a much larger initial population. The formation of globular clusters remains a mystery that can be better constrained by understanding cluster orbits. By obtaining definitive orbital data for the entire Galactic globular cluster system, *SIM* will clarify the range of extant cluster-satellite dynamical histories and how the Galactic ensemble evolved and depopulated.

At present, $\lesssim$25% of Galactic globular clusters have had *any* attempt at a measured proper motion, and reliable data generally exist only for those clusters closest to the Sun (see summaries in Dinescu et al. 1999; Palma et al. 2002). As in the case of the Galactic satellites (§ 10.4), even in the rare cases when appropriate data for proper-motion measurements exist, analyses are hampered by critical systematic errors, notably the tie-in to an inertial reference frame. Galaxies yield unreliable centroids and QSOs have too low of a sky density at typical magnitudes probed. Moreover, most of the outer halo globular

clusters, including some newly discovered examples (Carraro 2005; Willman et al. 2005a) have very sparse giant branches, reducing the effectiveness of averaging the motions of numerous members to obtain a precision bulk motion. *SIM* will immediately resolve these problems.

11. ASTROMETRIC MICROLENSING

What would an unbiased census of Galactic objects, dark and luminous, reveal? At a minimum, it would yield the frequency of black holes, neutron stars, and old brown dwarfs, which are either completely dark or so dim that they defy detection by normal methods. It might also find a significant component of the dark matter, although the majority of dark matter cannot be in the form of compact objects (Alcock et al. 2000; Tisserand et al. 2007). The only known way to conduct such a census is to put a high-precision astrometry telescope in solar orbit.

Masses of astronomical bodies can be measured only by the deflections they induce on other objects, typically planets and moons that orbit solar-system bodies and binary companions that orbit other stars. Masses of luminous isolated field stars can be estimated from their photometric and spectroscopic properties by calibrating these against similar objects in bound systems. Hence, photometric surveys yield a reasonably good mass census of luminous objects in the Galaxy.

Dark objects like black holes are another matter. Mass measurements of isolated field black holes can be obtained only by their deflection of light from more distant luminous objects. Indeed, it is difficult to even detect isolated black holes by any other effect. However, to go from detection to mass measurement (and therefore positive identification) of a black hole is quite challenging.

Gravitational microlensing experiments currently detect about 500 microlensing events per year. The vast majority of the lenses are ordinary stars, whose gravity deflects (and so magnifies) the light of a more distant "source star." As the source gets closer to and farther from the projected position of the lens, its magnification, A, waxes and wanes according to the Einstein (1936) formula

$$A(u) = \frac{u^2+2}{u\sqrt{u^2+4}}, \qquad u(t) = \sqrt{u_0^2 + \left(\frac{t-t_0}{t_{\rm E}}\right)^2}, \tag{4}$$

where u is the source-lens angular separation (normalized to the so-called Einstein radius $\theta_{\rm E}$), t_0 is the time of maximum magnification (when the separation is u_0) and $t_{\rm E}$ is the Einstein radius crossing time, i.e., $t_{\rm E} = \theta_{\rm E}/\mu$, where μ is the lens-source relative proper motion. The mass M cannot be directly inferred from most events because the only measurable parameter that it enters is $t_{\rm E}$, and this is a degenerate combination of M, μ, and the source-lens relative $\pi_{\rm rel}$:

$$t_{\rm E} = \frac{\theta_{\rm E}}{\mu}, \qquad \theta_{\rm E} = \sqrt{\kappa M \pi_{\rm rel}}, \tag{5}$$

where $\kappa \equiv 4G/(c^2\ {\rm AU}) \sim 8\ {\rm mas}\, M_\odot^{-1}$.

It follows immediately that to determine M, one must measure *three* parameters, of which only one ($t_{\rm E}$) is routinely derived from microlensing events. Another such parameter is $\theta_{\rm E}$, which could be routinely measured from the image positions, if it were possible to resolve their $O({\rm mas})$ separation. A third is the "microlens parallax" $\pi_{\rm E} = \pi_{\rm rel}/\theta_{\rm E}$. Hence the lens mass can be extracted from $\theta_{\rm E}$ and $\pi_{\rm E}$ alone (see, e.g., Gould 2000):

$$M = \frac{\theta_{\rm E}}{\kappa \pi_{\rm E}}. \tag{6}$$

Just as $\theta_{\rm E}$ is the Einstein radius projected onto the plane of the sky, $\pi_{\rm E}$ is related to $\tilde{r}_{\rm E} \equiv {\rm AU}/\pi_{\rm E}$, the Einstein radius projected onto the observer plane. And just as $\theta_{\rm E}$ could, in principle, be measured by resolving the two images on the sky, $\pi_{\rm E}$ could be routinely measured by simultaneously observing the event from two locations separated by $O(\tilde{r}_{\rm E})$ (Refsdal 1966; Gould 1995). "Routine" measurement of both $\pi_{\rm E}$ and $\theta_{\rm E}$ is essential. At this writing, there have been a few dozen measurements of these parameters separately (e.g., Poindexter 2005), but only one very exceptional microlensing event for which both were measured together with sufficient precision to obtain an accurate mass (Gould et al. 2005).

In fact, such routine measurements are possible by placing an accurate astrometric and photometric telescope in solar orbit. For current microlensing experiments carried out against the dense star fields of the Galactic bulge, $\pi_{\rm rel} \sim 40\ \mu$as, so for stellar masses, $\theta_{\rm E} \sim 500\ \mu$as and $\tilde{r}_{\rm E} \sim 10$ AU. Hence, a satellite in solar orbit would be an appreciable fraction of an Einstein radius from the Earth. As a result, the photometric event described by equation (4) would look substantially different than it would from the ground. From this difference, one could infer $\tilde{r}_{\rm E}$ (and so $\pi_{\rm E}$).

Determining $\theta_{\rm E}$ is more difficult. As mentioned above, this would be straightforward if one could resolve the separate images, but to carry this out routinely (i.e., for small as well as large values of $\theta_{\rm E}$) would require larger baselines than are likely to be available in next-generation instruments. Rather, one must appeal to a more subtle effect, the deflection of the *centroid* of the two lensed images. This deflection is given by (Miyamoto & Yoshii 1995; Høg et al. 1995; Walker 1995)

$$\Delta\theta = \frac{u}{u^2+2}\theta_{\rm E}. \tag{7}$$

Simple differentiation shows that this achieves a maximum at $u = \sqrt{2}$, for which $\Delta\theta = \theta_{\rm E}/\sqrt{8}$, roughly $1/3$ of an Einstein radius. Hence, if the interferometer can achieve an accuracy of O (10 μas) *at the time when this deflection is the greatest*, then $\theta_{\rm E}$ can be measured to a few percent.

There are some subtleties as well as some challenges. Satellite measurements of $\tilde{r}_{\rm E}$ are subject to a fourfold discrete degeneracy, which can only be resolved by appealing to higher-order

effects (Gould 1995). It is not enough to measure the centroid location to determine the astrometric deflection: one must also know the undeflected position to which the measured position is to be compared, and this can only be found by extrapolating back from late-time astrometry. And the precision of the mass measurement depends directly on the signal-to-noise ratio of the underlying photometric and astrometric measurements. This is important because space-based astrometric telescopes are likely to be photon challenged and so to require relatively bright (and hence rare) microlensing events to provide accurate mass measurements. Gould & Salim (1999) estimated that $\simeq$1200 hours of *SIM* time would yield 5% mass measurements for about 200 microlenses. Most of these lenses will be stars, but at least a few percent are likely to be black holes, and several times more are likely to be other dark or dim objects like neutron stars, old white dwarfs, and old brown dwarfs. Since such a census is completely new, it may also turn up unexpected objects.

12. DYNAMICS OF GALAXY MOTIONS: NUMERICAL ACTION AND *SIM*

If one could measure the proper motions of galaxies with global accuracies of a few microarcseconds per year, one could obtain another two components of phase space with which to construct flow models and determine histories and masses for galaxies and galactic groups. For a galaxy 1 Mpc away, $4\ \mu\mathrm{as\,yr^{-1}}$ corresponds to $19\ \mathrm{km\,s^{-1}}$ transverse motion, which is small compared to the expected transverse motions in the field, $\sim$100 $\mathrm{km\,s^{-1}}$. With an instrument such as *SIM*, one could measure accurate positions of a few dozen stars, with $V < 20$, in each galaxy and after $\sim$5 yr obtain proper motions with adequate accuracy. For a typical dwarf galaxy, after averaging randomly located stars, the contribution to the error from the internal motions would be only a few $\mathrm{km\,s^{-1}}$. For larger galaxies, simple rotation models, adjusted to the observed velocity profiles, can be removed from the motions for $< 20\ \mathrm{km\,s^{-1}}$ accuracy. There are 27 galaxies known (all within 5 Mpc) that have stars sufficiently bright.

Just beyond the outermost accessible 21 cm isophotes of galaxies, the dark matter distribution becomes unknown. Within the light-emitting parts of galaxies, rotation curves are flat and not falling according to Kepler's law, which implies that mass grows roughly linearly with radius. The total mass-to-light ratio depends critically on where this mass growth ends, but this is generally not observed. As a result, critical questions about dark matter on scales of galaxies to groups remain: Do dwarf galaxies have lower or higher mass-to-light ratios than regular galaxies? Do the dark matter halos of galaxies in groups merge into a common envelope? How do these mass components compare with the warmer dark matter particles smoothly distributed across superclusters or larger scales? At present, we can only detect dark matter through its gravitational effects; therefore, a careful study of the dynamics of nearby galaxies is one of the few ways to resolve these issues.

SIM measurements of the deviation from Hubble flow will be of lasting importance in the modeling of the formation of the Local Group, several nearby groups, and the plane of the Local Supercluster. Note that with *Gaia* only M31 and M33 have sufficient numbers of stars that are bright enough to attempt a proper-motion determination. If *Gaia* achieves $25\ \mu\mathrm{as\,yr^{-1}}$ (the currently stated goal) or $\sim$100 $\mathrm{km\,s^{-1}}$ at 1 Mpc, it will obtain only $\sim$1 σ detections for these two galaxies.

12.1. Peculiar Velocities

Most analyses of peculiar velocity flows have applied linear perturbation theory (appropriate for scales large enough that overdensities are $\ll 1$) to spherical infall (Peebles 1980). Peculiar velocity analysis (Shaya et al. 1992; Dekel et al. 1993; Pike & Hudson 2005) have proven the general concept that the observed velocity fields of galaxies result from the summed gravitational accelerations of overdensities over the age of the universe. They also agree with virial analyses of clusters and *WMAP* observations that indicate the existence of a substantial dark matter component strewn roughly where the galaxies are. But these studies apply only to large scales of > 10 Mpc, the scales of superclusters and large voids. Spherical infall (including "timing analysis" and "turnaround radius") studies do not presume low overdensities and have been applied to the smaller scale of the Local Group (Lynden-Bell & Lin 1977). These studies indicate mass-to-light ratios for the Local Group of roughly $M/L \sim 100\ M_\odot/L_\odot$, but the model is crude; nonradial motions and additional accelerations from tidal fields and subclumping are expected to be non-negligible and would substantially alter the deduced mass. A more complete treatment of solving for self-consistent complex orbits is required.

12.2. The Numerical Action Method

The application of the numerical action method (NAM; Peebles 1989) allows one to solve for the trajectories that result in the present distribution of galaxies (or more correctly, the centers of mass of the material that is presently in galaxies). By making use of the constraint that early time peculiar velocities were small, the problem becomes a boundary value differential equation with constraints at both early and late times. For each galaxy, a position on the sky, either a redshift or a distance and an assumed mass (usually taken to be the luminosity times an assumed mass-to-light ratio) are required inputs. In addition, one must presume an age of the universe (which is known from *WMAP*). Several studies comparing NAM with *N*-body solutions have shown that NAM can recover accurate orbits and positions or velocities (Branchini et al. 2002; Phelps 2002; Romano-Díaz et al. 2005). Sharpe et al. (2001) have used NAM to predict distances from redshifts and then compared these to Cepheid distance measures.

Figure 13 (*upper panel*) shows the output of a recent NAM calculation for the orbits of nearby galaxies and groups going out to the distance of the Virgo Cluster. The orbits are

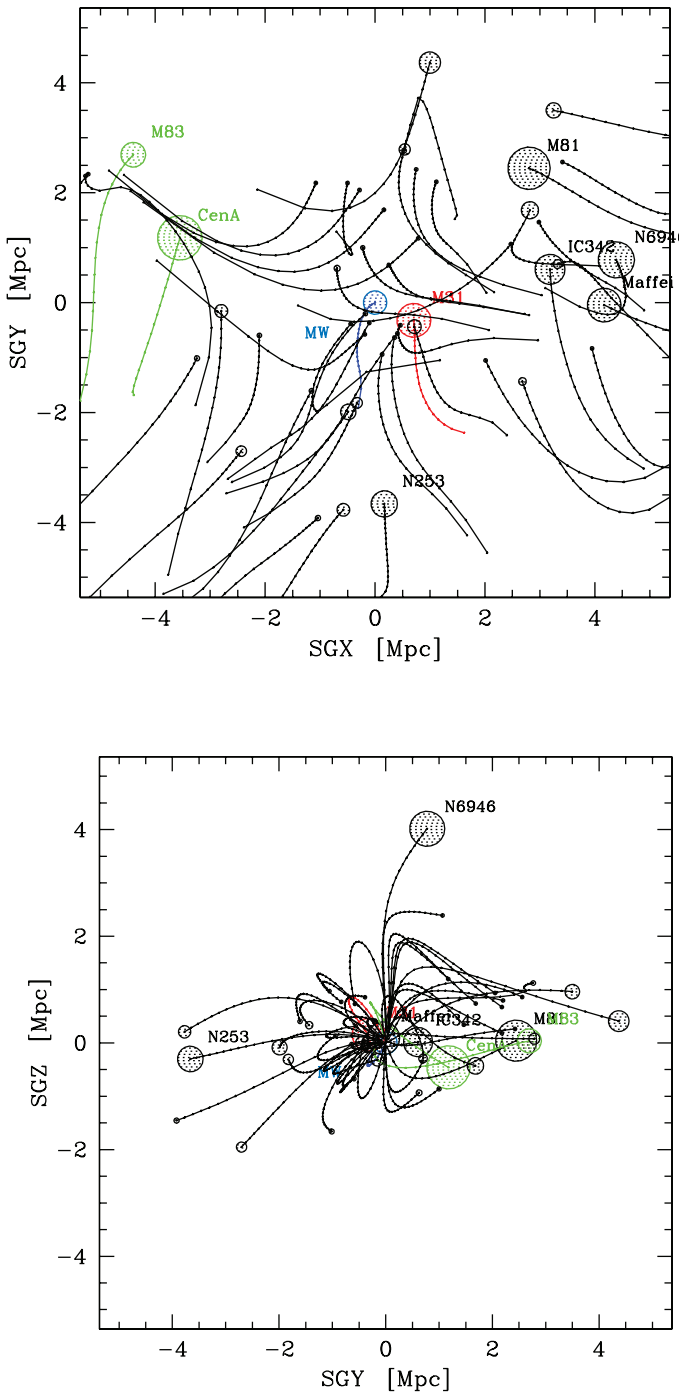

FIG. 13.—*Top*: Trajectories of nearby galaxies and groups going out to the distance of the Virgo Cluster from a numerical action method calculation with parameters $M/L = 90$ for spirals and 155 for ellipticals, $\Omega_m = 0.24$, $\Omega_\Lambda = 0.76$. The axes are in the supergalactic plane (SGX-SGY) in comoving coordinates. There are 21 time steps going from $z = 40$ to now. The large circle is placed at the present position and the radius is proportional to the square root of the mass. The present estimated distances were fixed and the present redshifts were unconstrained. *Bottom*: View of the galaxy trajectories, except that the coordinates here are real-space (proper) rather than comoving, and the axes are SGY-SGZ allowing a view of the collapse into a plane.

in comoving coordinates. This is just a single solution of a set of several solutions using present 3D positions as inputs. The four massive objects (Virgo Cluster, Coma Group, Cen A Group, and M 31) have been adjusted to provide best fit to observed redshifts. Figure 13 (*lower panel*) is the same calculation, but now the coordinates are real-space rather than comoving, and the supergalactic plane is viewed edge-on. It appears that the plane of the Local Supercluster was not created by matter raining in from large distances but rather that material has never achieved great heights away from the plane.

Assuming a constant mass-to-light ratio provides only a rough guess for the galaxy masses. Adding proper motions measured by *SIM* will allow us to solve for the actual masses of the dominant galaxies. The dwarf galaxies are essentially massless test particles of the potential. Also, the two components of proper motion would be extremely useful for determining several supplementary but crucial parameters: the halo sizes and density falloff rates at large radii, the mass associated with groups aside from that in the individual galaxies, and the amount of matter distributed on scales larger than 5 Mpc.

12.3. Preliminary Science Data

Ongoing ground- and space-based observations should help in the analyses of nearby galaxy dynamics. Accurate relative distances of nearby galaxies, often with accuracy as good as 5%, are being made at a rapid rate using methods such as Cepheids, tip of the red giant branch, eclipsing binaries, maser distances, etc. *SIM* should help reduce distance errors by providing better and therefore more consistent calibrations of these techniques. In addition, measurements of the proper motions of a few galaxies (only M 33 and IC 10 thus far) using masers supplement our knowledge. For the fortuitous cases in which both a maser and *SIM* measurements are made for the same galaxy, the maser information can be averaged to beat down errors from internal motions. However, it is unlikely that future maser proper-motion measurements, if any, will be in the same galaxies as those to be measured by *SIM* and thus they may provide completely complementary information.

12.4. Future NAM Studies Using *SIM* Data

It appears that the mass-to-light ratio for systems with early-type galaxies is higher than systems with late-type galaxies. Cluster mass-to-light ratios and elliptical galaxy X-ray data tend to $M/L \sim 300\ M_\odot/L_\odot$ while group virial masses, turnaround radii, and the timing analysis lead to ratios of 50–100 in the field. In NAM calculations, we are beginning to see this trend as well, with Virgo and Cen A requiring ratios of ~450 and ordinary groups at ~120. A detailed study of the flow on the 5 Mpc scale with all three components of velocity that *SIM* would allow, will be able to determine if the normal groups have additional dark matter at larger radii that could bring the baryon-to-dark matter ratios of the two species into better alignment.

The total masses of galaxies and the sizes of their halos are essential parameters for an understanding of dark matter and large-scale structure formation. It may be that the mass of the dark matter particle is in the range in which it is neither completely cold nor hot. If this is so, the clumping scale of the dark matter will provide a mass estimate of the dark matter particle. Or it may be that the dark matter particle is mildly dissipative. In which case, the halos will be flattened and the orbits of dwarf galaxies in different planes about some massive galaxy would be subjected to different effective masses. These would be important clues to revealing the physics and identity of the dark matter particle. If we combine the constraints on the 1–5 Mpc scale with flow studies on larger scales, it will be possible to strongly constrain a constant density component, resulting in a new astrophysical limit to the mass of the neutrino.

13. QUASAR JETS AND ACCRETION DISKS

Galaxies that possess spheroidal bulges also appear to possess central supermassive black holes whose mass is of order 0.1% of the bulge. Episodic accretion of gas, dust and stars onto the central black hole gives rise to the active galactic nucleus phenomenon. The potential *SIM* discovery space for AGN observations is broad because direct measurement on scales less than ~100 μas has previously been done only at radio wavelengths. Most of what is known about the optically emitting inner regions of AGN comes from optical variability studies of the broad line region: the intrinsic size scales are very small (light days to a light year, or ~0.1–10 μas) in extent. The ability of *SIM* to measure motions and position differences on microarcsecond scales means that we can study AGN on scales of tens to hundreds of Schwarzschild radii, perfect for studying accretion disks, jet collimation and possible orbital motion of binary black holes.

Key questions that *SIM* can answer include: (1) Does the most compact optical emission from an AGN come from an accretion disk or from a relativistic jet? Does this depend on whether the AGN is radio-loud or radio-quiet? (2) Do the cores of galaxies harbor binary supermassive black holes remaining from galaxy mergers? (3) Does the separation of the radio core and the optical photocenter of the quasars used for the reference frame tie change on the timescale of the photometric variability, or is the separation stable? The use of quasars in the astrometric grid to approximate a perfectly inertial frame is described in Appendix C. We first briefly review the basic properties of AGN and the physics of the current accretion disk-jet paradigm, and then describe how *SIM* will answer these questions, including examples of what *SIM* should see for specific targets.

13.1. Basic Quasar Properties: Radio-Quiet and Radio-Loud Sources

The observational signature of a quasar is an optically emitting source that is very bright intrinsically (up to $10^{13}\ L_{\odot}$) but very small in physical size (~10^{15} cm). At a 1 Gpc distance, for example, the size of the central quasar engine is of the order of 0.1 μas and that of the broad line region of the order of 1 μas. About 90% of all quasars are radio-quiet; their emission is dominated by optical and X-ray emission. The optical continuum spectrum consists of a fairly steep power law, sometimes with a big blue bump in the blue or near ultraviolet region (Band & Malkan 1989; Zheng et al. 1995). In addition, there are broad emission lines from highly ionized elements, which are produced rather close to the central source (~$10^{16–17}$ cm) and ionized by it.

The remaining 10% of quasars are radio-loud; they have strong diffuse radio emission in addition to all the properties of radio-quiet quasars, with radio jets extending on both sides of the optical source out to the external radio lobes. In many cases these jets flow at relativistic speeds (Lorentz factors of 10 or more). About 10% of these (i.e., about 1% of all quasars) are blazars—strong and variable compact radio sources, which also emit in the optical (mainly red and near-infrared), and in X-rays and γ-rays. They are believed to be normal radio-loud quasars viewed by us nearly end-on to the jet. Relativistic beaming toward the observer can produce an enhancement of an order of magnitude or more in apparent radio luminosity, as well as apparent proper motions of jet components of up to 1000 μas yr^{-1}. If they display similar internal proper motions in their optical jets, these would be readily detectable with *SIM*.

13.2. The Location of the Most Compact Optical Emission in the Accretion Disk-Jet Paradigm

In order to understand how *SIM* observations can provide insights into the physical processes in AGN, we need to briefly review the major components and current constraints on their parameters. A sketch of the canonical AGN model is presented in Figure 14. Observations on this size scale are indirect, so this picture is based largely on theoretical models. There are three possible sources of compact optical emission: the accretion disk, the disk corona or wind, and the relativistic jet. For a number of nearby AGN, *SIM* will be able to distinguish which component dominates and to study AGN properties on scales of 1 pc or less.

13.2.1. The Big Blue Bump and Hot Corona

In radio-quiet quasars, there should be two sources of optical-UV emission: (1) thermal accretion disk emission, which produces the big blue bump and dominates in the blue, and (2) a nonthermal corona whose origin is a steep power-law ionizing source, which dominates in the red. Both of these emission regions should be physically centered on the black hole within ~1 μas, and both should have a similar ~1 μas size.

In the high-accretion case, the disk produces a thermal peak in the near ultraviolet region. For a typical $10^9\ M_{\odot}$ black hole system, accreting at 10% of $\dot{M}_{\rm Edd}$, the diameter of the portion of

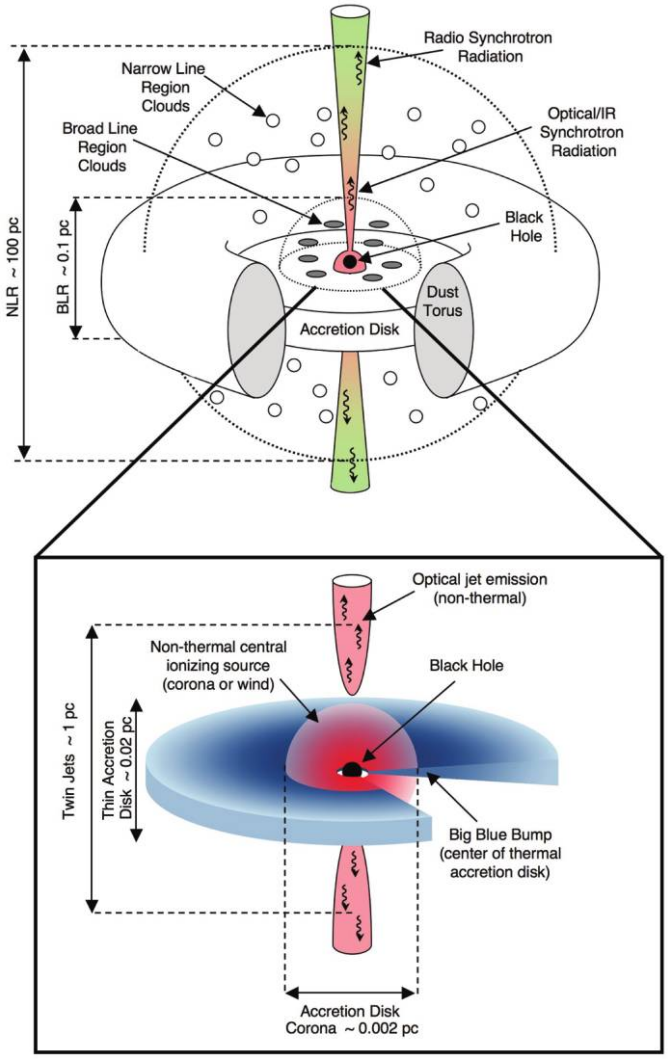

FIG. 14.—Schematic diagram of the structure of a typical quasar on scales from 0.002–100 pc, after Elvis (2000) and N. Smith (2007, private communication). *Top*: On scales from ~0.1–100 pc, the main components are the broad- and narrow-line emission clouds and a dust torus that obscures the black hole in certain orientations. In radio-loud quasars, powerful (and often relativistic) jets are ejected from the central engine (Königl 1981). These jets emit over the entire EM spectrum, with optical/IR dominating on scales $\lesssim 0.1$ pc, and radio emission dominating on larger scales. *Bottom*: On scales $\lesssim 1$ pc, a geometrically thin disk forms around the massive accreting black hole. In some quasars, the innermost portion of the accretion disk is seen as the big blue bump (Band & Malkan 1989). All quasars also have a source of nonthermal emission, a corona, which dominates in the red, and produces enough UV radiation to ionize the broad and even narrow-line regions. In radio-loud quasars, the base of jet also will produce nonthermal, typically highly variable, red emission that can outshine the central corona. *SIM* can probe the subparsec structure using time-dependent and color-dependent astrometry (see § 13.3). The blue disk and red corona are very compact and spatially coincident, so *SIM* would not expect to detect time- or color-dependent astrometric shifts in these components. However, if the jet dominates, then a color shift of ~0.5 pc (for a $z = 0.6$ quasar; see text) would be seen, and any variability would be along the direction of the jet. *SIM* will be able to test these predictions for radio-quiet and radio-loud quasars.

the disk that is radiating at a temperature of 10^4 K or above is $\sim 3.6 \times 10^{16}$ cm, or 0.012 pc (Shakura & Sunyaev 1973). At the distance of M 87 (16 Mpc) this region would subtend an angular size of ~160 μas, while at moderate redshift ($z = 0.5$) the angular size would be only ~2 μas.

The hot corona is believed to be responsible for exciting the observed emission lines of the high-ionization species of carbon, silicon, nitrogen, and oxygen, (Osterbrock & Matthews 1986). Coronal emission, therefore, is likely nonthermal—either optical synchrotron or inverse-Compton-scattered emission from a radio synchrotron source. Models of this ionizing source (e.g., Band & Malkan 1989) indicate a size of only ~70 Schwarzschild radii. At moderate redshift (e.g., 3C 345, $z = 0.6$) this subtends an angular size of only ~1 μas, centered on the black hole and comparable in size to the big blue bump.

13.2.2. The Beamed Relativistic Jet in Compact Radio-Loud Quasars

Radio-loud quasars possess powerful radio-emitting jets, in addition to the central optical-UV source seen in radio-quiet quasars. These jets are often relativistic flows, ejected in a direction approximately perpendicular to the accretion disk (see Fig. 14) by the effects of magnetic fields (Meier et al. 2001; McKinney 2006). If an AGN is radio-loud, and viewed at a small angle to the jet axis (a blazar), then a third source of optical continuum emission may be seen in addition to the big blue bump and hot disk corona: emission from the relativistic jet beamed toward the observer. This emission would be readily detectable by *SIM*, because it would be offset with respect to the other sources of emission, and highly variable. The Königl (1981) model for relativistic jets predicts that the majority of the optical emission comes not from synchrotron emission from the base of the jet but from synchrotron–self-Compton emission in the region of the jet where the synchrotron emission peaks in the radio or millimeter (Hutter & Mufson 1986). A detailed application of this model to 3C 345, for example, predicts the optical emission to be offset ~80 μas from the center of mass of the system and nearly coincident with the 22 GHz radio emission which lies ~70 μas or 0.4 pc from the black hole (Unwin et al. 1994). Not only is this readily detectable with *SIM*, but the vector position of the variability on the sky can be compared with the jet orientation seen on larger scales.

13.3. Distinguishing AGN Models Using Color-Dependent Astrometry

SIM can directly test the above modes by measuring a color-dependent shift in the astrometric position. A displacement in optical photocenter between the red and blue ends of the passband can be readily measured, and is very insensitive to systematic errors; measurements will be primarily limited by photon noise not instrument errors. This color-dependent dis-

placement, and its time-derivative in variable sources, is a vector quantity on the sky whose alignment can be compared to, say, the orientation of a radio jet imaged by VLBI or the VLA.

In radio-quiet quasars we do not expect to see a color shift, because of the absence of any contribution of a relativistic jet whose optical emission might introduce an astrometric asymmetry. The red emission from the corona and the blue emission from the disk both should be coincident with the central black hole within ~1 μas. Any color-dependent astrometric shift seen in radio-quiet quasars would challenge the current models of accreting systems in AGN.

By contrast, the astrometric position may be strongly color-dependent in any object with strong optical jet emission. So while the blue end of the spectrum should be dominated by the thermal disk, the red region may be dominated by the beamed relativistic jet. The relative contributions may vary as the activity level changes (see Ferrero et al. 2006). Furthermore, we would expect any variability to be aligned on the sky with the direction of the color shift itself.

An example of a moderate-redshift jet-dominated quasar is 3C 345 ($z = 0.6$) for which the red optical jet emission should be roughly coincident with the 22 GHz radio emission, at about 80 μas from the black hole. For 3C 273 ($z = 0.16$), the separation may be as large as 300 μas. Not only is such a large shift readily detectable, but *SIM* could also detect variations in the offset with time.

In the nearby radio galaxy M 87 we expect the red optical emission should be dominated by the accretion disk corona because its jets are not pointing within a few degrees of our line of sight. Therefore, *SIM* should not see a significant color shift in this source. However, M 87 is so close that we might see an absolute position shift between the measured radio photocenter and the overall optical photocenter. This shift should be even larger for this low-redshift radio galaxy than for 3C 345—perhaps in the 1000 μas range.

13.4. Finding Binary Black Holes

Do the cores of galaxies harbor binary supermassive black holes remaining from galaxy mergers? This is a question of central importance to understanding the onset and evolution of non-thermal activity in galactic nuclei. *SIM* can detect binary black holes in a manner analogous to planet detection: by measuring positional changes in the quasar optical photocenters due to orbital motion. If a quasar photocenter traces an elliptical path on the sky, then it harbors a binary black hole; if the motion is random, or not detectable, then the quasar shows no evidence of binarity. If massive binary black holes are found, we will have a new means of directly measuring their masses and estimating the coalescence lifetimes of the binaries.

An AGN black hole system (see Fig. 15) can occur near the end of a galactic merger, when the two galactic nuclei themselves merge. Timescales for the nuclei themselves to merge, and the black holes to form a binary of ~1 pc in size, are fairly short (on the order of several million years) and significantly shorter than the galaxy merger time (a few hundred million years). Furthermore, once the separation of the binary becomes smaller than 0.01 pc, gravitational radiation also will cause the binary to coalesce in only a few million years (Krolik 1999). However, the duration of the "hard" binary phase (separation of 0.01–1 pc) is largely unknown, and depends critically on how much mass the binary can eject from the nucleus as it interacts with ambient gas, stars, and other black holes (Yu 2002; Merritt & Milosavljevic 2005). Depending on what processes are at work, the lifetime in this stage can be longer than the age of the universe, implying that binary black holes are numerous—or as short as the "Salpeter" timescale $\sim(M_1 + M_2)/\dot{M}_{\rm Edd} \sim 5 \times 10^7$ yr, implying that binaries might be rare. Therefore, the search for binary black holes in the nuclei of galaxies will yield important information on their overall lifetime and on the processes occurring in galaxies that affect black holes and quasars.

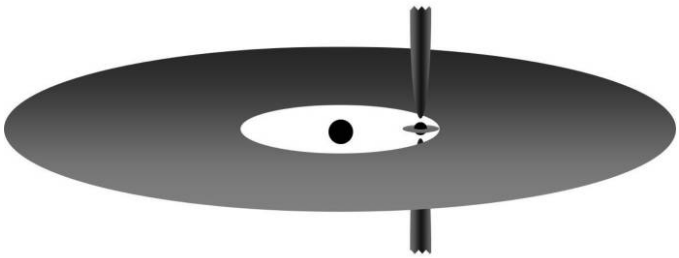

FIG. 15.—Schematic diagram of a binary black hole system. Binary separations of the order of 0.01–1 pc may be expected. While the larger object will have a large disk, the smaller will clear out the center of the disk, rendering the larger hole quiet, and leaving only the lower-mass black hole as a source of ionizing radiation and jets, as in Fig. 14. The orbital shift of the secondary hole will be readily detectable by *SIM* especially for nearby quasars ($z \lesssim 0.2$). Expected orbital periods for a 10^9 $M_\odot$ primary range from ~3 yr for a 0.01 pc orbit to ~90 yr for a 0.1 pc orbit.

A promising candidate would be an object that looks like a quasar (with broad lines and optical-UV continuum) but with absolute luminosity somewhat less than 10% of the Eddington limit expected from the central black hole. These might be objects with a large, but dark, primary central black hole that is orbited by a secondary black hole of smaller mass; the secondary would have cleared out the larger hole's accretion disk interior, but still will be accreting prodigiously from the inner edge of the primary's disk (Milosavljevic & Phinney 2005). In this case, the astrometric motion would indicate the full orbit of the secondary about the primary, which could be a few to a few hundred μas, depending on the source distance. Figure 15 is a simplified sketch of this situation. OJ 287 ($z = 0.3$) is a candidate, based on brightness variations with 12 yr periodicity (Kidger 2000; Valtonen et al. 2006), and we estimate that about 14 μas of orbital motion may be expected during a 5 yr span.

14. COSMOLOGY WITH *SIM*

In this section, we describe some contributions that *SIM* can make to the fields of cosmology and dark energy (DE). There are at least three distinct types of contributions: (1) the measurement of accurate stellar ages which provide a robust lower bound for the age of the universe (t_0), (2) the estimation of the primordial Helium abundance, and (3) the determination of percent-level distances to several galaxies in the Local Group. Stellar ages and helium abundances are best determined from spectrophotometry and accurate parallaxes of eclipsing binaries (Lestrade 2000). For the present purpose, we will assume that the Local Group distances are equivalent to determining the Hubble constant (H_0) itself. In fact, a robust maximum value for the equation of state of dark energy derives from the product t_0 and H_0 (Bothun et al. 2006).

An error level for H_0 of one to two percent is optimal for determining the EOS of dark energy and the total energy density of the universe. Errors of the order of 1% and 0.1% for w and $\Omega_{\rm tot}$, respectively, are achievable with Planck-like cosmic microwave background (CMB) data and a 2% error on H_0. Assuming $\sqrt{N}$ statistics, 2% distance errors may be achieved with *SIM* observations of 43 stars in M 31, 200 stars in M 33 and 2025 stars in the LMC. Local Group distances do not determine H_0; rather they allow for a recalibration of secondary distance indicators that extend beyond the Local Group, such as Cepheids and the tip of the red giant branch (TRGB; see § 7). The disks of these galaxies encompass a wide range in metallicity, extinction, and number density, and thus provide ample opportunity for an accurate calibration of methods such as the TRGB, Cepheids, RR Lyrae, surface-brightness fluctuations and so forth.

14.1. The Extragalactic Distance Scale

When assuming a flat ΛCDM (cold dark matter) model, the fluctuations of the CMB as observed by *WMAP* imply a value of $H_0 = 73 \pm 3$ km s^{-1} Mpc^{-1} (Spergel et al. 2003, 2007; hereafter referred to as WMAP07). This value is very close to the *HST*-derived value of $H_0 = 74 \pm 2$ (random) $\pm$ 7(systematic) km s^{-1} Mpc^{-1} (Freedman et al. 2001). However, if the flatness assumption is abandoned, *WMAP* by itself hardly constrains H_0 because *WMAP* measures the product of the normalized matter density (Ω_m) and h^2 (WMAP07, their Fig. 20), as well as the baryon density ($\Omega_b h^2$). Here, $h \equiv 100$ km s^{-1} Mpc$^{-1}/H_0$ and $\Omega_m h^2 \equiv \omega_m = 0.126 \pm 0.009$. Thus, an independent and accurate determination of H_0 would determine Ω_m and Ω_b, and, if we assume a flat universe, the dark-energy density ($\Omega_{\rm DE}$).

While an accurate determination of H_0 has many advantages, here we will concentrate on those with direct cosmological implications: (1) determining the EOS defined as the ratio of pressure to density ($w \equiv p/\rho$) of dark energy (WMAP07), and (2) determining the total density ($\Omega_{\rm tot}$) of the universe. The EOS of dark energy tells us something about its nature: the cosmological constant, strings, domain walls, and so forth predict different values for the equation of state (e.g., Peebles & Ratra 2003).

According to Hu (2005, hereafter H05), a change in the EOS of dark energy by 30% leads to a change in H_0 by 15% if a constant w is assumed, and by about one-half that much if w changes with redshift (H05; Figs. 3*a* and 3*b*). Thus, an accuracy of 1% in H_0 leads to a percent-level determination of the EOS of dark energy. However, the absolute value of w and its rate of change cannot be independently determined by fixing H_0. In fact, once H_0 is fixed locally, the determination of w and/or its slope and/or the curvature term requires subpercent-level determination of H_0 at $z \sim 0.1$–1.5 (H05, Figs. 3*c* and 3*d*).

As discussed above, if the CMB parameters are infinitely well known, we expect that uncertainties in the EOS of dark energy remain at the level of the uncertainty in H_0. Below, we estimate analytically the effects of increasing both the accuracy of the CMB data and of H_0. The results of this exercise are consistent with the H05 findings. Because *SIM* is a targeted mission, a *SIM*-based determination of H_0 can obtain, more or less, any required accuracy if an appropriate amount of observing time is allocated. Thus, our analytical results are useful in quantifying more precisely the resulting accuracy in the EOS of dark energy given a certain expenditure of *SIM* time, and vice versa.

WMAP and other data currently constrain the EOS: $w \sim (-0.826 \pm 0.109) - (0.557 \pm 0.058)\omega_m h^{-2} \sim -0.95 \pm 0.11$, where we follow WMAP07 and assume a constant w, but allow for a nonzero curvature term (Olling 2007a). This follows from various relations between the vacuum energy (Ω_Λ), the matter density, the spatial curvature of the universe (Ω_K) and the Hubble constant. Likewise, current data yield: $\Omega_{\rm tot} = \Omega_\Lambda + \Omega_m \sim (0.9438 \pm 0.0114) + 0.225\omega_m h^{-2} \sim 0.996 \pm 0.016$. Thus, current data allow for the determination of the total density of the universe to plus or minus 1%, while the EOS of dark energy is known to about 10%.

To eliminate the uncertainty associated with h, one would want to determine the Hubble constant via trigonometric parallaxes of nearby galaxies. Unfortunately, this is not possible with foreseeable or planned technology. However, the rotational parallax method (see § 14.2) should be almost as good (Peterson & Shao 1997; Olling & Peterson 2000 hereafter referred to as OP2000).

Olling (2007a) estimates the effects of more accurate CMB data and a better Hubble constant on the EOS of dark energy and finds that, even at Planck accuracy, the errors on w and $\Omega_{\rm tot}$ are only slightly smaller than the current values. The accuracy of the EOS of dark energy only improves significantly when the accuracy of H_0 is improved.

The results are summarized in Figure 16, which shows the attainable accuracy on w as a function of the improvement of our knowledge of the CMB, with respect to the *WMAP* 3 yr data, for four values of H_0 accuracy. As expected, the error on w (ϵ_w)

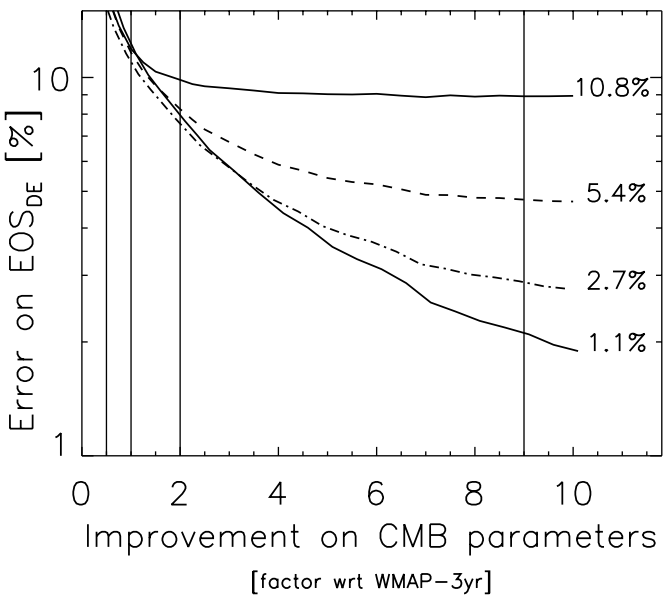

FIG. 16.—The accuracy of the EOS of dark energy w as a function of the uncertainty in the CMB data, essentially the factor by which the error on ω_m decreases, for four values of accuracy of the Hubble constant (curves labeled in % accuracy on H_0). Vertical lines (from left to right) indicate the accuracies in the CMB parameters using *WMAP* 1 yr, 3 yr, and 8 yr data, and expected Planck data (Efstathiou et al. 2005) normalized to the 3 yr *WMAP* data. The resulting w errors are 8.9%, 4.8%, 3.0%, and 2.3% for CMB accuracies at the level expected from Planck. A significant improvement in w requires both Planck CMB data *and* a more accurate Hubble constant.

decreases as knowledge of the CMB parameters improves. However, these curves show that ϵ_w approaches a limiting value. The curve that corresponds approximately to the current error on H_0 ($\epsilon_{H_0} \approx 11\%$; *top curve*) indicates that an error of only about 9% can be obtained for w, even with Planck-like CMB accuracies (Efstathiou et al. 2005). Note that this accuracy is only slightly better than our current knowledge as set by the *WMAP* 3 yr data. In order to significantly improve our knowledge of w, we need Planck data and also need H_0 to much better accuracy. Achieving $\epsilon_w = 2.3\%$, requires an accuracy of 1.1% on H_0. Errors on $\Omega_{\rm tot}$ behave much like those on w, but with roughly 10 times smaller amplitude.

Further improvements in our knowledge of the dark energy EOS may come from improvements in observations other than H_0, though reducing the uncertainty in H_0 makes the biggest difference. The other data sets used by WMAP07 are: large-scale structure observations, galaxy redshift surveys, distant Type Ia supernovae, big bang nucleosynthesis, Sunyaev-Zel'dovich fluctuations, Lyman-α forest, and gravitational lensing. The Dark Energy Task Force (Albrecht et al. 2006) considers how future instruments and space missions might significantly reduce the error in ϵ_w through improvements in these data sets in four stages. It defines Stage I to be the current state of the art, and Stage IV to comprise a Large Survey Telescope (LST), and/or the Square Kilometer Array (SKA), and/or a Joint Dark Energy Mission (JDEM). Each higher stage represents an improvement of ϵ_w by a factor of about three with respect to the previous stage (Albrecht et al. 2006). It concludes that when these data are of Stage IV quality, a reduction in the error on H_0 by a factor of 2 matters at most 50% for the accuracy of the dark energy EOS. However, Olling (2007a) argues that the effects of smaller errors on H_0 are especially important at the early stages, estimating that a decrease of ϵ_{H_0} by a factor of 10 yields an improvement of ϵ_w by factors of: 3.9, 3.0, 2.4, and 1.6 for Stages I, II, III, and IV, respectively.

14.2. Rotational Parallax Distances

The method of rotational parallaxes (RP) combines proper motions (μ) and radial velocities (V_r) of stars in external galaxies to yield bias-free single-step distances with attainable accuracies of the order of 1%. This method is analogous to the orbital parallax technique (Armstrong et al. 1992).

For a nearby spiral galaxy at distance D (in Mpc) which is inclined by i degrees and with a rotation speed of V_c km s^{-1}, the proper motion due to rotation is $V_c/(\kappa D)$ μas yr^{-1}, with $\kappa \sim 4.74$ km s^{-1}/(AU yr^{-1}). For M 33, M 31, and the LMC we find $\mu \sim 24$, ~74, and ~192 μas yr^{-1}, respectively, which will be easily measured by *SIM*. A simplified RP method uses stars on the major and minor axes at similar galactocentric distances of a galaxy with a flat rotation curve. The minor-axis proper motion measures the circular velocity divided by D, while the ratio of minor- to major-axis proper motions is simply $\cos i$ (Peterson & Shao 1997). However, stars need to be close to the principal axes, making it difficult to find enough targets. Generalizing this method we find

$$D = \frac{V_{\rm r}}{\kappa}\sqrt{\frac{-y'/\mu_{y'}}{x\mu_x + y'\mu_{y'}}}; \tag{8}$$

with x and y' the major-axis and minor-axis position of individual stars in the target galaxy (OP2000; Olling 2007a). The attainable distance errors per star are estimated to be 13%, 28%, and 90% for M 31, M 33, and the LMC, respectively.

14.3. Realistic Rotational Parallaxes

The rotational parallax method allows distances to be made to M 31, M 33, and the LMC in a single step, to accuracies of about 0.92%, 2.0%, and 6.4%, respectively. Achieving these bias-free single-step distances requires careful modeling of noncircular motions (due to spiral-arm streaming motions, perturbations from nearby galaxies, a bar, and warps) which could otherwise bias the distance determination (OP2000). These effects are likely to be significant for the LMC. In order to achieve errors of several percent, it will be necessary to correct for any sizable deviations from circular motion. OP2000 show that a correction can be achieved with *SIM*-quality proper motions.

For a disk geometry, the combination of *SIM* proper motions and ground-based radial velocities will yield four of the six phase-space coordinates for individual stars, where the missing components can be chosen to be, for example, the vertical displacement (z) of the star with respect to the galaxy plane and the average z velocity (Olling 2007a). For M 31 and M 33, this assumption is likely to be reasonable. Furthermore, we can make different assumptions regarding the fifth and sixth phase-space parameters and require consistency between the results. Thus, the rotational parallax method will yield very reliable distances. This contrasts other techniques that claim to yield extragalactic distances at the few-percent level, such as eclipsing binaries, Cepheids, and nuclear water masers. In fact, these other techniques rely on additional assumption, inaccurate slopes, and/or zero points, although many of those problems are likely to be calibrated by *SIM* and *Gaia* (see review in Olling 2007a).

Because noncircular motions can be correlated on large scales, a substantial number of stars need to be observed (spread out over a large area of the galaxy) to be able to apply reliable corrections. OP2000 estimate that at least 200 stars are required to achieve the 1% distance error for M 31 noted above.

14.4. Other Local Group Distances

SIM can be used to apply the orbital parallax technique to binary stars in other nearby Local Group dwarf galaxies. This would increase the number and the range of types of galaxies that can be used to calibrate other rungs of the distance ladder. Let us estimate the required accuracies by neglecting inclination effects and eccentricity. Then, the orbital velocity, v, the semimajor axis, a, and the period, P, for each of the components yield the distance:

$$D_{100\,\mathrm{kpc}} = 10\kappa \frac{2\pi a_{\mu\mathrm{as}}}{P_{\mathrm{yr}} v_{\mathrm{km\,s^{-1}}}} \sim 298 \frac{a_{\mu\mathrm{as}}}{P_{\mathrm{yr}} v_{\mathrm{km\,s^{-1}}}}, \qquad (9)$$

where $v_{\mathrm{km\,s^{-1}}} = \kappa 2\pi a_{\mathrm{AU}}/P$ and $a_{\mathrm{AU}} = a_{\mu\mathrm{as}}/D_{\mathrm{Mpc}}$. Because the distance error (Δ_D) scales according to $(\Delta_D/D)^2 = (\Delta_a/a)^2 + (\Delta_P/P)^2 + (\Delta_v/v)^2$, a 1% distance error requires that the errors on semimajor axis (Δ_a/a), period (Δ_P/P), and radial velocity (Δ_v) are all at the subpercent level.

Given sufficient observing time, the period and the orbital velocity and their errors can be determined from the ground with the required accuracy. Also, short-period binaries are unlikely to have survived the expansion of the primary, while long-period orbits will be poorly sampled during *SIM* and ground-based observations, so we will assume periods between 2 and 10 yr. We simulate a population of binaries at 100 kpc with a 1 $M_\odot$ primary. Secondaries are drawn from the stellar initial mass function and are in circular orbits with a period distribution according to Duquennoy & Mayor (1991). We assume a 100% binarity rate. The result is that 1% of stars lie in the required period range (median is 7 yr) if $a_{\mu\mathrm{as}} \geq 12.5$. For these systems, the median projected orbital velocity is $\bar{v}_{o;\mathrm{km\,s^{-1}}} \sim 1.9$. To achieve the 1% distance accuracy goal, *SIM* would need $(100/12.5)^2 = 64$ observations per star, while the RV program would need to reach an accuracy of 19 m s^{-1}. At 138 (200) kpc, only 0.4% (0.042%) of binaries satisfy these criteria and have $\bar{P}_{\mathrm{yr}} \sim 7.9$ (9.3), $\bar{a}_{\mu\mathrm{as}} \sim 14.9$ (13.2) and $\bar{v}_{o,\mathrm{km\,s^{-1}}} \sim 1.9$ (2.5), where 138 kpc corresponds to the Fornax distance.

Excluding the Sagittarius dwarf and the Magellanic Clouds, we identify five galaxies within 100 kpc in the Mateo (1998) compilation of Local Group dwarfs, and seven within 200 kpc. If we make the optimistic assumption that the total luminosity of these systems comes only from stars 1 mag below the TRGB, then these systems have about 10 TRGB binaries with the right properties per galaxy. These are all fainter than $V \sim 18$ and would be fairly expensive in *SIM* observing time, but binaries in the Sagittarius dwarf, the Magellanic Clouds, and possibly the Sculptor and Fornax dwarfs are observable.

15. IMAGING WITH *SIM*

SIM will demonstrate synthesis imaging at optical wavelengths in space, thereby showing the viability of this approach for the design of the next generation of UV-optical-IR imaging telescopes for space astronomy. The telescopes we now have in space at these wavelengths (*GALEX*, *HST*, & *Spitzer*) are all of the "filled aperture" type, which ultimately limits their angular resolution to that dictated by the size of the largest rockets available for launching them. High sensitivity is automatically provided with such high-resolution instruments, but precision collecting area is expensive and may not always be required. Synthesis imaging using phase-stable UV-optical-IR interferometers provides, for the first time, the possibility of separately choosing the resolution and the collecting area of space telescopes in order to provide a more cost-effective match to the specific astrophysical problems to be addressed. Such flexibility is essential for the future if instruments are to provide ever-increasing angular resolution and still be affordable. *SIM* will break new ground by demonstrating these imaging techniques at optical wavelengths in space.

Since *SIM* must have very high fringe phase stability over long periods of time in order to accomplish its astrometric goals, it behaves at optical wavelengths in much the same way as a ground-based radio interferometer. The results of the observations can be put into the same general form of complex fringe visibilities. Data can be obtained over a range of baseline orientations, mimicking the rotation of the Earth for ground-based synthesis instruments. *SIM* will also have two baselines available, one at 9.0 m and the other at 7.2 m, and data for imaging observations can be taken at both baselines (although not simultaneously). Figure 17 (*left panel*) shows a typical coverage of the aperture (u, v) plane which can be achieved. A software simulator for this mode of *SIM* is available, based on the initial work on this subject by Böker & Allen (1999). The current version of the *SIM* imaging simulator, *imSIM*, incorporates the latest information on the expected performance parameters

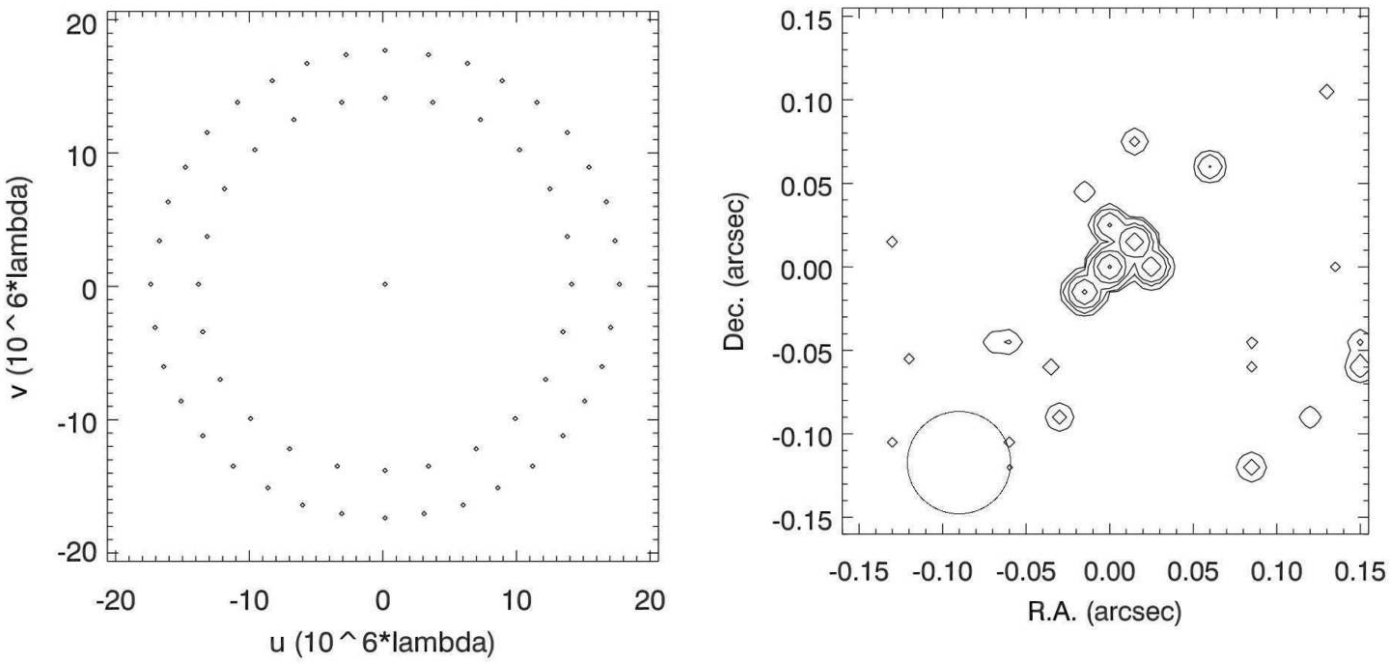

FIG. 17.—Left: Example of the (u, v) coverage for a single channel at mean wavelength $\lambda = 500$ nm. Both the long ($\simeq$9.0 m) and short ($\simeq$7.2 m) baselines are included, and data taken at increments of baseline orientations of 10° and 15°, respectively. Only half of the (u, v) plane needs to be observed; the rest can be computed using the fact that the field to be imaged is purely a real function. Note that *SIM* can provide its own zero-spacing data as well. The (u, v) coverage for longer wavelength channels would lie inside these circles, and the synthesized PSFs would be proportionally wider. Right: A model cluster of five stars observed for 10 s at each of the 30 (u, v) points shown in the left panel. The image has been cleaned and restored with a Gaussian beam of FWHM 0.010″, and the residuals added in. Contours are logarithmic at intervals of 1.25 mag. The brightest object (at 0,0) is a 15th magnitude A0 star, the faintest member of the cluster (at 0, 0.025) is a 17th magnitude G0 star. Other objects on this image are noise and artifacts of the restoration. The FWHM $\simeq 0.06''$ of the *HST*/ACS/HRC camera PSF is drawn in (*circle at lower left*) for comparison.

of *SIM*, and can generate simulated observations for a variety of source models.

Figure 17 (*right panel*) shows the image which could be produced by *SIM* on a (model) source field consisting of five stars ranging in brightness from $V = 15$ to 17, and the (u, v) coverage of the simulated data. The stars were observed for a total of 300 s of on-source integration time (30 points, 10 s per point). The point-spread function of *HST* (convolved with the pixels of the HRC) is shown for comparison.

For the imaging demonstration, targets of modest complexity but showing a wide range of surface brightness will be chosen, consistent with the limited number of physical baselines available in the *SIM* instrument. The observations for this demonstration will be carried out soon after the launch of *SIM* during the in-orbit checkout of the instrument. Subsequently, this capability will be available for general use.

15.1. Performance Features of *SIM* as a Synthesis Imaging Instrument

In addition to its high resolution, *SIM* as an imager has several other novel features. First, the instrument is a simple adding interferometer instead of a correlation interferometer (common in radio astronomy), so that the total flux of photons received in the FOV is retained in the measurement. If that value is not significantly contaminated by photons from extraneous objects in the FOV, it can provide an estimate of the "zero-spacing" data, as indicated by the dot at the origin in Figure 17 (*left panel*). Second, and perhaps most significant, images made synthetically with *SIM* will have exceptionally high dynamic range. This is a result of the extraordinarily high phase stability required of *SIM* in order to achieve its goal of *repeatable* microarcsecond astrometric precision. Since this stability means that the theoretically computed point-spread function (PSF) is an excellent approximation to the actual PSF, the former can be used to remove bright stars from the image, leaving only photon noise and low-level artifacts from residual phase instability. In marked contrast to the situation with filled apertures, these latter instabilities will be entirely uncorrelated from one measurement location in the (u, v) plane to the next. The result is that the remaining low-level artifacts make equal contributions everywhere over the synthesized image rather than piling up around the location of the bright stars. After PSF subtraction, the remaining faint sources can be detected anywhere in the difference images with equal sensitivity, even as close as one interferometer fringe ($\approx$11 mas at $\lambda = 500$ nm) from a bright star. Preliminary results from our simulations indicate that

we can expect the dynamic range (defined as the magnitude difference between the peak value on the brightest star and the faintest detectable companion) on *SIM* images to routinely exceed 6 mag for target stars with $V \lesssim 13$, which is comparable to that achieved at radio wavelengths with the VLA without any additional data processing. However, in contrast to the case with the VLA where values of dynamic range as high as 10 mag (factor 10^4) have been achieved by modeling the residual instrumental effects, the dynamic range on *SIM*'s synthetic images will ultimately be limited by the photon noise from the stars in the FOV. With *SIM*'s modest collecting area, it will be difficult to significantly improve the dynamic range on *SIM* images much further without large amounts of observing time.

15.2. Synthetic Imaging Secience with *SIM*

Although intended primarily as a technology demonstration, the synthesis imaging mode of *SIM* will also open new possibilities for science applications on targets of high surface brightness, and where resolving structure beyond the limits of the *HST*/ACS/HRC PSF would be significant to an understanding of their nature. Böker & Allen (1999) were the first to consider this question in some detail, and concluded that targets as varied as the cores of dense Galactic globular clusters, AGNs in galaxies, and dust disks around nearby stars were feasible. Based partly on their analysis, a proposal to map the stellar distributions and kinematics of the nuclear regions of M 31 was included in the initial science program for *SIM* (Unwin & Turyshev 2004). Since that time, instrument design changes have reduced the number of baselines available, and the nulling capability has been removed. These two reductions in scope of the *SIM* design have rendered the study of dust disks around nearby stars significantly more difficult. However, the M 31 project appears to be still feasible, as are observations of compact high–surface-brightness targets in general. The example of observations of a dense stellar cluster described in the previous section makes it clear that *SIM* will have significant things to say about such targets.

The successful demonstration of synthesis imaging at optical wavelengths with *SIM* is expected to have a significant impact on the design of future space-based instruments for astronomical imaging. *SIM* imaging will also offer new capabilities for the study of the structure of targets presently only barely resolved by *HST*, or otherwise confused by the inability to adequately remove diffraction spikes and scattered light from nearby bright stars. The design of *SIM* is now quite stable, and many details of just how the instrument will operate are now known. A new review of potential targets for imaging science with *SIM* is under way.

16. MEASURING THE PPN PARAMETER γ

Our current lack of understanding of quantum gravity and dark energy demands new physics. Searches for gravitational waves and attempts to understand the nature of dark matter are further motivated by the discovery of dark energy (Turyshev et al. 2006). Promising theoretical models involve new gravitational effects that differ from general relativity (GR), some of which could manifest themselves as violations of the equivalence principle, variation of fundamental constants, modification of the inverse square law of gravity at short distances, Lorenz-symmetry breaking, and large-scale gravitational phenomena. These effects are amenable to study with space-based experiments. For example, scalar-tensor extensions of gravity (Damour et al. 2002), brane-world gravitational models (Dvali et al. 2000), and modified gravity on large scales motivate new searches for deviations from a level of $10^{3–5}$ below the level currently tested by experiment (Turyshev et al. 2004; Turyshev et al. 2006).

The parameterized post-Newtonian (PPN) parameter γ (Will 2006) is currently measured to differ from unity by no more than $(2.1 \pm 2.3) \times 10^{-5}$, as obtained using radiometric tracking data received from the Cassini spacecraft (Bertotti et al.2003) during a solar conjunction experiment. This accuracy approaches the region where multiple tensor-scalar gravity models, consistent with the recent cosmological observations (Spergel et al. 2007), predict a lower bound for the present value of this parameter at the level of $(1 - \gamma) \sim 10^{-6}$–$10^{-7}$ (Damour et al. 2002), motivating the proposal of space-based experiments to improve the measurement of γ.

SIM will routinely operate at about this level of accuracy—the Sun produces an astrometric bend of 4 mas at 90°, more than 1000 times the accuracy of individual *SIM* grid stars. Gravitational effects in the solar system must therefore be included into the global astrometric model and the corresponding data analysis, formulated such that γ is a measured parameter. By performing differential astrometric measurements with an accuracy of a few μas over the instrument's FOV of 15° *SIM* will provide this precision as a by-product of its astrometric program and could measure the parameter γ with accuracy of a few parts in 10^6 (Turyshev 2002), a factor of 10 better than the Cassini result. A precision *SIM* measurement would aid the search for cosmologically relevant scalar-tensor theories of gravity by looking for a remnant scalar field in today's solar system.

17. CONCLUSIONS

The Space Interferometry Mission (*SIM*) represents a revolutionary step forward in the development of astronomy's most ancient measurement technique, determining the positions of celestial objects. With an absolute precision of 3 μas covering a wide range of magnitudes (from $V < 0$ mag to $V > 19$ mag), *SIM* will measure positions, distances, and proper motions for almost every type of astronomical object with a parallax accuracy of 10% or better across the entire Milky Way. Within a few parsecs, the parallax precision will be better than 1%. These precision measurements will challenge our theories of stellar (§ 5, 6) and galactic structure (§ 7), while adding to our under-

standing of dark matter and cosmology through refined knowledge of the distance to Cepheids (§ 8), the value of the Hubble constant (§ 14), the ages and distances of Globular Clusters (§ 9), and the motions of dwarf spheroidal and Local Group galaxies (§ 12). Precision *SIM* astrometry even promises to probe small-scale phenomena within the cores of quasars and active galactic nuclei, including the possible presence of binary supermassive black holes (§ 13).

With a differential astrometric precision of 1 μas, *SIM* will measure the orbital motions of many classes of multiple objects, including every sort of normal and exotic star from low-mass stars (§ 5) to X-ray binaries, evolved AGB stars, neutron star and black hole binaries (§ 6), and microlensing systems (§ 10). From these dynamical measurements, we will be able to determine masses for astronomical objects, perhaps the most fundamental single parameter in understanding their physical nature. Coupling new physical information from *SIM* with previously known characteristics of such systems, such as ages and metallicity, will allow a new level of understanding of the evolution of astronomical objects.

From a cultural standpoint and in the eyes of the public, as well as in the research community, *SIM*'s most dramatic contribution may come from opening up the next level of performance in the reconnaissance of our nearest stellar neighbors by looking for planets with masses that are equal to or just a few times above the mass of our own Earth and located in the range of orbits conducive to development of habitable environments (§ 2). As described in § 2.4, within a deep 5 yr survey, *SIM* could find planets with a mass of 1 $M_{\oplus}$ orbiting within the habitable zones of over 100 of the most favorable stars. *SIM* is the first step in a long-term strategy for searching for other habitable worlds suitable for subsequent follow-up with direct detections of planet light at visible or infrared wavelengths. *SIM* also offers dramatic new capabilities for finding planets orbiting stars not accessible to radial velocity or transit studies, such as young stars, very massive stars, or stars with highly variable photospheres or weak spectral lines. *SIM* will investigate the formation and migration of planets in young planetary systems, finding out whether Jupiter-mass planets are common or rare when orbiting stars younger than a few million years old (§ 3).

As we noted in § 1, this paper is intended to highlight some of the many areas of astrophysics that precision astrometry will address, specifically those problems amenable to flexibly targeted observations at very high precision. As a guide to possible opportunities, we show an overview of the assignment of *SIM* observing time in Table 6. Key project teams have the task of

TABLE 6

STRAWMAN KEY PROJECT AND GUEST OBSERVER TIME ASSIGNMENT

Science program	Number of targets	Target V magnitude	Observing mode	Accuracy (μas)[a]	Mission fraction
Prime mission					1.00
Science Team key projects	~10000	–1.4–20	Wide/Narrow	4–25	0.36
Guest observer call 1 (Terrestrial planets)	~75	6–9	Narrow	0.6–1.2	0.27[b]
Guest observer call 2 (Open)	~10000	12	Wide	8	0.05
Astrometric grid[c]	1302	9–10.5	Wide	3	0.24
Engineering[d]					0.08
Extended mission					1.00
Guest observer call 3 (Sample programs)					0.7
GO program 1	~180	6–9	Narrow	1.5	0.2[b]
GO program 2	~5000	12	Wide	5	0.1
GO program 3	~20000	12	Wide	8	0.1
GO program 4	~12000	14	Wide	10	0.1
GO program 5	~750	18	Wide	12	0.1
GO program 6	~1500	18	Wide	20	0.1
Astrometric grid	1302	9–10.5	Wide	2.5[e]	0.2
Engineering[d]					0.1

NOTES.—The *SIM* instrument and operations are designed for a 10 yr total lifetime. Prime mission has a duration of 5 yr; extended mission, a further 5 yr. Science Team key project time was assigned by NASA Announcement of Opportunity in 2000. All guest observer (GO) programs will be competed. The study of terrestrial planets described in § 2 assumes that the first GO call will be devoted to extending the target list for planet searches. GO call 3 is represented here by programs which span a range of magnitudes and accuracies, and which are purely intended to be illustrative.[a] In wide-angle mode, accuracy is midepoch position, one axis, at end of prime mission. In narrow-angle mode, accuracy is for a single measurement in a local reference frame, one axis

[b] Mission fraction is for 100 visits per target in each of two orthogonal axes

[c] Grid allocation also includes ~50 quasars (~1.5% mission fraction) to define the absolute reference frame (see Appendix C)

[d] Includes instrument calibration and scheduling margin

[e] Estimated accuracy of midepoch position, one axis, at end of extended mission

optimizing their science within their allocations, which requires a careful trade of the numbers of targets, their magnitudes, and the astrometric accuracy needed for the science objective. We note that for faint targets, say $V > 18$, accuracies of < 10 μas require hours of mission time, and such targets will be selected with substantial care; many of the sections in this paper discuss the considerations in target selection. As this process of target definition for the Science Team is still underway, we show only the formal allocation to the team. The remaining time will be allocated via a future peer-reviewed guest observer (GO) program, and will be completely open with respect to science topic. The number of selected programs will be set by NASA; it is expected that extended mission would be entirely open to competition. We show a set of hypothetical, but representative, programs that together would complete the *SIM* time assignment. The first GO program will likely be assigned to further searches for terrestrial planets to supplement the NASA Key Projects (see § 2). The number of targets, magnitudes, and accuracies in Table 6 should be viewed as illustrative, rather than the final word on target selection. Observing time calculations depend on the science objective (e.g., parallax and proper motion require different optimizations).

The technology pioneered by the *SIM* mission, the first long-baseline Michelson Interferometer in space, represents an important investment for the future of space astronomy. Visible and infrared imaging on the milliarcsecond scale demands widely separated apertures. *SIM*'s long-baseline interferometric capabilities (§ 15) will make simple images with 10 mas resolution on $V = 15$ objects. Future telescopes, potentially separated by hundreds of meters, will build upon the technology demonstrated by *SIM*.

The scientific measurements that *SIM* will provide cannot be duplicated by other means. As a pointed observatory, *SIM* will complement the all-sky survey planned for the *Gaia* mission by enabling observations of both very faint and very bright objects that are more precise by an order of magnitude. The combination of *SIM* and *Gaia* will move astronomy and astrophysics into a new era of precision dynamical and kinematic knowledge unprecedented in the 2000 year-old history of astrometric measurements.

The authors would like to thank their many colleagues, too numerous to mention, whose vision and determination over the course of more than a decade have brought *SIM PlanetQuest* to its current mature design. Through their efforts, we are now poised, technology in hand, to build the next generation of space astrophysics instruments based on interferometry. The research described in this paper was carried out at the Jet Propulsion Laboratory, California Institute of Technology, under contract with the National Aeronautics and Space Administration. This research has made use of the NASA/IPAC Infrared Science Archive, which is operated by the Jet Propulsion Laboratory, California Institute of Technology, under contract with the National Aeronautics and Space Administration. This work was supported by NSF grant AST-0307851 (RJP, SRM), NASA grant JPL 1228235 (S. R. M., C. G., K. V. J., R. J. P., S. T.), NASA grant NAG5-9064, and NSF CAREER award AST-0133617 (K. V. J.).

APPENDIX A

NARROW-ANGLE ASTROMETRY

SIM is designed to perform narrow-angle (relative) astrometry in three different modes where it is capable of measuring periodic motions with a precision of 0.6 μas per axis in a narrow-angle frame. The modes include the standard narrow-angle (NA) mode, gridless narrow-angle astrometry (GNAA) mode (Shaklan et al. 2003), and grid-based differential astrometry (GBDA) mode (Pan et al. 2005). Because of its high efficiency, NA mode will be used for the vast majority of narrow-angle observations. Early-mission results can be obtained with GNAA, while GBDA is useful once grid stars are known to the level of 0.1″.

NA mode is linked to the wide-angle grid campaign. It uses the end-of-mission grid star positions to determine the instrument baseline orientation and length at the time that a target and reference stars were observed. Two roughly orthogonal baseline orientations are needed to make a two-dimensional measurement of the target-star motion relative to the reference frame. Because all measurements are tied to the absolute grid, the target parallax and proper motion are determined with high precision, and their errors do not contribute significantly to the single-measurement error. A single visit typically requires < 30 min to achieve 0.6 μas precision.

GNAA is akin to traditional relative astrometry with a single telescope. Relative astrometry typically employs a photographic plate, a CCD, or Ronchi Ruling (Gatewood 1987) to record the positions of a target star and a reference stars over several months to years. The reference stars are used to anchor a least-squares conformal transformation that matches the scale, rotation, translation, and potentially higher-order field-dependent and time-dependent terms into a common reference frame, which is then applied to the target. GNAA mode combines measurements of a target, at least four reference stars, and at least three baseline orientations (Shaklan et al. 2003), and uses a conformal model to solve for instrument parameters (baseline length and orientation, and a phase-delay constant term). Since the parallaxes and proper motions of the target

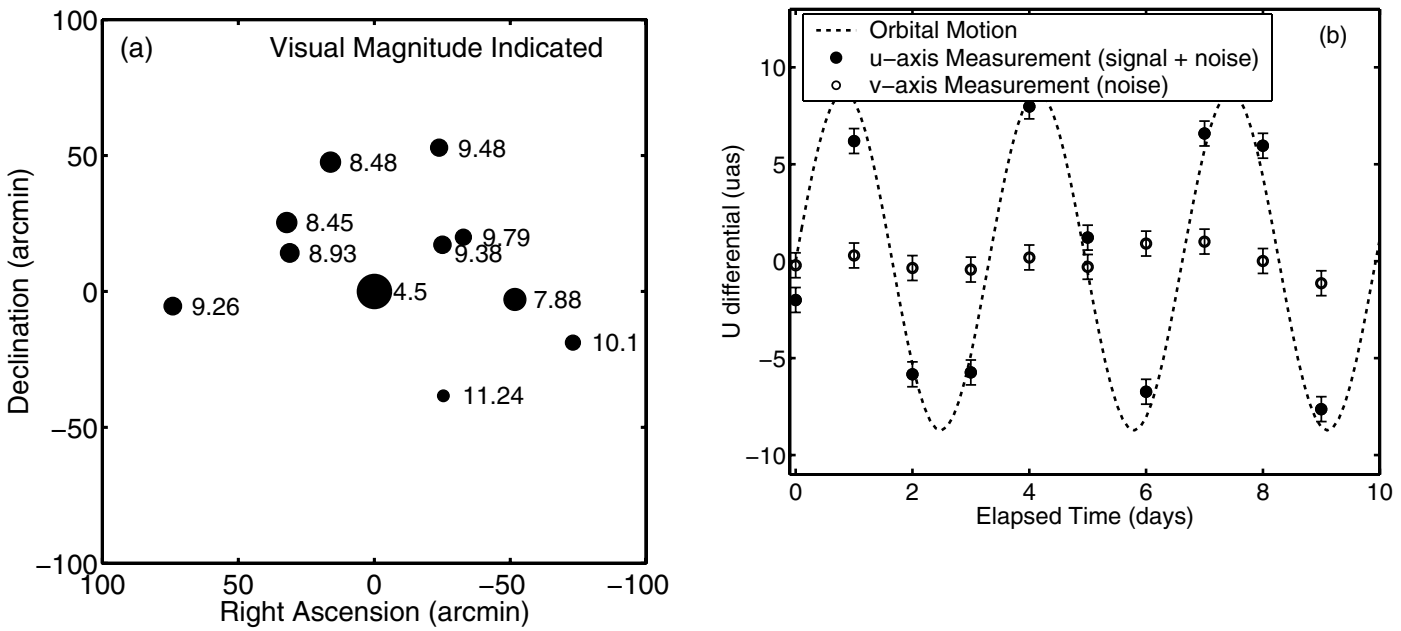

FIG. 18.—Simulation of GBDA with *SIM* of the 3.9 $M_{\rm Jup}$ planet around Tau Boo. (*a*) 10 brightest reference stars within 75′ of Tau Boo. (*b*) Simulated measurement of the 9 μas amplitude signal (assumed to be along one axis). Residual proper motion and parallax are removed from the plot but were included as error sources in the astrometric model.

and reference stars are not known to microarcsecond precision, this approach is not useful for long-period (>0.5 yr) signals.

GBDA is a hybrid mode that uses coarse (early-mission) grid star positions to solve for baseline parameters. GBDA requires the measurement of several grid stars using two nearly orthogonal baseline orientations in addition to the target and reference star measurements. It is more efficient than GNAA (two vs. three baselines) but is still limited to the detection of short periods. In GBDA, grid catalog errors combine with stochastic baseline repointing errors to cause baseline orientation, length, and constant-term errors. These in turn mix with reference frame catalog errors resulting in random noise on the target-star estimate. To keep the errors between the target and reference stars below a fraction of a microarcsecond, the baseline reorientation requirements for subsequent visits are 0.1° (around the line of sight) and 0.01° (tilt toward the target). These are easily met using star trackers.

To demonstrate the GBDA approach, we modeled the detection of the known planet orbiting Tau Boo (Butler et al. 1997). The planet has a measured period of 3.3 days and (minimum) mass 3.9 $M_{\rm Jup}$, from which we derive that the astrometric amplitude is 9.0 μas. In the model we assumed that the stellar reflex motion was on one axis in order to demonstrate that the magnitude of the astrometric errors is independent of the signal amplitude. Tau Boo's proper motion was assumed to be known to 1 mas yr^{-1}. We modeled 20 GBDA measurements over a 10 day period. We used realistic catalog errors for the reference and target-star positions and proper motions. The NA reference frame consisted of the 10 brightest reference stars within a 75′ radius of Tau Boo (Fig. 18*a*). We modeled instrument systematic errors based on the flight instrument design, and added signal-dependent noise in quadrature to the target and reference star observations. For our adopted observing scheme, this yields an astrometric error of 0.65 μas per axis per visit. Figure 18*b* shows the simulated signal and measurements, and that the Tau Boo planet is easily detected by the GBDA technique.

APPENDIX B

ALL-SKY ASTROMETRIC GRID

SIM observes stars sequentially within a 15° patch of sky termed a "tile," while the instrument is held inertially stable by observing a pair of guide stars with guide interferometers. One guide star lies close in angle to the target star; the other is roughly 15° away. Details of the operation of *SIM* and how the guide stars are used to derive microarcsecond precisions on science targets is discussed in, e.g., Laskin (2006). Here we describe the development of the astrometric grid of

stars to which the science measurements are referenced, the astrophysical selection of those stars, and the "frame tie" of the grid to an inertial frame defined by distant quasars.

SIM will construct an all-sky astrometric grid including 1302 preselected stars and a smaller number of quasars. The grid accuracy is expected to be about 3 μas in mean-epoch position, based on the current best estimate of instrument performance. Each grid object will be observed about 200 times during the nominal 5 yr mission. The limited number of grid objects and the moderate density of the grid is explained by its special role that is more utilitarian than research-driven. *SIM* will largely rely on self-calibration of the instrument and on the determination of the baseline orientation from its own interferometric measurements of the grid objects interspersed with routine measurements of science targets. A number of key instrument parameters (for example, the baseline length) cannot be determined to the required picometer-level accuracy by external metrology techniques and, therefore, should be derived from observations of stars.

Because the number of instrument and attitude parameters is large, it is necessary to observe a global grid of stars multiple times during the mission to construct an overdetermined system of linear equations. The grid solution is a one-step direct least-squares adjustment of a system of $\sim 300,000$ linear equations of $\sim 160,000$ unknowns. Of the latter set, only some 6500 unknown parameters are related to the grid objects (i.e., the mean positions, parallaxes, and proper motions that constitute the actual astrometric grid). An efficient and fast algorithm has been developed to solve the grid equations eliminating of the numerous attitude terms by QR factorization, described in Makarov & Milman (2005).

The astrometric accuracy of the grid can be directly evaluated from the global covariance, as far as random errors of measured positions are concerned. Systematic errors are not always possible to predict or to model, and are less amenable to straightforward covariance analysis. However, the manageable size of the reduced design matrix allows us to employ rigorous mathematical analysis of *possible* systematic errors and compute the complete space of those perturbations that have a strong adverse effect on the grid accuracy. As explained in more detail in Makarov & Milman (2005), measurement errors (accidental and systematic alike) propagate nonuniformly in different singular vectors spanning the parameter space, which is likely to result in large-scale (so-called "zonal") correlated spatial errors in the grid. They may be represented by spherical orthogonal functions for the parallax error distribution, and by vector spherical harmonics for the proper motion error distribution, which is a vector field on the unit sphere (Kopeikin & Makarov 2006). The spatial power spectrum of grid errors is red, meaning the signal is larger at low frequencies.

We explored the grid performance for a wide range of possible instrument systematic errors developed as a by-product of the detailed flight instrument design. This allows us not only to evaluate the expected rms grid performance and the properties of the zonal errors but also to estimate confidence levels, for instance, how likely the actual *SIM* grid will be better than a given value.

An effective way to mitigate these zonal errors is to use a number of quasars as grid objects; quasar parallaxes are vanishingly small and can be constrained to zero in the global solution. Numerical simulations and covariance analysis have shown that with only 25 additional optically bright quasars in the grid program, the grid parallax astrometric accuracy improves by $\sim 28\%$, meeting the mission goal (4 μas) with considerable margin. Using the current best estimate for the instrument performance, the grid should achieve 3 μas. Quasars also dramatically improve the grid confidence: the 99% confidence limit on grid parallax error drops from 6.2 μas to 3.1 μas (with the same simulated mission but with quasars included in the grid).

Analytical considerations showed that the astrometric accuracy on bright, frequently observed science program stars should be equal to or slightly surpassing that of grid stars. Spreading observation times evenly across the mission time is not the best strategy for parallax. Significantly better parallax can be obtained for a given star by simply scheduling the chosen number of observation at the most favorable times, determined by a semiempirical optimization algorithm implemented in the wide-angle processing code. In a similar way, the observation schedule can be optimized for any object on proper-motion performance, or a combination of all three types of astrometric parameters. A realistic *SIM* schedule takes into account the desired science objectives of the measurements and optimizes across the ensemble of all science targets both the integration time invested and the observation epochs. While this ideal is likely impossible to realize in practice, observation planning will definitely play a major role in extracting the best astrometric performance from the instrument.

APPENDIX C

ASTROMETRIC REFERENCE FRAME

SIM will define a reference frame accurate to 3 μas using 50–100 quasars to "tie" the stellar grid to a presumed inertial frame. The *SIM* frame will complement the *Gaia* catalog, as the *SIM* frame will have much more precise positions than *Gaia*'s, albeit for a smaller number of sources. These distant sources are assumed to have negligible parallaxes and proper motions, and, as noted above, quasar observations will also reduce the amplitude of zonal errors in the astrometric grid. Because of the physical

effects discussed in § 13, radio-quiet quasars are to be preferred, as there are less likely to be asymmetries, or worse, time-dependent position shifts, in the optical photocenters relative to the massive black holes that serve as inertial reference points (§ 13.2). Most *SIM* science programs are not affected by frame rotation. For instance, parallaxes are quite insensitive to a rotation rate. Some topics require the frame to be inertial to $\sim$2 μas yr^{-1}. Examples include galactic structure, including tidal tails (§ 9) and extragalactic rotational parallaxes (§ 13). This requirement should be easily met using 50–100 radio-quiet quasars, selected from bright quasar catalogs. Note that a tie to the *radio* (ICRF) frame plays no direct role in these investigations.

Tying the *SIM* inertial frame (defined by radio-quiet quasars and grid stars) to the ICRF serves two fundamental purposes. First, future astrometric catalogs will require a registration with the ICRF since that frame is the basis for all current astrometric data. Second, accurate registration between reference frames is important for science that combines astrometric data in two frames, for instance *SIM* and VLBI data. This requires a tie to the ICRF, and hence *SIM* will include (radio-loud) quasars in the astrometric grid. The study of nonthermal radio emission associated with stars will lead to a better understanding of the mechanisms giving rise to an individual source's spectral energy distribution (see § 6.6). We showed in § 13 that astrometry is a powerful tool for probing the structure of blazars. A tie to radio (VLBI) images is important for a full understanding of the physical processes in quasars that manifest themselves as astrometric motion.

The tie must of course be done using radio-loud quasars, since the ICRF is fundamentally a radio reference frame. The accuracy of the radio-optical frame tie will therefore depend on the quasars in common between the two frames. Since the *SIM* reference frame will be much more accurate than the ICRF, errors in tying the frames are likely to be dominated by the VLBI observations that define the ICRF. Quasars will be chosen from the 212 ICRF sources; there is approximately one ICRF quasar per 15° diameter *SIM* tile, with fewer in the southern hemisphere and in the plane of the Milky Way Galaxy. By establishing an accurate link between the optical *SIM* frame and the radio ICRF, high-resolution imaging data at these disparate wavelengths can be accurately aligned to allow absolute positional correlation.

Quasars with radio emission may not make ideal astrometric reference targets, due to variability. It is not yet clear how the known structure changes seen at milliarcsecond levels (from VLBI imaging) in the most variable radio-loud objects translate into astrometric shifts in the optical. Section 13 discusses the physical models that allow us to make estimates of the effects, prior to *SIM* launch. Although there is a lot of experience with the ICRF defined by radio observations, the physics is not understood well enough to make a simple prediction. Indeed, we fully expect that *SIM* will provide key insights into this problem.

The quality of the radio-optical frame tie can be improved in a number of ways. First, the quasars in common should be selected to avoid the most highly variable targets. Second, repeated astrometric measurements taken during the *SIM* 5 yr mission can be checked for consistency and obvious outliers can be rejected. Third, the number of quasars in common should be large to allow us to average out the offsets, which will be uncorrelated from target to target. Since the investment of *SIM* observing time may be traded between the number of quasars and the accuracy of the astrometric measurements, intrinsic astrometric variability would lead one to prefer to increase the number of quasars in common; this would also make the identification of outliers easier. Those objects which show astrometric signatures as large as perhaps 15–20 μas will be easily eliminated from the reference frame program but will make for very interesting astrophysical studies. Finally, we note that detailed studies of the physical processes in quasars, as probed by the astrometric program described in § 13, can provide insights into the most effective selection of quasars to use in the end-of-mission solution for the reference frame, allowing some quasars to be selectively omitted from the solution.

APPENDIX D

SELECTION OF *SIM* GRID STARS

The *SIM* grid comprises 1302 K-giant stars spread quasi-uniformly over the sky. K-giant stars were chosen for several reasons. K-giant stars are numerous and located at all galactic latitudes. K-giant stars are intrinsically much brighter than dwarf stars. Compared to similarly numerous F and G dwarfs (the most common dwarfs in a $V \approx 9$–12 mag limited sample), K giants are intrinsically brighter by 4–5 mag at V. Thus, for a given brightness, K-giant stars are 5–10 times more distant than F and G dwarfs. Astrometric motions induced by unseen stellar and planetary companions are of course minimized by the increased distance (e.g., Gould 2001; Frink et al. 2001; Peterson et al. 2002).

Candidate K-giant stars were selected from the Tycho-2 and 2MASS catalogs based upon a compiled catalog of photometric colors ($BVJHK_s$), proper motions, and distances (if known) of the stars. A near-infrared reduced proper-motion diagram was constructed to separate candidate K-giant stars from dwarf stars of similar color (Gould & Morgan 2003). The visual extinction for each candidate K-giant star was estimated to produce extinction corrected magnitudes and colors (i.e., spectral types) and

distance estimates (Ciardi 2004). The Tycho-2 catalog giant star extraction was supplemented with a ground-based survey, sparsely covering the whole sky with a roughly uniform pattern of "bricks," each covering ≈ 0.5 deg^2 per brick (Patterson et al. 2001). The survey utilized the Washington M, T_2, and DDO51 filter system to identify candidate low metallicity K-giant stars (Majewski et al. 2000). Together the two methods provided a total of $\sim 170,000$ K-giant stars from which the grid star candidates could be selected. For each brick, six candidate grid stars were selected for a total of 7812 candidate grid stars. A minimum distance of 500 pc was required for candidate selection. The candidate grid stars have a median visual magnitude of $V = 9.9$ mag, with 90% of the stars between $V = 9.0$–10.5 mag. The median distance of the grid stars is $d = 600$ pc, with 90% of the stars between $d = 500$ and 1000 pc.

Detailed simulations of the effectiveness of RV "screening" of grid star candidates has been performed by Catanzarite (2004), using reasonable assumptions about the population of binary companions that induce astrometric perturbations in the primary star. The results show that without RV screening, the grid is likely to be significantly contaminated, but that screening to a fairly modest precision of 50 m s^{-1}, with three observations spread over at least 3 yr, are sufficient to reduce the contamination to a very low level (Fig. 19). RV screening mostly fails to reject brown dwarfs and giant planets, but most of the companions remaining produce small astrometric signatures, and have a negligible effect on the grid as a whole. A pilot study of the RV stability of K-giant stars by Frink et al. (2001) showed that early K-giant stars ($B - V \approx 0.8$–1.1 mag) were intrinsically stable at a level of 20–30 m s^{-1}. Analytic studies and Monte Carlo simulations (Gould 2001; Frink et al. 2001; Peterson et al. 2002) indicated that a modest RV screening program (30–50 m s^{-1}) would reduce the fraction of grid stars with unmodeled astrometric motions detectable by *SIM* to less than 1%–10%. In September 2004, a high-precision (< 50 m s^{-1}) RV monitoring campaign was begun to remove those stars from the candidate list with unseen stellar companions. Observations are currently being performed at the 1.2 m Euler Telescope at La Silla. The RV program spans four years and is structured such that half of the candidates (3 per brick) are observed twice in years 1 and 2 with a minimum separation between observations of 9 months. Those stars which display large RV excursions ($\chi^2_\nu > 4$) are removed from the candidate list. The removed stars are replaced and are observed during years 3 and 4, along with the surviving candidates from years 1 and 2. The program has finished its second year.

The effective sensitivity of the radial-velocity program to detect companions is a convolution of the stellar atmospheric jitter and the instrumental jitter. Thus, the effective precision of the RV measurements is given by $\sigma_{\rm total} = (\sigma^2_{\rm inst} + \sigma^2_\star)^{1/2}$ where $\sigma_{\rm inst}$ is the RV precision of the instrument or data reduction, and $\sigma_\star$ is the intrinsic stellar atmospheric jitter. In Figure 20, we present the frequency distribution of the difference between two consecutive RV measurements separated by 300+ days for 847 candidate grid stars. The precision for each RV measurement is approximately $\sigma_{\rm inst} = 20$–30 m s^{-1}. The intrinsic stellar jitter of early K giants, as found by Frink et al. (2001), is $\sigma_\star \approx 25$ m s^{-1}, yielding an expected distribution width (in the absence of companions) of $\sigma_{\rm total} \approx 30$–$35$ m s^{-1}. The central por-

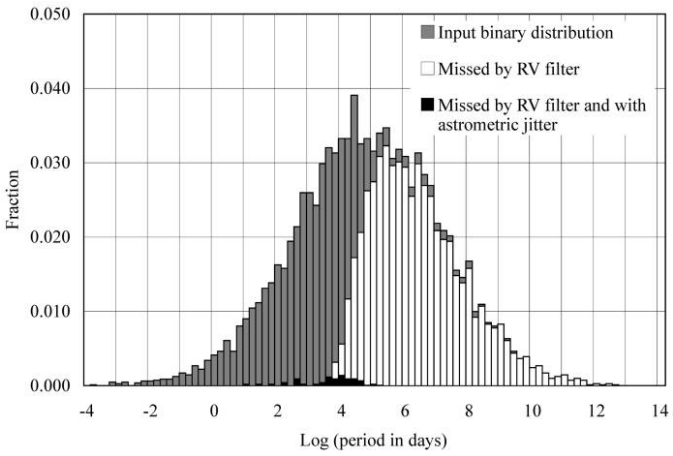

FIG. 19.—Histogram of the simulated period distribution of stellar companions to candidate *SIM* grid stars, showing the effectiveness of RV screening in eliminating binary stars with significant astrometric signatures from the grid. The binary mass and orbit distributions are assumed to be those of Duquennoy & Mayor (1991). Gray symbols represent the input period distribution. RV filters virtually all binaries with periods less than 104 days, leaving only the long-period companions (white symbols). Very few of these remaining (i.e., missed) long-period companions produce astrometric motion detectable by *SIM* (jitter > 4 μas rms, shown in black).

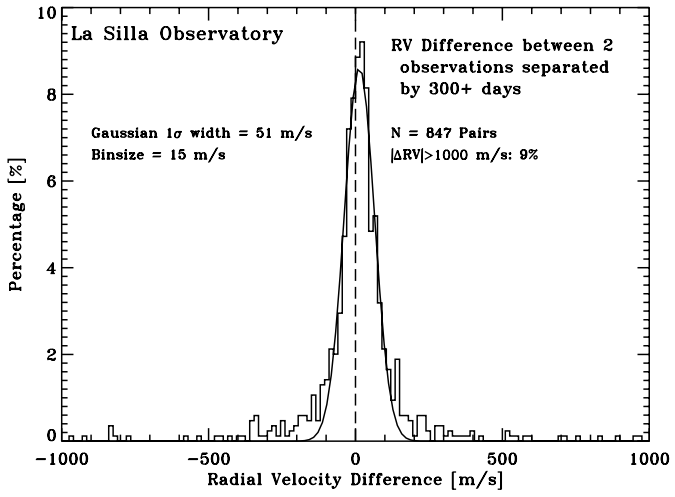

FIG. 20.—Frequency distribution of the difference between consecutive radial-velocity measurements separated by more than the 300 days. Data taken at La Silla Observatory as part of the *SIM* grid star RV monitoring program.

tion of the distribution is well modeled with a Gaussian of width $\sigma_{\rm total} = 51\ {\rm m\,s^{-1}}$, slightly larger than the expected width, indicating the presence (not unexpectedly) of binaries in the sample or a slightly higher atmospheric jitter (40 vs. 25 $\rm m\,s^{-1}$). Additionally, the high velocity wings ($|\Delta{\rm RV}| > 100\ {\rm m\,s^{-1}}$) are likely the result of the presence of unseen companions to the grid stars. Using a reduced χ^2 of $\chi^2_\nu < 4$ as the cutoff for acceptance, approximately 60% of the stars in this subsample would pass through for further radial-velocity vetting in years 3 and 4 of the program.

REFERENCES

Albrecht, A., et al. 2006, preprint (astro-ph/0609591)
Alcock, C., et al. 2000, ApJ, 542, 281
Alibert, Y., Mordasini, C., Benz, W., & Winisdoerffer, C. 2005, A&A, 434, 343
Andersen, J. 1991, A&A Rev., 3, 91
Anguita, C., Loyola, P., & Pedreros, M. H. 2000, AJ, 120, 845
Antokhina, E. A., Moffat, A. F. J., Antokhin, I. I., Bertrand, J.-F., & Lamontagne, R. 2000, ApJ, 529, 463
Armandroff, T. E. 1989, AJ, 97, 375
Armandroff, T. E., Olszewski, E. W., & Pryor, C. 1995, AJ, 110, 2131
Armstrong, J. T., et al. 1992, AJ, 104, 241
Bahcall, J. 1991, The Decade of Discovery in Astronomy and Astrophysics (Decadal Survey), (Washington, DC: National Academies Press)
Balick, B., & Frank, A. 2002, ARA&A, 40, 439
Band, D. L., & Malkan, M. A. 1989, ApJ, 345, 122
Baraffe, I., Chabrier, G., Allard, F., & Hauschildt, P. H. 1998, A&A, 337, 403
Baraffe, I., Chabrier, G., Allard, F., & Hauschildt, P. H. 2002, A&A, 382, 563
Barziv, O., Kaper, L., Van Kerkwijk, M. H., Telting, J. H., & Van Paradijs, J. 2001, A&A, 377, 925
Bellazzini, M., Ferraro, F. R., & Ibata, R. 2002, AJ, 124, 915
Bellazzini, M., Ferraro, F. R., & Ibata, R. 2003, AJ, 125, 188
Bellazzini, M., Ibata, R., Monaco, L., Martin, N., Irwin, M. J., & Lewis, G. F. 2004, MNRAS, 354, 1263
Belokurov, V., Evans, N. W., Irwin, M. J., Hewett, P. C., & Wilkinson, M. I. 2006a, ApJ, 637, L29
Belokurov, V., et al. 2006b, ApJ, 642, L137
Belokurov, V., et al. 2006c, ApJ, 647, L111
Benson, A. J. 2005, MNRAS, 358, 551
Benz, W., Alibert, Y., Mordasini, C., & Naef, D. 2006, in IAU Colloq. 200, Direct Imaging of Exoplanets: Science & Techniques, ed. C. Aime & F. Vakili, 1
Bertotti, B., Iess, L., & Tortora, P. 2003, Nature, 425, 374
Bildsten, L., et al. 1997, ApJS, 113, 367
Bisikalo, D. V., Harmanec, P., Boyarchuk, A. A., Kuznetsov, O. A., & Hadrava, P. 2000, A&A, 353, 1009
Bjork, S. R., & Chaboyer, B. 2006, ApJ, 641, 1102
Boboltz, D. A., & Diamond, P. J. 2005, ApJ, 625, L978
Boboltz, D. A., Fey, A. L., Johnston, K. J., Claussen, M. J., de Vegt, C., Zacharias, N., & Gaume, R. A. 2003, AJ, 126, 484
Boboltz, D. A., Fey, A. L., Puatua, W. K., Zacharias, N., Claussen, M. J., Johnston, K. J., & Gaume, R. A. 2007, AJ, 133, 906
Boboltz, D. A., & Marvel, K. B. 2005, ApJ, 627, L45
Böker, T., & Allen, R. J. 1999, ApJS, 125, 123
Bono, G., Castellani, V., & Marconi, M. 2000, ApJ, 529, 293
Boss, A. 2001, ApJ, 551, L167
Bothun, G., Hsu, S. D. H., & Murray, B. 2006, preprint (astro-ph/0612106)
Bouvier, J., & Bertout, C. 1989, A&A, 211, 99
Bouvier, J., et al. 1995, A&A, 299, 89
Branchini, E., Eldar, A., & Nusser, A. 2002, MNRAS, 335, 53
Brown, W. R., Geller, M. J., Kenyon, S. J., & Kurtz, M. 2006, ApJ, 640, L35
Burrows, A., et al. 1997, ApJ, 491, 856
Butler, R. P., Marcy, G. W., Williams, E., Hauser, H., & Shirts, P. 1997, ApJ, 474, L115
Butler, R. P., Vogt, S. S., Marcy, G. W., Fischer, D. A., Wright, J. T., Henry, G. W., Laughlin, G., & Lissauer, J. J. 2004, ApJ, 617, 580
Butler, R. P., Wright, J. T., Marcy, G. W., Fischer, D. A., Vogt, S. S., Tinney, C. G., Jones, H. R. A., Carter, B. D., Johnson, J. A., McCarthy, C., & Penny, A. J. 2006, ApJ, 646, 505
Caldwell, J. A. R., & Coulson, I. M. 1986, MNRAS, 218, 223
Caldwell, J. A. R., & Coulson, I. M. 1987, AJ, 93, 1090
Carraro, G. 2005, ApJ, 621, L61
Catanzarite, J. H. 2004, BAAS, 36, 1489
Catanzarite, J., Shao, M., Tanner, A., Unwin, S., & Yu, J. 2006, PASP, 118, 1319
Chaboyer, B. 1995, ApJ, 444, 9
Chaboyer, B., Demarque, P., Kernan, P., Krauss, L., & Sarajedini, A. 1996, MNRAS, 283, 683
Chambers, K. C. 2005, in ASP Conf. Ser. 338, Astrometry in the Age of the Next Generation of Large Telescopes, ed. P. K. Seidelmann & A. K. B Monet (San Francisco: ASP), 134
Charlot, S., Worthey, G., & Bressan, A. 1996, ApJ, 457, 625
Chauvin, G., Lagrange, A.-M., Dumas, C., Zuckerman, B., Mouillet, D., Song, I., Beuzit, J.-L., & Lowrance, P. 2005, A&A, 438, L25
Chiang, E. I., & Murray, N. 2002, ApJ, 576, 473
Ciardi, D. R. 2004, BAAS, 36, 770
Clark, J. S., Goodwin, S. P., Crowther, P. A., Kaper, L., Fairbairn, M., Langer, N., & Brocksopp, C. 2002, A&A, 392, 909
Coburn, W., Heindl, W. A., Rothschild, R. E., Gruber, D. E., Kreykenbohm, I., Wilms, J., Kretschmar, P., & Staubert, R. 2002, ApJ, 580, 394
Crane, J. D., Majewski, S. R., Rocha-Pinto, H. J., Frinchaboy, P. M., Skrutskie, M. F., & Law, D. R. 2003, ApJ, 594, L119
Da Costa, G. S., & Armandroff, T. E. 1995, AJ, 109, 2533
Damour, T., Piazza, F., & Veneziano, G. 2002, Phys. Rev. D, 66, 046007
Dekel, A., Bertschinger, E., Yahil, A., Strauss, M. A., Davis, M., & Huchra, J. P. 1993, ApJ, 412, 1
Demarque, P. 1980, in IAU Symp. 85, Star Clusters, ed. J. E. Hesser (Dordrecht: Reidel), 281
Dinescu, D. I., Girard, T. M., & van Altena, W. F. 1999, AJ, 117, 1792
Dinescu, D. I., Keeney, B. A., Majewski, S. R., & Girard, T. M. 2004, AJ, 128, 687

Dinescu, D. I., Majewski, S. R., Girard, T. M., & Cudworth, K. M. 2000, AJ, 120, 1892
Duquennoy, A., & Mayor, M. 1991, A&A, 248, 485
Dvali, G., Gabadadze, G., & Porrati, M. 2000, Phys. Lett. B, 485, 208
G., Efstathiou, C., Lawrence, Tauber, J., & the Planck Science Team2005,The Planck Blue Book, www.rssd.esa.int/index.php?project=PLANCK
Eisner, J. A., & Kulkarni, S. R. 2002, ApJ, 574, 426
Einstein, A. 1936, Science, 84, 506
Elvis, M. 2000, ApJ, 545, 63
Endl, M., Cochran, W. D., Kürster, M., Paulson, D. B., Wittenmyer, R. A., MacQueen, P. J., & Tull, R. G. 2006, ApJ, 649, 436
ESA, 1997, The *Hipparcos* and Tycho Catalogs (ESA SP-1200; Garching: ESA)
Feast, M., & Whitelock, P. 1997, MNRAS, 291, 683
Fender, R. 2006, in Compact Stellar X-ray Sources (Cambridge: Cambridge Univ. Press), 381
Ferrero, E., Wagner, S. J., Emmanoulopoulos, D., & Ostorero, L. 2006, A&A, 457, 133
Fey, A. L., et al. 2004, AJ, 126, 484
Ford, E. B. 2005, AJ, 129, 1706
Ford, E. B. 2006, PASP, 118, 364
Franciosini, E., Massi, M., Paredes, J. M., & Estalella, R. 1999, A&A, 341, 595
Freedman, W. L., et al. 2001, ApJ, 553, 47
Frinchaboy, P. M., Majewski, S. R., Crane, J. D., Reid, I. N., Rocha-Pinto, H. J., Phelps, R. L., Patterson, R. J., & Muñoz, R. R. 2004, ApJ, 602, L21
Frink, S., Quirrenbach, A., Fischer, D., Röser, S., & Schilbach, E. 2001, PASP, 113, 173
Fröhlich, C. 2006, Space Sci. Rev., 125, 53
Gatewood, G. 1987, AJ, 94, 213
Gerhard, O. E., & Spergel, D. N. 1992, ApJ, 389, L9
Ghigna, S., Moore, B., Governato, F., Lake, G., Quinn, T., & Stadel, J. 1998, MNRAS, 300, 146
Giacconi, R., Gursky, H., Paolini, F. R., & Rossi, B. B. 1962, Phys. Rev. Lett., 9, 439
Gieren, W., Storm, J., Barnes, T. G., III, Fouqué, P., Pietrzyński, G., & Kienzle, F. 2005, ApJ, 627, 224
Gliese, W. 1969, Veröff. Astron. Rechen-Inst. Heidelberg, 22, 1
Goldreich, P., Lithwick, Y., & Sari, R. 2004, ApJ, 614, 497
Gnedin, O. Y., Gould, A., Miralda-Escudé, J., & Zenter, A. R. 2005, ApJ, 634, 344
Gnedin, O. Y., Lee, H.-M., & Ostriker, J. P. 1999, ApJ, 522, 935
Goerdt, T., Moore, B., Read, J. I., Stadel, J., & Zemp, M. 2006, MNRAS, 368, 1073
Gould, A. 1995, ApJ, 441, L21
Gould, A. 2000, ApJ, 542, 785
Gould, A. 2001, ApJ, 559, 484
Gould, A., Bennett, D. P., & Alves, D. R. 2005, ApJ, 614, 404
Gould, A., & Morgan, C. W. 2003, ApJ, 585, 1056
Gould, A., & Salim, S. 1999, ApJ, 524, 794
Gould, A., et al. 2006, ApJ, 644, L37
Grillmair, C. J. 2006a, ApJ, 645, L37
Grillmair, C. J. 2006b, ApJ, 651, L29
Grillmair, C. J., & Dionatos, O. 2006a, ApJ, 641, L37
Grillmair, C. J., & Dionatos, O. 2006b, ApJ, 643, L17
Grillmair, C. J., & Johnson, R. 2006, ApJ, 639, L17
Harries, T. J., Hilditch, R. W., & Hill, G. 1998, MNRAS, 295, 386
Harris, H. C., et al. 2005, in ASP Conf. Ser. 338, Astrometry in the Age of the Next Generation of Large Telescopes, ed. P. K. Seidelmann & A. K. B. Monet, 122
Harris, W. E. 1996, AJ, 112, 1487
Henry, T. J., Franz, O. G., Wasserman, L. H., Benedict, G. F., Shelus, P. J., Ianna, P. A., Kirkpatrick, J. D., & McCarthy, D. W., Jr. 1999, ApJ, 512, 864
Henry, T. J., Kirkpatrick, J. D., & Simons, D. A. 1994, AJ, 108, 1437
Henry, T. J., & McCarthy, D. W., Jr. 1993, AJ, 106, 773
Herrero, A., Kudritzki, R. P., Gabler, R., Vilchez, J. M., & Gabler, A. 1995, A&A, 297, 556
Herrero, A., Puls, J., & Villamariz, M. R. 2000, A&A, 354, 193
Hills, J. G. 1988, Nature, 331, 687
Hillwig, T. C., Gies, D. R., Huang, W., McSwain, M. V., Stark, M. A., van der Meer, A., & Kaper, L. 2004, ApJ, 615, 422
Høg, E., Novikov, I. D., & Polanarev, A. G. 1995, A&A, 294, 287
Hu, W. 2005, in ASP Conf. Ser. 339, Observing Dark Energy, ed. S. C. Wolff & T. R. Lauer, 215 (H05)
Hummel, C. A., et al. 1994, AJ, 108, 326
Hutter, D. J., & Mufson, S. L. 1986, ApJ, 301, 50
Ibata, R. A., Gilmore, G., & Irwin, M. J. 1995, MNRAS, 277, 781
Ibata, R. A., Lewis, G. F., Irwin, M. J., & Quinn, T. 2002, MNRAS, 332, 915
Ida, S., & Lin, D. N. C. 2005, ApJ, 626, 1045
Imai, H., Obara, K., Diamond, P. J., Omodaka, T., & Sasao, T. 2002, Nature, 417, 829
Johnson, J. A., et al. 2007, ApJ, in press
Johnston, K. J., de Vegt, C., & Gaume, R. A. 2003, AJ, 125, 3252
Johnston, K. J., et al. 1995, AJ, 110, 880
Johnston, K. V. 1998, ApJ, 495, 297
Johnston, K. V. 2001, ASP Conf. Ser. 230, Galaxy Disks and Disk Galaxies, ed. J. G. Funes, S. J. & E. M. Corsini, 417
Johnston, K. V., Spergel, D. N., & Haydn, C. 2002, ApJ, 570, 656
Johnston, K. V., Zhao, H., Spergel, D. N., & Hernquist, L. 1999, ApJ, 512, L109
Jones, B. F., Klemola, A. R., & Lin, D. N. C. 1994, AJ, 107, 1333
Jordi, C., et al. 2006, MNRAS, 367, 290
Kallivayalil, N., van der Marel, R. P., Alcock, C., Axelrod, T., Cook, K. H., Drake, A. J., & Geha, M. 2006, ApJ, 638, 772
Kenyon, S. J., & Bromley, B. C. 2006, AJ, 131, 1837
Keller, S. C., & Wood, P. R. 2006, ApJ, 642, 834
Kidger, M. 2000, AJ, 119, 2053
Kley, W., Lee, M. H., Murray, N., & Peale, S. J. 2005, A&A, 437, 727
Kleyna, J., Wilkinson, M. I., Evans, N. W., Gilmore, G., & Frayn, C. 2002, MNRAS, 330, 792
Klypin, A. A., Kratsov, A. V., Valenzuela, O., & Prada, F. 1999, ApJ, 522, 82
Königl, A. 1981, ApJ, 243, 700
Kopeikin, S. M., & Makarov, V. V. 2006, AJ, 131, 1471
Kovalevsky, J., et al. 1997, A&A, 323, 620
Krolik, J. 1999, Active Galactic Nuclei (Princeton: Princeton Univ. Press)
Kroupa, P. 1997, NewA, 2, 139
Kroupa, P., & Bastian, U. 1997, NewA, 2, 77
Kroupa, P., Röser, S., & Bastian, U. 1994, MNRAS, 266, 412
Kuhn, J. R. 1993, ApJ, 409, L13

Kunkel, W. E. 1979, ApJ, 228, 718
Lane, B. F., & Muterspaugh, M. W. 2004, ApJ, 601, 1129
Laney, C. D., & Stobie, R. S. 1994, MNRAS, 266, 441
Laskin, R. A. 2006, Proc. SPIE, 6268, 6268-23
Lattimer, J. M., & Prakash, M. 2004, Science, 304, 536
Law, D. R., Johnston, K. V., & Majewski, S. R. 2005, ApJ, 619, 807
Lestrade, J.-F. 2000, Proc. 5th EVN Symp., ed. J. E. Conway, A. G. Polatidis, R. S. Booth, & Y. Pihlström (Onsala, Sweden: Onsala Space Observatory), 155
Lestrade, J.-F, Preston, R. A., Jones, D. L., Phillips, R. B., Rogers, A. E. E., Titus, M. A., Rioja, M. J., & Gabuzda, D. C. 1999, A&A, 344, 1014
Lestrade, J.-F., et al. 1993, ApJ, 410, 808
Libeskind, N. I., Frenk, C. S., Cole, S., Helly, J. C., Jenkins, A., Navarro, J. F., & Power, C. 2005, MNRAS, 363, 146
Lin, D. N. C., & Faber, S. M. 1983, ApJ, 266, L21
Lin, D. N. C., Papaloizou, J. C. B., Terquem, C., Bryden, G., & Ida, S. 2000, Protostars and Planets IV, ed. V. Mannings, A. P. Boss, & S. S. Russell (Tucson: Univ. Arizona Press), 1111
Liu, Q. Z., van Paradijs, J., & van den Heuvel, E. P. J. 2000, A&AS, 147, 25
Liu, Q. Z., van Paradijs, J., & van den Heuvel, E. P. J. 2001, A&A, 368, 1021
Luyten, W. J. 1979, The Luyten Half-Second (LHS) Catalog (2nd ed.; Minneapolis: Univ. Minnesota)
Lynden-Bell, D. 1982, Observatory, 102, 202
Lynden-Bell, D., & Lin, D. N. C. 1977, MNRAS, 181, 37
Lynden-Bell, D., & Lynden-Bell, R. M. 1995, MNRAS, 275, 429
Ma, C., et al. 1998, AJ, 116, 516
Macri, L. M., Stanek, K. Z., Bersier, D., Greenhill, L. J., & Reid, M. J. 2006, ApJ, 652, 1133
Majewski, S. R. 1992, ApJS, 78, 87
Majewski, S. R., Law, D. R., Polak, A. A., & Patterson, R. J. 2006, ApJ, 637, L25
Majewski, S. R., Ostheimer, J. C., Kunkel, W. E., & Patterson, R. J. 2000, AJ, 120, 2550
Majewski, S. R., Skrutskie, M. F., Weinberg, M. D., & Ostheimer, J. C. 2003, ApJ, 599, 1082
Majewski, S. R., et al. 2004, AJ, 128, 245
Majewski, S. R., et al. 2005, AJ, 130, 2677
Makarov, V. V., & Kaplan, G. H. 2005, AJ, 129, 2420
Makarov, V. V., & Milman, M. 2005, PASP, 117, 757
Marcy, G., Butler, R. P., Fischer, D., Vogt, S., Wright, J. T., Tinney, C. G., & Jones, H. R. A. 2005, Prog. Theor. Phys. Suppl., 158, 24
Margon, B. 1984, ARA&A, 22, 507
Marr, J. C., IV 2006, Proc. 57th IAC (Reston, VA: AIAA), IAC-06-A3.1.01
Mashchenko, S., Sills, A., & Couchman, H. M. 2006, ApJ, 640, 252
Mateo, M. L. 1998, ARA&A, 36, 435
Mayor, M. 1974, A&A, 32, 321
McKee, C., & Taylor, J. 2001, Astronomy and Astrophysics in the New Millennium (Decadal Survey) (Washington, DC: National Academies Press)
McKinney, J. 2006, MNRAS, 368, 1561
Mei, S., Blakeslee, J. P., Tonry, J. L., Jordán, A., Peng, E. W., Côté, P., Ferrarese, L., West, M. J., Merritt, D., & Milosavljevic, M. 2005, ApJ, 625, 121
Meier, D. L., Koide, S., & Uchida, Y. 2001, Science, 291, 84
Mekkaden, M. V. 1998, A&A, 340, 135
Merritt, D., & Milosavljevic, M. 2005, Living Rev. Relativ., 8, 8
Metzger, M. R., Caldwell, J. A. R., & Schechter, P. L. 1998, AJ, 115, 635
Milosavljevic, M., & Phinney, S. 2005, ApJ, 622, L93
Minniti, D. 1996, ApJ, 459, 175
Mirabel, I. F., & Rodrigues, I. 2003, A&A, 398, L25
Mirabel, I. F., Rodriguez, L. F., Cordier, B., Paul, J., & Lebrun, F. 1992, Nature, 358, 215
Miyamoto, M., & Yoshii, Y. 1995, AJ, 110, 1427
Momany, Y., & Zaggia, S. 2005, A&A, 437, 339
Monnier, J. D., et al. 2004, ApJ, 605, 436
Moore, B., Ghigna, S., Governato, F., Lake, G., Quinn, T., Stadel, J., & Tozzi, P. 1999, ApJ, 524, L19
Moore, B., Governato, F., Quinn, T., Stadel, J., & Lake, G. 1998, ApJ, 499, L5
Muñoz, R. R., Carlin, J. C., Frinchaboy, P. F., Nidever, D. L., Majewski, S. R., & Patterson, R. J. 2006a, ApJ, 650, L51
Muñoz, R. R., et al. 2005, ApJ, 631, L137
Muñoz, R. R., et al. 2006b, ApJ, 649, 201
Mutel, R. L., Molnar, L. A., Waltman, E. B., & Ghigo, F. D. 1998, ApJ, 507, 371
Navarro, J. F., Frenk, C. S., & White, S. D. M. 1997, ApJ, 490, 493
Neuhauser, R., et al. 2005, A&A, 435, L13
Nice, D. J., Splaver, E. M., Stairs, I. H., Löhmer, O., Jessner, A., Kramer, M., & Cordes, J. M. 2005, ApJ, 634, 1242
Olling, R. P. 2005, ASP Conf. Ser. 338, Astrometry in the Age of the Next Generation of Large Telescopes, ed. P. K. Seidelmann, & A. K. B. Monet, 272
Olling, R. P. 2007a, MNRAS, 378, 1385
Olling, R. P. 2007b, preprint (astro-ph/0704.3059)
Olling, R. P., & Peterson, D. M. 2000, preprint (astro-ph/0005484) (OP2000)
Osterbrock, D. E., & Matthews, W. G. 1986, ARA&A, 24, 171
Pakzad, S. L., et al. 2004, BAAS, 36, 1582
Palma, C., Majewski, S. R., & Johnston, K. V. 2002, ApJ, 564, 736
Palma, C., Majewski, S. R., Siegel, M. H., Patterson, R. J., Ostheimer, J. C., & Link, R. 2003, AJ, 125, 1352
Pan, X., & Shaklan, S. 2005, BAAS, 37, 454
Pan, X., Shaklan, S., Hunyadi, S., Unwin, S., & Wehrle, A. 2005, BAAS, 37, 1355
Pan, X., Shao, M., & Colavita, M. M. 1993, ApJ, 413, L129
Patterson, R. J., et al. 2001, IAU Colloq. 183, Small Telescope Astronomy on Global Scales, ed. W.-P. Chen, C. Lemme, & B. Paczynski (ASP Conf. Ser. 246; San Francisco: ASP), 65
Pedreros, M. H., Costa, E., & Méndez, R. A. 2006, AJ, 131, 1461
Peebles, P. J. E. 1980, The Large-Scale Structure of the Universe (Princeton, NJ: Princeton University Press)
Peebles, P. J. E. 1989, ApJ, 344, L53
Peebles, P. J., & Ratra, B. 2003, Rev. Mod. Phys., 75, 559
Peñarrubia, J., Benson, A. J., Martínez-Delgado, D., & Rix, H. W. 2006, ApJ, 645, 240
Perryman, M. A. C. 2002, Ap&SS, 280, 1
Perryman, M. A. C., et al. 2001, A&A, 369, 339
Peterson, D., Liu, Y., & Portegies Zwart, S. 2002, PASP, 114, 955
Peterson, D., & Shao, M. 1997, ESA SP-402, Hipparcos—Venice '97, 749
Phelps, S. D. 2002, ApJ, 575, 1

Piatek, S., et al. 2002, AJ, 124, 3198
Pietrzyński, G., et al. 2006, AJ, 132, 2556
Pike, R. W., & Hudson, M. J. 2005, ApJ, 635, 11
Poindexter, S. 2005, ApJ, 633, 914
Pollack, J., Hubickyj, O., Bodenheimer, P., Lissauer, J. J., Podolak, M., & Greenzweig, Y. 1996, Icarus, 124, 62
Pont, F., Mayor, M., & Burki, G. 1994, A&A, 285, 415
Pont, F., Queloz, D., Bratschi, P., & Mayor, M. 1997, A&A, 318, 416
Popper, D. M. 1980, ARA&A, 18, 115
Pravdo, S. H., Shaklan, S. B., & Lloyd, J. 2005, ApJ, 630, 528
Prieto, J. L., & Gnedin, O. Y. 2006, in Rev. Mexicana Astron. Astrofis. Ser. Conf. 26, ed. L. Infante, M. Rubio, & S. Torres-Peimbert, 184
Psaltis, D. 2004, in AIP Conf. Proc. 714, X-ray Timing 2003: Rossi and Beyond, ed. P. Kaaret, F. K. Lamb, & J. H. Swank (New York: AIP), 29
Ransom, R. R., Bartel, N., Bietenholz, M. F., Lebach, D. E., Ratner, M. I., Shapiro, I. I., & Lestrade, J.-F. 2002, ApJ, 572, 487
Refsdal, S. 1966, MNRAS, 134, 315
Remillard, R. A., & McClintock, J. E. 2006, ARA&A, 44, 49
Renzini, A. 1991, in Observational Tests of Cosmological Inflation, ed. T. Shanks, et al. (Dordrecht: Kluwer), 131
Richstone, D. O., & Tremaine, S. 1986, AJ, 92, 72
Rivera, E. J., Lissauer, J. J., Butler, R. P., Marcy, G. W., Vogt, S. S., Fischer, D. A., Brown, T. M., Laughlin, G., & Henry, G. W. 2005, ApJ, 634, 625
Rix, H. W., et al. 2004, ApJS, 152, 163
Romano-Díaz, E., Branchini, E., & van de Weygaert, R. 2005, A&A, 440, 425
Rood, R. T. 1990, in Astrophysical Ages and Dating Methods, ed. E. Vangioni-Flan, et al. (Gif sur Yvette: Ed. Frontières), 313
Rutledge, R. E., Bildsten, L., Brown, E. F., Pavlov, G. G., Zavlin, V. E., & Ushomirsky, G. 2002, ApJ, 580, 413
Schaller, G., Schaerer, D., Meynet, G., & Maeder, A. 1992, A&AS, 96, 269
Scholz, R.-D., & Irwin, M. J. 1994, in IAU Symp. 161, Astronomy from Wide-Field Imaging, ed. H. T. MacGillivray, et al. (Dordrecht: Kluwer), 535
Schüssler, M., Caligari, P., Ferriz-Mas, A., Solanki, S. K., & Stix, M. 1996, A&A, 314, 503
Schweickhardt, J., Schmutz, W., Stahl, O., Szeifert, T., & Wolf, B. 1999, A&A, 347, 127
Schweitzer, A. E., Cudworth, K. M., & Majewski, S. R. 1997, ASP Conf. Ser. 127, Proper Motions and Galactic Astronomy, ed. R. M. Humphreys, 103
Schweitzer, A. E., Cudworth, K. M., Majewski, S. R., & Suntzeff, N. B. 1995, AJ, 110, 2747
Searle, L., & Zinn, R. 1978, ApJ, 225, 357
Shaklan, S. B., Milman, M. H., & Pan, X. 2003, Proc. SPIE, 4852, 161
Shakura, N. I., & Sunyaev, R. A. 1973, A&A, 55, 155
Shao, M. 1993, Proc. SPIE, 1947, 89
Shao, M. 2006, Proc. SPIE, 6268, 62681Z
Sharpe, J., et al. 2001, MNRAS, 322, 121
Shaya, E. J., Tully, R. B., & Pierce, M. J. 1992, ApJ, 391, 16
Shklovskii, I. S. 1967, ApJ, 148, L1
Sohn, S. T., et al. 2007, ApJ, 663, 960
Sozzetti, A. 2005, PASP, 117, 1021
Sozzetti, A., Casertano, S., Brown, R. A., & Lattanzi, M. G. 2002, PASP, 114, 1173
Sozzetti, A., Casertano, S., Brown, R. A., & Lattanzi, M. G. 2003, PASP, 115, 1072
Spergel, D. N., et al. 2003, ApJS, 148, 175
Spergel, D. N., et al. 2007, ApJS, 170, 377 (WMAP07)
Strassmeier, K. G., & Rice, J. B. 1998, A&A, 339, 497
Strigari, L. E., Bullock, J. S., & Kaplinghat, M. 2007, ApJ, 657, 1
Strigari, L. E., Bullock, J. S., Kaplinghat, M., Kravtsov, A. V., Gnedin, O. Y., Abazajian, K., & Klypin, A. A. 2006, ApJ, 652, 306
Szabados, L. 2003, Inf. Bull. Variable Stars, 5394, 1
Szczerba, R., Szymczak, M., Babkovskaia, N., Poutanen, J., Richards, A. M. S., & Groenewegen, M. A. T. 2006, A&A, 452, 561
Tabachnik, S., & Tremaine, S. 2002, MNRAS, 335, 151
Tanaka, H., & Ward, W. R. 2004, ApJ, 602, 388
Tanner, A., et al. 2007, PASP, 119, 747
Thorsett, S. E., & Chakrabarty, D. 1999, ApJ, 512, 288
Tisserand, P., et al. 2007, A&A, 469, 387
Tolstoy, E., et al. 2004, ApJ, 617, L119
Tomsick, J. A., Quirrenbach, A., & Reffert, S. 2005, BAAS, 207, 117.02
Tonry, J. L., & Schneider, D. P. 1988, AJ, 96, 807
Turnbull, M. C., & Tarter, J. C. 2003, ApJS, 145, 181
Turyshev, S. G. 2002, preprint (gr-qc/0205061)
Turyshev, S. G., Shao, M., & Nordtvedt, K. 2007, in Lasers, Clocks, and Drag-Free Technologies for Future Exploration in Space and Tests of Gravity, Astrophysics and Space Science Library, Vol. 349, ed. H. Dittus, C. Lämmerzahl, & S. G. Turyshev (New York: Springer Verlag), 473
Turyshev, S. G., Williams, J. G., Nordtvedt, K., Shao, M., & Murphy, T. W., Jr. 2004, 35 Years of Testing Relativistic Gravity, Lecture Notes in Physics, Vol. 648 (Berlin/Heidelberg: Springer), 311
Unwin, S. C. 2005, in ASP Conf. Ser. 338, Astrometry in the Age of the Next Generation of Large Telescopes, ed. P. K. Seidelmann, & A. K. B. Monet, 37
Unwin, S. C., & Turyshev, S. G. 2004, Science with the Space Interferometry Mission (JPL Publication), 2004-19
Unwin, S. C., Wehrle, A. E., Urry, C. M., Gilmore, D. M., Barton, E. J., Kjerulf, B. C., Zensus, J. A., & Rabaca, C. R. 1994, ApJ, 432, 103
Valtonen, M., et al. 2006, ApJ, 6423, L9
VandenBerg, D. A. 1990, in Astrophysical Ages and Dating Methods, ed. E. Vangioni-Flan, et al. (Gif sur Yvette: Ed. Frontières), 241
Vlemmings, W. H. T., Diamond, P. J., & Imai, H. 2006, Nature, 440, 58
Walker, M. A. 1995, ApJ, 453, 37
Walker, M. G., Mateo, M., Olszewski, E. W., Pal, J. K., Sen, B., & Woodroofe, M. 2006, ApJ, 642, L41
Welch, D. 1998, McMaster Cepheid Photometry and Radial Velocity Data Archive, http://crocus.physics.mcmaster.ca/Cepheid/
Wenzler, T., Solanki, S. K., & Krivova, N. A. 2005, A&A, 432, 1057
Westfall, K. B., Majewski, S. R., Ostheimer, J. C., Frinchaboy, P. M., Kunkel, W. E., Patterson, R. J., & Link, R. 2006, AJ, 131, 375
Wielen, R., Lenhardt, H., Schwan, H., & Dettbarn, C. 2001, A&A, 368, 298
Wilkinson, M. I., Kleyna, J. T., Evans, N. W., Gilmore, G. F., Irwin, M. J., & Grebel, E. K. 2004, ApJ, 611, L21
Will, C. M. 2006, Living Rev. Relativ., 9, 3
Willman, B., et al. 2005a, AJ, 129, 2692
Willman, B., et al. 2005b, ApJ, 626, L85

Wittkowski, M., Boboltz, D. A., Ohnaka, K., Driebe, T., & Scholz, M. 2007, A&A, 470, 191
Wolf, C., et al. 2004, A&A, 421, 913
Worthey, G. 1994, ApJS, 95, 107
Worthey, G. 1998, PASP, 110, 888
Wuchterl, G., & Tscharnuter, W. M. 2003, A&A, 398, 1081
Yencho, B. M., Johnston, K. V., Bullock, J. S., & Rhode, K. L. 2006, ApJ, 643, 154
Yu, Q. 2002, MNRAS, 331, 935
Yu, Q., & Tremaine, S. 2003, ApJ, 599, 1129
Zacharias, N., Urban, S. E., Zacharias, M. I., Wycoff, G. L., Hall, D. M., Monet, D. G., & Rafferty, T. J. 2004, AJ, 127, 3043
Zentner, A. R., Kravtsov, A. V., Gnedin, O. Y., & Klypin, A. A. 2005, ApJ, 629, 219
Zheng, W., et al. 1995, ApJ, 444, 632
Zhu, Z. 2000, Ap&SS, 271, 353
Zinn, R. 1996, in ASP Conf. Ser. 92, Formation of the Galactic Halo Inside and Out, ed. H. Morrison, & A. Sarajedini, 211
Zucker, D. B., et al. 2006, ApJ, 650, L41